A Spherical Vortex Model for Homogeneous Turbulence

Thesis by

Keri A. Aivazis

In Partial Fulfillment of the Requirements

for the Degree of

Doctor of Philosophy

California Institute of Technology

Pasadena, California

1999

(Submitted May 26, 1999)

To MacKenzie and Alec

and

To the memory of my mother

Acknowledgements

I would like to thank my advisors, Professors Philip Saffman and Dale Pullin, for their patience, unrelenting support and guidance throughout my investigations. Their outstanding mathematical and physical understanding of turbulent fluid mechanics yielded critical insights into the most difficult aspects of this work.

I wish to express my appreciation to the ARCS Foundation for their generous support the last four years and to the National Science Foundation for the fellowship I received in the academic years 1994-1995, 1995-1996, and 1996-1997.

I would also like to thank my dear friend and office mate, James Gleeson, for the many helpful conversations and for his great sense of humor. Special thanks are also due to Sheila Shull in the Applied Mathematics department.

I owe the deepest gratitude to my daughter, MacKenzie, and to my son, Alec, for their understanding and sacrafice during my years as a graduate student. Finally, I extend thanks to Michael Aivazis for his wealth of wisdom and encouragement.

Abstract

We investigate a stochastic model for homogeneous, isotropic turbulence based on Hill's spherical vortex. This is an extension of the original work done by Synge and Lin in the early 1940's. The spherical vortex is an inviscid, steady, rotational solution to Euler's equation and its structure makes it a natural candidate for a model of a turbulent eddy. The model assumes that a field of locally isotropic turbulence is generated by a homogeneous distribution of Hill's vortices. The cascade process of eddy breakdown is incorporated into the statistical model through an average over vortex size. Dissipation field characteristics are assumed for the vortex size distribution. We are interested in the statistical properties of the model, in particular order-n structure functions defined by rank-n tensors for the ensemble average of a set of incremental differences in a given field property. We are primarily concerned with the second order pressure structure function, $D_p = \left\langle \left(p\left(\mathbf{x}+\xi\right)-p\left(\mathbf{x}\right)\right)^2 \right\rangle / \rho^2$, and the velocity structure functions, orders 2-6, where $D_{i...s} = \left\langle \left(u_i\left(\mathbf{x}+\xi\right)-u_i\left(\mathbf{x}\right)\right)...\left(u_s\left(\mathbf{x}+\xi\right)-u_s\left(\mathbf{x}\right)\right)\right\rangle$ and $\langle ... \rangle$ denotes the ensemble average.

Specifically D_p, D_{ij}, D_{ijkl}, and the longitudinal component of D_{ijklmn} are calculated. Comparing D_{ij} and D_{ijkl} with experimental curves fixes the two independent model parameters while the sixth-order longitudinal velocity structure function is a predicted result. The pressure structure function is calculated both from first principles and directly from its integral relation with the fourth-order velocity structure function and compared with direct numerical simulation.

Contents

List of Figures

List of Tables

Chapter 1 Introduction

1.1 Introduction

Turbulence is a highly unpredictable state of fluids in which small disturbances are generally amplified, rendering their deterministic evolution intractable. Turbulent motion is by nature unstable; it describes a regime dominated by the quadratic nonlinearities in the momentum equation. The degree of instability is characterized by the Reynolds number which measures the relative importance of the nonlinear convective motions over the linear dissipative damping. This work is concerned with fully developed turbulence which refers to the limit of very large Reynolds numbers. Such a limit corresponds to large velocities (convective dominance) or small viscosity (weak viscous damping).

Classical theory relies on the premise that turbulent motion is so complex and unpredictable that statistically averaged quantities provide the most meaningful information. A decomposition of the velocity and pressure fields into mean and fluctuating fields gives rise to the Reynolds equations which are analogous to the Navier-Stokes equations for the mean velocity and pressure but include a supplementary term involving the second order moment of the velocity fluctuations, the so called Reynolds stress tensor. It is a simple exercise to show that the evolution of the second order moment depends on the third order moment, or more generally, that the n-order moment depends on the $(n+1)$-order moment [3]. This generates a hierarchy of equations which constitute the well known closure problem. To close the set of equations, an additional phenomenological hypothesis or model can be adopted. For statistically inhomogeneous flows and when the average quantities depend on only one point in space, one point closure models have been proposed [4]. One such hypothesis proposed by Prandtl in 1925, introduced a characteristic scale and velocity for the turbulent fluctuations. Borrowing ideas from molecular diffusion, Prandtl expressed

the Reynolds stress as a turbulent diffusion which regularizes the mean velocity gradients for scales smaller than the characteristic length. The analogy with molecular diffusion however is very misleading. As pointed out by Farge [5], molecular diffusion is decoupled from the large scale dynamics, whereas turbulence is characterized by non-linear interactions at all scales. A separation of scales decoupling large scale dynamics from small scale ones does not exist. The more modern renormalization group techniques [6] suffer from the same obstacle. Hence, the adequacy of one point closure models remain an open question.

Significant simplifications are made when the flow is statistically invariant under translation (homogeneous) and rotation (isotropic). Homogeneity permits the assumption that the mean velocity is zero, and interest is turned to two point closure modeling and correlations. For homogeneous flows it is convenient to work in Fourier space where many of the statistical properties have physically significant meanings, and the modes make additive contributions to the energy spectrum. Since Taylor's famous paper in 1935 [7] where he characterized turbulent flows by their energy spectrum tensors, the vast majority of turbulence research has been based on analysis in Fourier space. Taylor's initial assumption that ensemble averages are homogeneous and isotropic has remained a pivotal assumption to progress in the last sixty years. Shortly after Taylor's work, Kolmogorov and his student, Obukhov, applied probability theory to turbulence and published four significant papers in 1941 [8, 9, 10, 11] laying the foundation for dimensional analysis and statistical theory of fully developed turbulence. Batchelor also made substantial contributions, and published his famous book, *Homogeneous Turbulence*, in 1953. To study the distribution of energy across the scales, Kolmogorov assumed that external forces inject energy at the large scales, while the effects of viscosity are limited to the small scales. For fully developed flows, this leaves an intermediate bandwidth of scales, the inertial range, in which a uni-directional cascade of energy on average from large to small scales at a constant rate, ϵ, was assumed. Kolmogorov further assumed a constant skewness which led him to introduce the K41 model, which predicts the famous $k^{-5/3}$ law for the shell

averaged energy spectrum function,

$$E(k) = C_o \epsilon^{2/3} k^{-5/3}. \tag{1.1}$$

In response to criticism by Landau, the assumption that ϵ is constant was later relaxed and Kolmogorov proposed a model in which only a fraction, β, of energy is transferred between scales [12]. Assuming a log-normal probability distribution for the dissipation field, Kolmogorov introduced the K62 model which predicts the following scaling for $E(k)$:

$$E(k) = C_o \epsilon^{2/3} k^{-5/3} \ln\left(\frac{k}{k_I}\right)^{\beta}. \tag{1.2}$$

The constant C_o is called the Kolmogorov constant and k_I is the modulus of the wavenumber at which energy is injected. The log-normal distribution function has since played an important role in understanding dissipation and eddy structure in turbulent flows [13, 14].

Advances in scientific computing have refocused attention from the classical ensemble average to independent flow realizations in which the role of vorticity and the presence of coherent structures can be appreciated. An important manifestation of turbulent flows is the production of vorticity. Owing to the inherent instabilities of continuous vortex distributions, regions of intensely rotational motion form into well-localized coherent structures which are characterized by distinct shapes and life spans that exceed the typical eddy turnover time. The nucleation of coherent structures plays a significant role in non-deterministic flows such as turbulent mixing layers [13].

Presently, the direct numerical simulation of turbulence is constrained by the large range of scales present in fully developed flows. The number of degrees of freedom necessary to fully resolve a turbulent flow scales like $\mathrm{Re}_I^{9/4}$ for three-dimensional flows and Re_I^2 for two-dimensional flows, where Re_I is the turbulent Reynolds number based on the integral scale of turbulence [3]. Such memory and cpu requirements far exceed present computing capabilities when Re_I is very large. However, advances

in scientific computing have led to promising areas such as Large Eddy Simulation [15] which resolves the large scale motion yet contains inaccuracies introduced by our lack of fully understanding the role of the small scales. The promise of vortex models would be to bridge the deterministic approach (DNS) to the stochastic approach by providing statistical information about the dynamical impact of the unresolved, fine scales on the larger ones. This is encouraging as subgridscale modeling is required for filtering techniques such as LES so that kinetic energy can be taken from the large, filtered scales and transferred to the subgrid scales and dissipated by viscous damping.

Vortex models for turbulence are thus emerging rapidly in tandem with numerical models, attempting to encompass the inherent complexities of turbulent flows. However, the pursuit of a comprehensive statistical model which reflects both experiment and direct numerical simulation is slow, as the structures which appear and subsequently contribute to the statistical field properties are seemingly flow dependent. Qualitatively, turbulence can be described as a superposition of vortex structures with varying length scales, but the physical nature of the eddy structure changes dramatically in the presence of boundaries, and fluid property variations. The topological features of the turbulent boundary layer elucidate this [16]. Near the wall, structures are tube-like, lying in the spanwise direction; their existence owing to the alignment of the vorticity and the intermediate principal strain rate direction [17]. As revealed by Vincent and Meneguzzi [18, 19], the alignment is most prominent in regions of high viscous dissipation. At the boundary, the mean flow enstrophy reaches its maximum and appears as a distorted sheet, while the perturbation enstrophy results in cylindrical structures emanating from the wall. As expected, downstream, and away from the wall, the structures begin to arch, their shape becoming less discernable. As the boundary effects become less appreciable the flow tends to a more homogeneous state and the dynamic role of tube-like structures becomes less significant.

This work is concerned with a statistical model for turbulence in a range of scales void of concentrations of high viscous dissipation of kinetic energy. In the case of the turbulent boundary layer or channel flow, this would apply far from the wall. For

such a region, homogeneity and isotropy become plausible assumptions.

In the early 1940's, Synge and Lin [20] initially considered Hill's sperical vortex as a model for homogeneous turbulence. While the spherical vortex provides a statistically tractable steady solution to Euler's equation, it lacks dissipation and an energy transfer mechanism such as vortex stretching consistent with small scale dynamics. Since the seminal work of Synge and Lin, there have been numerous investigations of vortex based models for turbulent flows [21, 22, 23, 24, 25]. A simple solution to the Navier-Stokes equations which encapsulates a mechanism for vortex stretching is given by the steady Burgers [26] vortex,

$$\omega(s) = \frac{\mu\Gamma_o}{4\pi\nu}\exp\left(-\frac{s^2\mu}{4\gamma}\right), \tag{1.3}$$

where s denotes the radial distance to the vortex center, Γ_o is the total circulation, ν is the viscosity and γ is the strain rate of a uniform straining field. Equation (1.3) coupled with a similar equation for a stretched shear layer constitute a dynamical balance between vorticity diffusion and vortex stretching. Together they form a model consistent with the Kármán-Howarth equation for turbulence (1.32), which at zero separation suggests that vortex line stretching by the local straining field and viscous dissipation of the mean square vorticity are in statistical equilibrium. In 1951, Townsend [21] calculated the one-dimensional velocity spectrum for isotropic turbulence using an ensemble of axisymmetric and plane Burgers vortices. In the case where each realization in the ensemble consists of a single axisymmetric Burgers vortex, the shell-summed energy spectrum is

$$E(k) = \frac{N\tau\Gamma_o^2}{4\pi k}\exp\left(-\frac{2k^2\nu}{\gamma}\right), \tag{1.4}$$

where N and τ are model parameters. The spectrum for the plane Burgers vortex behaves like $k^{-2}G(k)\exp\left(-\frac{2k^2\nu}{\gamma}\right)$, where $G(k)$ is a slowly varying function of k. Hence, as noted by Pullin and Saffman [27], the K41 model suggests vorticity distributions for inertial range properties should have both sheet-like and tube-like structure. It

should be mentioned that volume filling ensembles of such vortices yield poor results for higher order velocity derivative moments [28].

In the same spirit that Townsend introduced a physical model describing a distribution of vorticity embedded in a straining field, Lundgen introduced the stretched-spiral vortex model in 1982 [25]. The model consists of axisymmetric straining combined with a slender spiral vortex. The stretching represents the effect of instabilities while the internal spiral structure provides a source of dissipation. Lundgren related the energy spectrum to a time integration involving the enstrophy spectrum of the evolving 2-D cross-sectional flow and gave examples in which a $k^{-5/3}$ spectrum was obtained [29]. The structure of the Lundgren model offered a great deal of promise for developing a robust model for the intermittent fine structure and since its introduction it has received significant attention [30, 31, 32, 27, 2, 33]. Pullin and Saffman [31] used the model to compute one-point statistics of vorticity and velocity derivative moments and later calculated higher order velocity structure functions with mixed results. While the model has had some success recovering local properties for small separation, its predictive capability for larger scales is questionable.

The majority of vortex based models have embodied the tube and sheet-like structures occurring in the turbulent boundary layer resulting from the concentration of dissipation. Other coherent turbulent structures include the Karman vortices observed by Roshko [34] and vorticity tubes which form in statistically homogeneous flows [35]. The precise source of coherent structures in homogeneous flows is unknown; however, large scale instability manifested in the roll-up of thin vortex layers has been suggested. In addition, direct numerical simulation suggests vortex cores spontaneously nucleate from a random two-dimensional vorticity field [36]. Although tube-like structures exist in a homogeneous field, it is unlikely that they serve as the base flow and strongly impact the statistical properties. One might conjecture that large scale instability gives rise to a region of intense kinetic energy dissipation, increasing the probability for alignment between the vorticity and the intermediate principal rate of strain direction, resulting in the formation of a tubular coherent structure. These local condensations of the vorticity field nucleate randomly and are

thereafter advected by the base flow in a homogeneous and isotropic fashion. Their effect is essentially lost during the ensemble averaging. In three-dimensional flows, vorticity tubes become highly unstable and their temporal and spatial support may be very small. Therefore, the presence of coherent structures only affect high-order velocity structure functions which are most sensitive to unusual or extreme events [5].

Utilizing tube-like structures as in the Burgers and stretched-spiral model aims at modeling the small scales where dissipation becomes important. We are, however, in need of a different model for the larger structures defined by scales for which stretching is not the dominant dynamic. This paper is primarily concerned with a model for the base flow for a statistically homogeneous turbulent field. We assume the flow is locally isotropic which forces all finite dimensional probablity distribution functions to be unaffected by rotations about the origin and mirror reflections about any plane passing through the origin. In such an idealized, isotropic, homogeneous field, the eddy would have an unbiased orientation and shape. The spherical vortex is a natural candidate for such an eddy – symmetrical, rotational flow is secluded from potential flow by a sphere of radius a.

A stochastic model for turbulence includes a physical model for the topology of the fine scale motion as well as information regarding at least one probability distribution function for the flow. In turbulence, focus is generally directed toward the joint distribution function which provides the statistical connection between random values of the velocity field at different points in space-time. It is the joint probability distribution function which is essential to most hypothesis regarding the mechanism of turbulence decay. Once the machinery for computing averages is established, numerous statistical properties can be computed and tested against theory, observation and numerical simulation.

Synge and Lin were able to compute the velocity correlation for the Hill's spherical vortex model, hereafter referred to as HSV, and present strong data suggesting that the spherical vortex provides a reasonable representation of a large scale turbulent eddy. We modify and extend the work of Synge and Lin by incorporating cascade characteristics into the statistical model, and investigate both velocity and pressure

statistics. We compute the high-order velocity structure function tensors D_{ij}, D_{ijkl}, the longitudinal component of D_{ijklmn} and the pressure structure function, D_p, for a field of locally isotropic turbulence generated by a homogeneous distribution of Hill's vortices. The model is based on an ensemble of statistically independent vortex spheres advancing with constant velocity through a fluid which is at rest at infinity. Initially field averages are computed under the assumption of a single vortex type. The assumption of fixed vortex size is later relaxed with the introduction of the log-normal distribution function governing vortex radius which embodies the cascade process of eddy breakdown.

1.2 Governing equations for turbulent flows

This work is concerned with fluid motion which can be regarded as incompressible (constant density of fluid elements) and Newtonian (deformation stress proportional to velocity gradients). The fundamental equations governing the dynamics of such a motion are the equation of continuity and conservation of momentum,

$$\nabla \cdot \mathbf{U} = \mathbf{0}, \tag{1.5}$$

$$\partial_t \mathbf{U} + (\mathbf{U} \cdot \nabla)\,\mathbf{U} + \frac{1}{\rho}\nabla P = \nu \nabla^2 \mathbf{U} + \mathbf{F}, \tag{1.6}$$

where $\mathbf{U}(\mathbf{x}, t)$ is the fluid velocity at position $\mathbf{x}$ and time t, P the pressure, F the resultant of external forces per unit mass, ρ the density, and ν the kinematic viscosity of the fluid. These equations can be derived from kinetic theory [37] or via the methods of continuum mechanics [38]. They describe the dynamics of such common fluids as water, air and most gases. A more physically illuminating framework for studying turbulence is given by the vorticity equation which results by taking the curl of (1.6),

$$\partial_t \omega + (\mathbf{U} \cdot \nabla)\,\omega = (\omega \cdot \nabla)\,\mathbf{U} + \nu \nabla^2 \omega + \nabla \times \mathbf{F}. \tag{1.7}$$

The vorticity equation describes the effect of three distinct processes on the time dependence of the vorticity of fluid elements (disregarding external forcing). Corresponding to the second, third and fourth terms in (1.7) respectively, these are the convection of vortex lines with the fluid, the intensification of vorticity due to vortex stretching and the diffusion of vorticity. The Burgers vortex [26] is an exact solution to the Navier-Stokes equations and involves all three processes. Radially outward diffusion of vorticity is countered by a straining field which sweeps vorticity back toward the vortex axis and intensifies the vorticity by stretching fluid elements in the axial direction.

A simplification in the momentum and vorticity equation results for an ideal inviscid fluid motion commonly referred to as Eulerian flow. For conservative forcing, $F = -\nabla H$ where H is a potential, (1.6) and (1.7) reduce to

$$\partial_t \mathbf{U} + (\mathbf{U} \cdot \nabla)\,\mathbf{U} + \frac{1}{\rho}\nabla P = -\nabla H, \tag{1.8}$$

$$\frac{D\omega}{Dt} = (\omega \cdot \nabla)\,\mathbf{U}. \tag{1.9}$$

The operator $\frac{D}{Dt}$ denotes the total derivative. Equation (1.9) also results by beginning with the Navier-Stokes equation and considering a stationary state of turbulence in which the net energy injected into the flow by external forcing is dissipated by viscosity. In 3-D, (1.9) shows that vortex tubes may be stretched by velocity gradients, a phenomenon suggested as a mechanism for energy transfer from large to small scales. In 2-D, $(\omega \cdot \nabla)\,\mathbf{U}$ is zero, so that the vorticity and its infinitely many moments are Lagrangian invariants of the motion. Without a mechanism for the cascade, energy tends to accumulate in the large scales [5].

Reynolds introduced statistics to turbulence in 1894 [39] and decomposed the velocity and pressure fields into a mean field and a fluctuating field,

$$\mathbf{U} = \overline{\mathbf{U}}\,(\mathbf{x}, t) + \mathbf{u}'\,(\mathbf{x}, t)\,, \tag{1.10}$$

$$P = \overline{P}\,(\mathbf{x}, t) + p'\,(\mathbf{x}, t)\,. \tag{1.11}$$

The overbar denotes time average which is generally replaced by a suitable volume average under the assumption that the flow is ergodic. It follows from $\overline{\overline{\mathrm{U}}} = \overline{\mathrm{U}}$ that the fluctuations have zero mean. Substituting this decomposition back into (1.6) and averaging yields the Reynolds equations,

$$\partial_t \overline{U}_i + \overline{U}_j \frac{\partial \overline{U}_i}{\partial x_j} + \frac{1}{\rho}\frac{\partial \overline{P}}{\partial x_i} = \frac{\partial}{\partial x_j}\left(\nu \frac{\partial \overline{U}_i}{\partial x_j} - \left\langle u_i' u_j' \right\rangle\right) + \overline{F}_i. \tag{1.12}$$

The equation for the mean is just the Navier-Stokes equation for the mean variables with the inclusion of a term involving $\left\langle u_i' u_j' \right\rangle$ due to turbulent fluctuations. Note that we have replaced $\overline{u_i' u_j'}$ with its ergodic equivalent $\left\langle u_i' u_j' \right\rangle$ which denotes volume averaging. Thus, the dynamical equations for turbulent flows contain three independent unknowns. This is perhaps the simplest version of the closure problem. Subtracting (1.12) from (1.6) yields an equation for the fluctuating velocity,

$$\partial_t u_i' + u_j' \frac{\partial \overline{U}_i}{\partial x_j} + \overline{U}_j \frac{\partial u_i'}{\partial x_j} + \frac{\partial}{\partial x_j}\left\{u_i' u_j' - \left\langle u_i' u_j' \right\rangle\right\} = -\frac{1}{\rho}\frac{\partial p'}{\partial x_i} + \nu \nabla^2 u_i'. \tag{1.13}$$

While this equation vanishes upon averaging, multiplying through by $u_i'(\mathbf{x}, t)$ prior to averaging generates the one-point moment hierarchy common to engineering approaches to closure. Multiplying through by $u_\gamma'(\tilde{\mathbf{x}}, t)$ prior to averaging generates the two point moment hierarchy which forms the basis for the fundamental approach. The role of one-point and two-point statistical models is thus to provide closure information for the moment problem.

In practice a correlation is measured by averaging over the lifetime of a signal. The turbulent velocity and pressure signals vary in space and time for each realization. Mathematically, computing correlations requires replacing the signal average with a suitable ensemble average. Substituting the ensemble average with a space average supposes the turbulent motion is ergodic. Two point correlations underly the basis of classical theory, and their Fourier transforms dominate themes of research in

turbulence. In general, a two-point correlation of a field quantity is given by

$$Q_{ij}\left(\mathbf{x},\tilde{\mathbf{x}};t,\tilde{t}\right)=\left\langle q_i\left(\mathbf{x},t\right)q_j\left(\tilde{\mathbf{x}},\tilde{t}\right)\right\rangle. \tag{1.14}$$

In the laboratory, correlations are measured by allowing the distance between points $\mathbf{x}$ and $\tilde{\mathbf{x}}$ to vary in a controlled way while allowing relative transverse motion between the vector connecting the two points and the reference frame. This is equivalent to introducing the change of variables,

$$\mathbf{R} = \frac{\mathbf{x}+\tilde{\mathbf{x}}}{2}, \tag{1.15}$$

$$\xi = \mathbf{x}-\tilde{\mathbf{x}}, \tag{1.16}$$

where $\mathbf{R}$ is the centroid (absolute) coordinate and ξ is the separation (relative) coordinate. A similar transformation exists for the time variables t and $\tilde{t}$,

$$T = \frac{t+\tilde{t}}{2}, \tag{1.17}$$

$$\tau = t-\tilde{t}, \tag{1.18}$$

so that, in general, two point correlations have the form,

$$Q_{ij}\left(\mathbf{x},\tilde{\mathbf{x}};t,\tilde{t}\right)=Q_{ij}\left(\xi,\mathbf{R};\tau,T\right). \tag{1.19}$$

1.2.1 Isotropic regimes

Assuming the turbulent field is stationary, homogeneous and isotropic, correlation tensors depend solely on the magnitude of the relative position vector and the relative time,

$$\left\langle q_i\left(\mathbf{x},t\right)q_j\left(\tilde{\mathbf{x}},\tilde{t}\right)\right\rangle=Q_{ij}\left(\xi,t\right). \tag{1.20}$$

Such a tensor is invariant under the Euclidean group $E\left(3\right)$. Isotropic two-point tensors can be written in terms of invariants of the rotation group, $SO\left(3\right)$. Robertson [40]

showed that all the requisite symmetries of a second order isotropic tensor are satisfied by a relationship with two scalar, even functions of $|\xi| = \xi$,

$$Q_{ij}(\xi) = A(\xi)\,\xi_i\xi_j + B(\xi)\,\delta_{ij}. \tag{1.21}$$

Although the explicit time dependence has been omitted, it is understood that the scalar functions and the correlation tensor are time dependent in general. In the case where $Q_{ij}(\xi)$is the two-point velocity correlation $R_{ij}(\xi)$, $A(\xi)$ and $B(\xi)$ are related via continuity. Having introduced the relative position vector ξ, a preferred coordinate system can be introduced based on the configuration of the two points where one of the Cartesian axes is colinear with the separation vector. Based on such a configuration, a correlation can be established between longitudinal velocity components $(u_\xi, \tilde{u}_\xi)$ and transverse components $(u_\gamma, \tilde{u}_\gamma)$. Thus, longitudinal and transverse (lateral) velocity scalar functions can be introduced through the following relationships:

$$\left\langle u^2 \right\rangle f(\xi) = \left\langle u_\xi \tilde{u}_\xi \right\rangle, \tag{1.22}$$

$$\left\langle u^2 \right\rangle g(\xi) = \left\langle u_\gamma \tilde{u}_\gamma \right\rangle, \tag{1.23}$$

where

$$\left\langle u^2 \right\rangle = \frac{1}{3}\left(\left\langle u_1^2 \right\rangle + \left\langle u_2^2 \right\rangle + \left\langle u_3^2 \right\rangle\right). \tag{1.24}$$

In terms of $f(\xi)$ and $g(\xi)$ the two-point velocity correlation tensor is

$$R_{ij}(\xi) = \langle u_i \tilde{u}_j \rangle = \left\langle u^2 \right\rangle \left(\frac{f-g}{\xi^2}\xi_i\xi_j + g\ \delta_{ij}\right). \tag{1.25}$$

These relationships are fully developed in Batchelor's book on homogeneous turbulence [41]. Continuity translates into requiring $\frac{\partial}{\partial \xi_i} R_{ij}(\xi) = 0$ which fixes the relationship between the scalar functions,

$$g = f + \frac{1}{2}\xi f'. \tag{1.26}$$

Two important length scales can be computed from the longitudinal correlation function $f(\xi)$. One is a differential length scale, the Taylor microscale λ, and the other is the integral length scale L_p, defined respectively by

$$f_o'' = -\frac{1}{\lambda^2}, \tag{1.27}$$

$$L_p = \int_0^\infty f(\xi)\, d\xi. \tag{1.28}$$

The longitudinal length scale represents the spatial extent to which the longitudinal velocities are correlated. The physical significance of the Taylor microscale is indicated by its relationship to the mean-square vorticity and the rate of energy dissipation. The two-point vorticity correlation is given by

$$\langle \omega_i(\mathbf{x})\, \tilde{\omega}_j(\tilde{\mathbf{x}}) \rangle = \epsilon_{ilm}\epsilon_{jpq} \left\langle \frac{\partial u_m}{\partial x_l} \frac{\partial \tilde{u}_q}{\partial \tilde{x}_p} \right\rangle, \tag{1.29}$$

$$= -\delta_{ij}\nabla^2 R_{ll}(\xi) + \frac{\partial^2 R_{ll}(\xi)}{\partial \xi_i \partial \xi_j} + \nabla^2 R_{ij}(\xi). \tag{1.30}$$

Contracting the indices and letting $\xi = 0$ yields an interesting result for the mean-square vorticity,

$$\langle \omega_i \tilde{\omega}_i \rangle = -\left(\nabla^2 R_{ii}(\xi)\right)_{\xi=0} = -15 \langle u^2 \rangle f_o'' = \frac{15\langle u^2 \rangle}{\lambda^2}. \tag{1.31}$$

The relationship between the Taylor microscale and the rate of energy dissipation is found directly from the Kármán-Howarth equation. The Kármán-Howarth equation describes the relationship between the time rate of change of $\langle u^2 \rangle f(\xi)$, derivatives of the triple velocity correlation $S_{ilj}(\xi)$ (which can be expressed in terms of a single scalar function $\langle u^3 \rangle k(\xi)$), and derivatives of $f(\xi)$ arising from the viscous dissipation term in the Navier-Stokes equation,

$$\partial_t \langle u^2 \rangle f(\xi) = \langle u^3 \rangle \left(\frac{\partial}{\partial \xi} + \frac{4}{\xi} \right) k(\xi) + 2\nu \langle u^2 \rangle \left(\frac{\partial^2}{\partial \xi^2} + \frac{4}{\xi}\frac{\partial}{\partial \xi} \right) f(\xi). \tag{1.32}$$

Like the momentum equation, (1.32) is not closed. Attempts to obtain equations

for $k(\xi)$ generates the moment hierarchy observed with the averaged momentum equation. Putting $\xi = 0$ gives the connection between λ and the rate of energy dissipation,

$$\varepsilon = \frac{3}{2}\frac{d\langle u^2\rangle}{dt} = \frac{15\nu\langle u^2\rangle}{\lambda^2}. \tag{1.33}$$

Aside from two-point correlations of field properties, structure functions provide another fundamental two-point quantity in classical turbulence theory [41, 42]. The structure function of order-p is a statistical average of an incremental difference of a field quantity raised to the power p,

$$S_p(\xi) = \langle [q(\mathbf{x}) - q(\tilde{\mathbf{x}})]^p \rangle . \tag{1.34}$$

As p increases, $S_p(\xi)$ becomes increasingly dominated by extreme events. A great deal of attention is placed on possible power law behavior of structure functions,

$$S_p(\xi) = \xi^{\varsigma(p)}, \tag{1.35}$$

where $\varsigma(p)$ denotes the explicit dependence of the exponent on the order. Based on similarity principles, Kolmogorov [8] predicted the general result for the velocity structure functions, namely, $\varsigma(p) = p/3$. This contradicts more recent experiments [43] which suggest the exponents tend to increase less quickly with p for $p > 5$. Fine structure intermittency has been suggested as the probable cause.

Chapter 2 Statistical representation of a turbulent field

We are interested in computing statistical properties for a vortex model of turbulence. We imagine a fluid stirred up into a state of turbulence by a locally isotropic, homogeneous distribution of Hill's vortices. To compute two-point correlations we must first focus our attention on a fixed region in space, and imagine collecting a number of separate observations of vortex distributions. Upon superimposing all such observations, we obtain an ensemble in which the frequency distribution for the field variables tends to a continuous limit.

To proceed with the average, we must make several assumptions. First we assume that fluctuations in the number of vortices in the region under consideration are statistically insignificant. Secondly, because the velocity field of the spherical vortex is zero at infinity in a fixed reference frame, we will find it convenient to treat the region as infinite in extent. However, since we are imposing homogeneity, the ratio of the number of vortices to the volume of our region remains finite. Therefore, we cannot pass to the limit, $V \to \infty$, without simultaneously allowing $N \to \infty$ so that $N/V = n$ is a finite number.

We begin by labeling each vortex $1, ..., N$. In a given observation, the k^{th} vortex is characterized by seven quantities, $x_1^k, x_2^k, x_3^k, \theta^k, \phi^k, U^k$ and a^k, three coordinates fixing its position, two coordinates fixing its orientation and two coordinates fixing its type. Therefore, we have 7N different quantities that characterize each observation. Let $\alpha_\mathbf{k}$ be the seven-dimensional vector that characterizes vortex k. We assume that frequency distributions exist for the quantities characterizing the field, and in the limit that the number of observations becomes very great, we obtain a continuous distribution denoted by $\Phi(\alpha_1, \alpha_2, \ldots, \alpha_N)$. The ensemble average of any field

property B is then given by

$$\langle B \rangle = \int \dots \int B\Phi d\alpha_1 \dots d\alpha_N. \tag{2.1}$$

Solving (2.1) requires knowledge of the distribution function Φ. If we assume the N vortices are stochastically independent, we can express the distribution function as the product of the distribution functions governing each vortex, i.e.,

$$\Phi(\alpha_1 \dots \alpha_N) = \Psi^{(1)}(\alpha_1) \dots \Psi^{(N)}(\alpha_N). \tag{2.2}$$

We must further remove any dependence on the initial numbering of vortices. Essentially, this requires

$$\Psi^{(1)} = \Psi^{(2)} = \dots = \Psi^{(N)}. \tag{2.3}$$

Assuming there is zero correlation between orientation, position and type, the vortex distribution function can be decomposed into the product of three distribution functions. Letting $\zeta(U, a)$ be the frequency distribution in type, $\mu(l^m)$ the distribution in orientation, and $\sigma(\mathbf{x})$ the distribution in position, we have

$$\Psi^{(k)}(\alpha_k) = \zeta(U_k, a_k)\, \mu(l_k^m)\, \sigma(\mathbf{x}_k), \tag{2.4}$$

where ζ, μ, and σ are subject to the normalization conditions,

$$\begin{aligned} \int \mu(l) d\Omega &= 1, \\ \int \zeta(U, a) dU da &= 1, \\ \int \sigma(\mathbf{x}) dx_1 dx_2 dx_3 &= 1. \end{aligned} \tag{2.5}$$

We assume the vortex distribution function is both isotropic and homogeneous. Therefore, $\mu(l)$ is the inverse of the surface area of a unit sphere, $(4\pi)^{-1}$ and $\sigma(\mathbf{x})$ is V^{-1}. A distribution function for vortex type will be chosen to reflect the fractal

nature of the cascade process and will be discussed later.

In a probabalistic fluid system, it is natural to seek statistical information on the pressure and velocity fields. By measuring individual events in the laboratory, averages of such observables are obtained in the obvious manner,

$$\langle X_N \rangle = \frac{1}{N} \sum_{n=1}^{N} X(n). \tag{2.6}$$

As N becomes large, $\langle X_N \rangle$ tends to the mean $\langle X \rangle$. In general, the moments $\langle X^p \rangle$ are the statistical quantities of interest, as these are often the easiest to measure and calculate from theory. Since probability densities are required to have finite support, we see that higher moments yield information regarding the properties of unlikely large values of X. Higher order moments are therefore sensitive to extreme events.

2.1 Velocity field statistics

In theoretical turbulence research, we begin by considering a reference frame in which the fluid under observation has a zero mean in each of its velocity components. This is consistent with experimental work in which the scientist collects data solely on the fluctuations in a given variable. Formally, the mean velocity is defined as the first moment, which is constructed by integration given the probability distribution, $P(\mathbf{u})$, of the velocity field,

$$\langle \mathbf{u}(\mathbf{x}) \rangle = \int \mathbf{u} P(\mathbf{u}) \, d\mathbf{u}. \tag{2.7}$$

Higher order statistics, in particular, the two point velocity product mean values of orders 2, 3, and 4 have become the working tools of practical theories in tubulence research. The second order two point velocity correlation tensor, $R_{ij}(\mathbf{r})$, has obvious significance as it relates directly by Fourier transform to the energy spectrum

tensor $\Phi_{ij}(\mathbf{k})$,

$$R_{ij}(\mathbf{r}) = \langle u_i(\mathbf{x})\, u_j(\mathbf{x}+\mathbf{r})\rangle\,, \tag{2.8}$$

$$\Phi_{ij}(\mathbf{k}) = \frac{1}{8\pi^3}\int R_{ij}(\mathbf{r})\, \mathrm{e}^{-i\mathbf{k}\cdot\mathbf{x}} d\mathbf{r}. \tag{2.9}$$

Fourier space has served as the traditional setting for turbulence analysis as it allows a decomposition of the turbulent motion into a number of components which additively contribute to the energy of the motion. $\Phi_{ij}(\mathbf{k})$ is hence the repository of knowledge about the distribution of energy over various wavenumbers, and has formed the basis for most theories concerning the decay of energy containing eddies.

The structure function tensors of varying order for the turbulent velocity field and the second order pressure structure function have become other fundamental quantities in classical turbulence theory. A velocity structure function is a two point average of a set of incremental differences in velocity components. We begin by defining the velocity structure function tensors of orders 2, 3 and 4. The first order structure function is obviously defined by the mean which is taken to be zero. The second order structure function is given by

$$D_{ij}(\xi) = \langle (u_i(\mathbf{x}+\xi) - u_i(\mathbf{x}))(u_j(\mathbf{x}+\xi) - u_j(\mathbf{x}))\rangle\,. \tag{2.10}$$

For simplicity, we write $\tilde{u}_i = u_i(\mathbf{x}+\xi)$ and $u_i = u_i(\mathbf{x})$. This allows for the more concise set of definitions,

$$D_{ij}(\xi) = \langle (\tilde{u}_i - u_i)(\tilde{u}_j - u_j)\rangle\,, \tag{2.11}$$

$$D_{ijk}(\xi) = \langle (\tilde{u}_i - u_i)(\tilde{u}_j - u_j)(\tilde{u}_k - u_k)\rangle\,, \tag{2.12}$$

$$D_{ijkl}(\xi) = \langle (\tilde{u}_i - u_i)(\tilde{u}_j - u_j)(\tilde{u}_k - u_k)(\tilde{u}_l - u_l)\rangle\,. \tag{2.13}$$

Orders higher than 4 are constructed in the obvious manner. The *longitudinal structure function of order p* refers to a particular component of the structure function

tensor, assuming the vector ξ lies along a coordinate axis. To avoid any potential confusion, we let u_ξ denote the velocity component along the vector ξ, the *longitudinal* component, and u_γ or u_λ denote orthogonal or *lateral* components. The p^{th} order longitudinal structure function is defined as

$$D_{\underbrace{\xi\xi\ldots\xi}_{p}} = \langle(\tilde{u}_\xi - u_\xi)^p\rangle\,, \tag{2.14}$$

and the p^{th} order lateral structure function is defined as

$$D_{\underbrace{\gamma\gamma\ldots\gamma}_{p}} = \langle(\tilde{u}_\gamma - u_\gamma)^p\rangle\,. \tag{2.15}$$

We return now to the vortex model for turbulence and allow $\mathbf{U}(\mathbf{x}+\xi)$ and $\mathbf{U}(\mathbf{x})$ to denote the velocities induced by the N vortices at positions $\mathbf{x}+\xi$ and $\mathbf{x}$ respectively. We will differentiate between lower and capital letters to distinguish between the field quantity induced by the set of N vortices and the field quantity induced by a single vortex. Each vortex makes an additive contribution to the velocity at the two points. Let $\tilde{u}_i(\alpha_k)$ refer to the i^{th} velocity component at position $\mathbf{x}+\xi$ and $u_i(\alpha_k)$ denote the i^{th} velocity component at position $\mathbf{x}$, both due to vortex k. The explicit dependence of these values on the position, orientation and size of vortex k is shown by its functional dependence on the vector α_k. Summing over the N vortices, we have

$$U_i(\mathbf{x}+\xi) = \sum_{k=1}^{N} \tilde{u}_i(\alpha_k) \tag{2.16}$$

and

$$U_i(\mathbf{x}) = \sum_{k=1}^{N} u_i(\alpha_k). \tag{2.17}$$

Invoking the definition of the ensemble average (2.1), we obtain the most general expression for the p^{th} order structure function tensor based on a field on N non-

interacting vortices,

$$D_{\underbrace{i...s}_{p}} = \int ... \int \Psi^{(1)}(\alpha_1)...\Psi^{(N)}(\alpha_N) \sum_{k=1}^{N} (\tilde{u}_i(\alpha_k) - u_i(\alpha_k)) ... \sum_{k=1}^{N} (\tilde{u}_s(\alpha_k) - u_s(\alpha_k))\, d\alpha_1...d\alpha_N. \tag{2.18}$$

2.2 Pressure field statistics

In many applications, the turbulent pressure field is the desired quantity. Unfortunately much less is known about the fluctuating pressure than the velocity, primarily due to the difficulty of its measurement. Statistical properties of the pressure field are therefore subjected to abundant conjecture and scaling arguments. The two point pressure correlation $P(\xi)$ and the second order structure function $D_p(\xi)$ are the classical statistical quantities for the turbulent pressure field,

$$P(\xi) = \frac{1}{\rho^2} \langle p(\mathbf{x}) \tilde{p}(\mathbf{x}+\xi) \rangle , \tag{2.19}$$

$$D_p(\xi) = \frac{1}{\rho^2} \left\langle (p(\mathbf{x}) - \tilde{p}(\mathbf{x}+\xi))^2 \right\rangle , \tag{2.20}$$

where p and $\tilde{p}$ denote the pressure at points $\mathbf{x}$ and $\mathbf{x}+\xi$ respectively and ρ is the fluid density. Reliable data for these statistical quantities is difficult to obtain. Therefore, relationships between pressure statistics and measurable velocity statistics are extremely useful for understanding the stochastic nature of the turbulent pressure field. Early progress was made in relating pressure statistics to velocity statistics and velocity-derivative statistics. Independently, Batchelor [44] and Obukhov [45] related $D_p(\xi)$ to a fourth-order velocity derivative correlation. Yaglom [46] built on Obukhov's work to derive the mean squared pressure gradient which was independently obtained by Heisenberg [47]. To obtain useful results, Batchelor [44], Obukhov [45] and Obukhov and Yaglom [48] imposed a joint-Gaussian assumption for velocities

and velocity derivatives at two spatial points. Assuming (1.1) they were able to show that the pressure structure function varies as $\xi^{4/3}$ within the inertial range and were further able to relate the scaling constant to the Kolmogorov constant. Without the joint-Gaussian assumption, Obukhov and Yaglom [48] used dimensional arguments to obtain similar results, i.e., $D_p(\xi) \propto \varepsilon^{4/3}\xi^{4/3}$.

In terms of analytically predicting pressure field statistics for a particular vortex model, one may pursue three different approaches. Two methods rely on functional relations between the pressure statistics and velocity statistics while a third approach employs model equations for the pressure field based on N non-interacting vortices. Following the work of Batchelor, Obukhov and Yaglom, the joint-normal hypothesis can be introduced to relate the pressure covariance to the longitudinal velocity correlation function $f(\xi)$. Alternatively, based on more recent work by Hill and Wilczak [49, 50], $D_p(\xi)$ can be related to the fourth order structure function tensor without appealing to the joint-Gaussian assumption.

2.2.1 Joint-normal hypothesis for the velocity field

One approach to estimating the pressure covariance relies on the joint-Gaussian hypothesis used by Heisenberg, Obukhoff and Batchelor. If we assume that the velocity field associated with the energy-containing eddies is normal, the Navier-Stokes equation enables us to relate the pressure statistics of an isotropic flow to the velocity correlation tensor, $R_{ij}(\xi)$, and thence to the longitudinal velocity correlation coefficient $f(\xi)$ [41]. The product of the divergence of the Navier-Stokes equation applied at two separate points, $\mathbf{x}$, and $\mathbf{x}+\xi$, yields a relation between the pressure covariance and the fourth-order velocity-product mean value,

$$\frac{1}{\rho^2}\nabla^4 \langle p\tilde{p}\rangle = \frac{\partial^4 \langle u_i u_j \tilde{u}_l \tilde{u}_m\rangle}{\partial\xi_i \partial\xi_j \partial\xi_l \partial\xi_m}. \tag{2.21}$$

Without a simplified form for the fourth-order product mean value, the above expression is of little help. There is a heuristic argument, developed first by M. Millionshtchikov [51], which suggests that the part of the probablility distribution

function for the velocity field $\mathbf{u}$ generated by the energy-containing eddies is approximately normal, the deviation from normality occurring at the tail of energy containing range of eddy size. Although some quantities such as the triple velocity correlation are highly sensititve to departures from Gaussian behavior, there is some empirical evidence to support relations between the fourth and secord-order product means developed from a joint Gaussian hypothesis. The assumption of a joint normal probability distribution of $\mathbf{u}$ and $\tilde{\mathbf{u}}$ yields the following relation between the fourth-order product mean value and the second-order product mean value [41],

$$\langle u_i u_j \tilde{u}_l \tilde{u}_m \rangle = \langle u_i u_j \rangle \cdot \langle \tilde{u}_l \tilde{u}_m \rangle + \langle u_i \tilde{u}_l \rangle \cdot \langle u_j \tilde{u}_m \rangle + \langle u_i \tilde{u}_m \rangle \cdot \langle u_j \tilde{u}_l \rangle . \tag{2.22}$$

Combining equations (2.21) and (2.22), we obtain a well known relation between the pressure covariance and the scalar function $f(\xi)$,

$$P_{JNH}(\xi) = 2u^4 \int_{\xi}^{\infty} \left(y - \frac{\xi^2}{y} \right) [f'(y)]^2 \, dy. \tag{2.23}$$

The subscript JNH refers to *joint-normal hypothesis*. It must be emphasized that this result depends entirely on the assumption that the major contribution to the velocity field and hence, pressure field, arises from the influences of the energy-containing eddies.

2.2.2 Relationships between fourth-order velocity statistics and the pressure structure function

The joint-probability distribution of the velocity field measured at two points is known generally to be not accurately normal. The fourth-order structure function is a sensitive measurement of such departures from Gaussian behavior, and is used to define the flatness factor,

$$F = \frac{\left\langle (\tilde{u}_\xi - u_\xi)^4 \right\rangle}{\left\langle (\tilde{u}_\xi - u_\xi)^2 \right\rangle^2}. \tag{2.24}$$

The flatness factor for a Gaussian joint-probability distribution would be 3.0. Measurements of grid turbulence made by R. W. Stewart [52] show large departures from 3.0 for small separations; a maximum near 3.6 occurs at $\xi = 0$. As the separation increases, the velocities at the two points become statistically independent resulting in a flatness factor near 3.0.

Without imposing the joint-Gaussian assumption, Hill [49] and Hill and Wilczak [50] related the pressure structure function to integrals of components of the fourth-order velocity structure function tensor under the assumptions of local homogenity and local isotropy. The derivation begins by expanding the fourth order tensor as follows:

$$\begin{aligned} D_{ijkl}(\xi) &\equiv \langle (u_i - \tilde{u}_i)(u_j - \tilde{u}_j)(u_k - \tilde{u}_k)(u_l - \tilde{u}_l) \rangle , \qquad (2.25) \\ &= \langle u_i u_j u_k u_l \rangle - \langle \tilde{u}_i u_j u_k u_l \rangle - \langle u_i \tilde{u}_j u_k u_l \rangle + \langle \tilde{u}_i \tilde{u}_j u_k u_l \rangle - \\ &\quad \langle u_i u_j \tilde{u}_k u_l \rangle + \langle \tilde{u}_i u_j \tilde{u}_k u_l \rangle + \langle u_i \tilde{u}_j \tilde{u}_k u_l \rangle - \langle \tilde{u}_i \tilde{u}_j \tilde{u}_k u_l \rangle - \\ &\quad \langle u_i u_j u_k \tilde{u}_l \rangle + \langle \tilde{u}_i u_j u_k \tilde{u}_l \rangle + \langle u_i \tilde{u}_j u_k \tilde{u}_l \rangle - \langle \tilde{u}_i \tilde{u}_j u_k \tilde{u}_l \rangle + \\ &\quad \langle u_i u_j \tilde{u}_k \tilde{u}_l \rangle - \langle \tilde{u}_i u_j \tilde{u}_k \tilde{u}_l \rangle - \langle u_i \tilde{u}_j \tilde{u}_k \tilde{u}_l \rangle + \langle \tilde{u}_i \tilde{u}_j \tilde{u}_k \tilde{u}_l \rangle . \end{aligned}$$

Adding and subtracting $3\langle u_i u_j u_k u_l \rangle$ and $3\langle \tilde{u}_i \tilde{u}_j \tilde{u}_k \tilde{u}_l \rangle$, $D_{ijkl}(\xi)$ can be factored into

$$D_{ijkl}(\xi) = -S_{ijkl}(\xi) - S_{ikjl}(\xi) - S_{iljk}(\xi) + M_{ijkl}(\xi) , \qquad (2.26)$$

where

$$\begin{aligned} S_{ijkl}(\xi) &\equiv \langle (u_i u_j - \tilde{u}_i \tilde{u}_j)(u_k u_l - \tilde{u}_k \tilde{u}_l) \rangle , \qquad (2.27) \\ &= \langle u_i u_j u_k u_l \rangle + \langle \tilde{u}_i \tilde{u}_j \tilde{u}_k \tilde{u}_l \rangle - R_{ijkl}(\xi) - S_{klij}(\xi) , \\ M_{ijkl}(\xi) &\equiv B_{ijkl}(\xi) + B_{jikl}(\xi) + B_{kijl}(\xi) + B_{lijk}(\xi) , \qquad (2.28) \\ B_{ijkl}(\xi) &\equiv \langle (u_i - \tilde{u}_i) u_j u_k u_l \rangle + \langle (\tilde{u}_i - u_i) \tilde{u}_j \tilde{u}_k \tilde{u}_l \rangle . \qquad (2.29) \end{aligned}$$

R_{ijkl} denotes the usual fourth-order velocity product mean value tensor,

$$R_{ijkl}(\xi) = \langle u_i u_j \tilde{u}_k \tilde{u}_l \rangle . \tag{2.30}$$

Taking the fourth-order divergence of (2.26), we find

$$D_{ijkl}(\xi)_{|ijkl} = 6Q(\xi), \tag{2.31}$$

which is valid under homogeneity for $Q(\xi)$defined as

$$\begin{aligned} Q(\xi) &\equiv \left\langle \partial_{ij}\left(u_i u_j\right) \tilde{\partial}_{kl}\left(\tilde{u}_k \tilde{u}_l\right) \right\rangle, \\ &= \left\langle \partial_j u_i \partial_i u_j \tilde{\partial}_l \tilde{u}_k \tilde{\partial}_k \tilde{u}_l \right\rangle . \end{aligned} \tag{2.32}$$

The right-hand side of (2.31) is related to the pressure structure function through the Navier-Stokes equation and incompressibility. Taking the divergence of the Navier-Stokes equation, we obtain the following relationship between the Laplacian of the pressure and velocity derivatives for an incompressible fluid (cf. [44]),

$$\frac{1}{\rho}\partial_{ii} p = -\partial_{ij}\left(u_i u_j\right), \tag{2.33}$$

where ∂_{ij} denotes differentiation with respect to coordinates x_i and x_j while $\tilde{\mathbf{x}}$ is held fixed, and $\tilde{\partial}_{kl}$ denotes differentiation with respect to coordinates $\tilde{x}_k$ and $\tilde{x}_l$ while $\mathbf{x}$ is held fixed. Applying (2.33) at two points in space separated by a vector ξ, and imposing homogeneity, Obukhov [53] and Obukhov and Yaglom [48] obtained

$$\partial_{ii}\tilde{\partial}_{kk} D_P(\xi) = D_P(\xi)_{|iikk} = -2Q(\xi). \tag{2.34}$$

(2.34) was solved for an isotropic field by Obukhov and independently by Batchelor [44] for the pressure correlation. They found

$$D_P(\xi) = \frac{1}{3\xi}\int_0^{\xi} \left(y^4 - 3\xi y^3 + 3\xi^2 y^2\right) Q(y)\, dy + \frac{\xi^2}{3}\int_{\xi}^{\infty} yQ(y)\, dy. \tag{2.35}$$

(2.31) provides a direct relationship between the fourth-order divergence of the fourth-order structure function tensor and the function $Q(\xi)$. Knowledge of $Q(\xi)$ allows us to solve the above equation for the pressure structure function. Introducing a Cartesian coordinate system (our preferred coordinate system) with unit vectors (e_1, e_2, e_3) and the separation vector colinear with the 3-axis, Hill [49] derived the fourth-order divergence of $D_{ijkl}(\xi)$,

$$\begin{aligned} D_{ijkl}(\xi)_{|ijkl} &= D^{(4)}_{3333}(\xi) + \frac{8}{\xi} D^{(3)}_{3333}(\xi) + \frac{12}{\xi^2} D^{(2)}_{3333}(\xi) - \\ &\quad \frac{12}{\xi} D^{(3)}_{33\gamma\gamma}(\xi) - \frac{60}{\xi^2} D^{(2)}_{33\gamma\gamma}(\xi) - \frac{24}{\xi^3} D^{(1)}_{33\gamma\gamma}(\xi) + \\ &\quad \frac{24}{\xi^4} D_{33\gamma\gamma}(\xi) + \frac{8}{\xi^2} D^{(2)}_{\lambda\lambda\lambda\lambda}(\xi) + \frac{8}{\xi^3} D^{(1)}_{\lambda\lambda\lambda\lambda}(\xi) - \\ &\quad \frac{8}{\xi^4} D_{\lambda\lambda\lambda\lambda}(\xi), \end{aligned} \tag{2.36}$$

where λ and γ are either 1 or 2. By isotropy, λ and γ can be the same or different. In equation (2.36), the order of differentiation is denoted by the superscripts in parentheses. Integrating by parts they obtained an integral equation for $D_P(\xi)$,

$$\begin{aligned} D_P(\xi) &= -\frac{1}{3} D_{3333}(\xi) \\ &\quad + \frac{4}{3}\xi^2 \int_\xi^\infty y^{-3} \left[D_{3333}(y) + D_{\lambda\lambda\lambda\lambda}(y) - 6 D_{33\gamma\gamma}(y) \right] dy \\ &\quad + \frac{4}{3} \int_0^\xi y^{-1} \left[D_{3333}(y) - 3 D_{33\gamma\gamma}(y) \right] dy. \end{aligned} \tag{2.37}$$

2.2.3 A mathematical model for pressure statistics for a field of stochastically independent vortices

An alternative to relating pressure statistics to velocity statistics is to directly calculate the statistical quantities using the model pressure field. Let $p(\alpha_m)$ and $\tilde{p}(\alpha_m)$ be the contributions of vortex m to the pressure at points $\mathbf{x}$ and $\mathbf{x}+\xi$ respectively. Our model for the turbulent pressure field is based on the assumption that the vortices present make additive contributions to the pressure at a given point. However, the

pressure field resulting from an additive velocity field is determined in part by the non-linearities of the Navier-Stokes equation, and is therefore, generally, non-additive. However, we propose strictly as a model,

$$p(\mathbf{x}) = \sum_{m=1}^{N} p(\alpha_m), \qquad p(\mathbf{x}+\xi) = \sum_{m=1}^{N} \tilde{p}(\alpha_m), \tag{2.38}$$

$$\langle p(\mathbf{x}) p(\mathbf{x}+\xi) \rangle = \sum_{m,n} \langle p_m \tilde{p}_n \rangle . \tag{2.39}$$

Under the assumption that the N vortices are statistically independent, we have

$$\langle p_m \tilde{p}_m \rangle = \int p(\alpha_m)\, \tilde{p}(\alpha_m)\, \Psi(\alpha_m)\, d\alpha_m \qquad m = n, \tag{2.40}$$

$$\langle p_m \tilde{p}_n \rangle = \int p(\alpha_m)\, \Psi(\alpha_m)\, d\alpha_m \int \tilde{p}(\alpha_n)\, \Psi(\alpha_n)\, d\alpha_n \qquad m \neq n. \tag{2.41}$$

Therefore,

$$\begin{aligned} \langle p(\mathbf{x}) p(\mathbf{x}+\xi) \rangle &= \sum_{m=1}^{N} \int p(\alpha_m)\, \tilde{p}(\alpha_m)\, \Psi(\alpha_m)\, d\alpha_m + \\ &\quad \sum_{n=1}^{N} \sum_{m=1}^{N} \int p(\alpha_m)\, \Psi(\alpha_m)\, d\alpha_m \int \tilde{p}(\alpha_n)\, \Psi(\alpha_n)\, d\alpha_n - \\ &\quad \sum_{m=1}^{N} \int p(\alpha_m)\, \Psi(\alpha_m)\, d\alpha_m \int \tilde{p}(\alpha_m)\, \Psi(\alpha_m)\, d\alpha_m, \\ &= N(N-1) \langle p_m \rangle^2 + N \langle p_m \tilde{p}_m \rangle . \end{aligned} \tag{2.42}$$

The two point pressure correlation $P(\xi)$ depends on the mean pressure as well as the two point average resulting from the presence of a single vortex. By homogeneity, $\langle p_m \rangle = \langle \tilde{p}_m \rangle$. Its actual value is the result of

$$\langle p_m \rangle = \frac{1}{4\pi V} \int \zeta(U, a)\, da \int d\Omega \int d\mathbf{x}\; p(\mathbf{x}, \Omega, U, a) . \tag{2.43}$$

The second order pressure structure function is immediately derivable from the

two-point correlation,

$$D_p(\xi) = 2\left\langle p^2 \right\rangle [1 - h(\xi)], \tag{2.44}$$

where $\langle p^2 \rangle$ is the mean-square pressure and $h(\xi)$ is the pressure correlation function defined by

$$P(\xi) = \left\langle p^2 \right\rangle h(\xi). \tag{2.45}$$

Chapter 3 Hill's spherical vortex

3.1 Equations of motion

Hill's spherical vortex defines an ideal flow in which rotational fluid is confined within a sphere translating with constant velocity through a region of potential flow. The spherical vortex provides us with a steady rotational solution to Euler's equation for incompressible, inviscid fluid flow. The entire flow field is symmetrical about the line of vortex advancement and characterized by the simple vorticity distribution, $\omega = (0, \omega_\phi, 0)$, where

$$\omega_\phi = \begin{cases} AR & (R^2 + z^2 < a^2) \\ 0 & (R^2 + z^2 > a^2)\,. \end{cases} \tag{3.1}$$

Here (R, ϕ, z) refer to cylindrical polar coordinates in which the z-axis lies along the axis of symmetry. Hill [54] defines the whole motion by the following velocity and pressure fields.

$$v_R = \begin{cases} 3UR\frac{(z-Z)}{(2a^2)} & (r \le a) \\ 3a^3UR\frac{(z-Z)}{(2r^5)} & (r \ge a) \end{cases}, \tag{3.2}$$

$$v_z = \begin{cases} U\frac{5a^2-3(z-Z)^2-6R^2}{2a^2} & (r \le a) \\ a^3U\frac{3(z-Z)^2-r^2}{2r^5} & (r \ge a) \end{cases}, \tag{3.3}$$

$$\frac{p}{\rho} + \mathcal{V} - \frac{\Pi}{\rho} = \begin{cases} \frac{9U^2}{8a^4}\left[\begin{array}{l} \left(R^2 - \frac{1}{2}a^2\right)^2 + a^4 - \\ \left((z-Z)^2 - a^2\right)^2 \end{array}\right] & (r \le a) \\ \frac{U^2}{8}\left[\begin{array}{l} \frac{9}{4} + \left(5 - 4\left(\frac{a}{R}\right)^3 - \left(\frac{a}{R}\right)^6\right) + \\ 3\cos^2\theta\left(4\left(\frac{a}{R}\right)^3 - \left(\frac{a}{R}\right)^6\right) \end{array}\right] & (r \ge a)\,. \end{cases} \tag{3.4}$$

The vortex motion is along the $z-$axis; its actual position given by Z. The distance between the $z-$axis and any point is given by the cylindrical coordinate R.

Furthermore, θ and r are defined so that

$$R = r\sin\theta, \tag{3.5}$$

$$z - Z = r\cos\theta. \tag{3.6}$$

The entire flow is fixed by the constants, U, a, and Π. The pair (U, a) define the vortex type where U is its speed and a its radius. Π is the minimum value of $\frac{P}{\rho} + \mathcal{V}$, where $\mathcal{V}$ is the potential of the impressed forces. The component of $\mathbf{r}$ along the direction of advancement is $r\cos\theta$. We introduce l^i $(i = 1, 2, 3)$ as the direction cosines of the direction of advancement referred to an arbitrary set of axes,

$$l_1 = \sin\theta\cos\varphi, \tag{3.7}$$

$$l_2 = \sin\theta\sin\varphi, \tag{3.8}$$

$$l_3 = \cos\theta. \tag{3.9}$$

We can replace R by $r(1-\cos^2\theta)^{\frac{1}{2}}$ and $\cos\theta$ by $(r_i l^i)/|r|$. After careful algebra, the velocity and pressure fields can be recast in the following form more convenient to the calculation of averages:

$$u_i = \alpha_{ij} l^j \qquad \alpha_{ij} = \frac{3Ua^3 r_i r_j}{2r^5} - \frac{Ua^3\delta_{ij}}{2r^3} \qquad (r \geq a), \tag{3.10}$$

$$u_i = \beta_{ij} l^j \quad \beta_{ij} = \frac{3Ur_i r_j}{2a^2} + U\left(\frac{5}{2} - \frac{3r^2}{a^2}\right)\delta_{ij} \quad (r \leq a), \tag{3.11}$$

$$p + \Pi = \frac{9\rho U^2}{8a^4}\left\{ \begin{array}{c} \left[r^2 - \frac{1}{2}a^2 - (r_i l^i)^2\right]^2 - \\ \left[(r_i l^i)^2 - a^2\right]^2 + a^4 \end{array} \right\} \quad (r \leq a), \tag{3.12}$$

$$p + \Pi = \frac{\rho U^2}{8}\left\{ \begin{array}{c} \frac{29}{4} - 4\left(\frac{a}{r}\right)^3 - \left(\frac{a}{r}\right)^6 + \\ 3\left[4\left(\frac{a}{r}\right)^3 - \left(\frac{a}{r}\right)^6\right]\frac{(r_i l^i)^2}{r^2} \end{array} \right\} \quad (r \geq a). \tag{3.13}$$

The tensors α_{ij} and β_{ij} are clearly symmetrical and it follows from continuity that

they are divergence free with respect to either index,

$$\frac{\partial \alpha_{ij}}{\partial x_i} = 0 \quad \frac{\partial \alpha_{ij}}{\partial x_j} = 0 \quad \frac{\partial \beta_{ij}}{\partial x_i} = 0 \quad \frac{\partial \beta_{ij}}{\partial x_j} = 0. \tag{3.14}$$

Furthermore,

$$\alpha_{ij} = \frac{\partial \varphi_i}{\partial x_j} = \frac{\partial \varphi_j}{\partial x_i} = \alpha_{ji} \quad \text{where } \varphi_i = \frac{1}{2} U a^3 \left(\frac{-r_i}{r^3} \right). \tag{3.15}$$

Note that except for derivative operators, there is an implied sum only over repeated indices at different levels.

3.2 Statistical equations for the spherical vortex

Using Hill's spherical vortex, turbulent properties can be calculated by explicit ensemble averaging. We derive the governing integral equations for the velocity structure functions, orders two through six, and the pressure correlation. Explicit calculation of the statistical quantities will be provided in subsequent chapters.

One of the significant features of the spherical vortex is that the velocity field is proportional to the direction cosines. This ensures that the mean is zero and greatly simplifies the average over orientation. The spatial dependence of $\mathbf{u}$ can be removed from the two-dimensional integral over the Euler angles which then reduces to averaging a rank-p tensor of direction cosines. Let $\overline{B}^{\Omega}$ denote the average of field property $B(\theta, \varphi)$ over orientation. The general expression for $\overline{B}^{\Omega}$ is given by the spherical-polar integral,

$$\overline{B}^{\Omega} = \int_0^{2\pi} d\varphi \int_0^{\pi} d\theta \sin\theta \; B(\theta, \varphi). \tag{3.16}$$

For B equal to a product of direction cosines, the following relations will prove useful:

$$\overline{l_i}^{\Omega} = 0, \tag{3.17}$$

$$\overline{l_i l_j}^{\Omega} = \frac{1}{3}\delta_{ij}, \tag{3.18}$$

$$\overline{l_i l_j l_k}^{\Omega} = 0, \tag{3.19}$$

$$\overline{l_i l_j l_k l_m}^{\Omega} = \frac{1}{15}\left(\delta_{ij}\delta_{km} + \delta_{ik}\delta_{jm} + \delta_{im}\delta_{jk}\right), \qquad \text{etc.} \tag{3.20}$$

It is immediately evident that the high degree of symmetry of the spherical vortex ensures all odd order correlations vanish. This contradicts experimental evidence that the third order correlation is non-zero. However, since the spherical vortex model is a local solution to the steady Euler's equation ($\partial_t = 0, \nu = 0$), the Kármán-Howarth equation (1.32) is not violated. As noted by Synge and Lin [20], a more realistic model might include terms quadratic in the direction cosines, so that odd order correlations would not vanish in general.

The second order velocity structure function, D_{ij}, assumes a particularly simple form. Since the mean value is zero, the cross terms in the expansion of equation (2.18) for $p = 2$ vanish leaving the sum of N identical integrals. Furthermore, isotropy ensures $D_{ij} = D_{ij}\delta_{ij}$. Hence,

$$D_{ii} = N \int \Psi^{(k)}\left(\alpha_k\right)\left(\tilde{u}_i\left(\alpha_k\right) - u_i\left(\alpha_k\right)\right)^2 d\alpha_k, \tag{3.21}$$

where $i = \xi, \gamma$, or λ. The script k denotes a typical vortex. For $p = 4, 6, 8...$ cross terms of even powers remain. Referring to our preferred coordinate system, fourth order isotropic tensor of the form (2.13) can be fully specified by three independent scalar functions [40]. For the fourth-order velocity structure function, these are the longitudinal structure function $D_{\xi\xi\xi\xi}$, the lateral structure function $D_{\gamma\gamma\gamma\gamma}$, and the

cross structure function $D_{\xi\xi\gamma\gamma}$, defined respectively by

$$D_{iiii} = \int ... \int \Psi^{(1)}(\alpha_1) ... \Psi^{(N)}(\alpha_N) \times \left[\sum_{k=1}^{N} \left(\widetilde{u}_i(\alpha_k) - u_i(\alpha_k) \right) \right]^4 d\alpha_1 ... d\alpha_N, \tag{3.22}$$

with $i = \xi$ or γ, and

$$D_{\xi\xi\gamma\gamma} = \int ... \int \Psi^{(1)}(\alpha_1) ... \Psi^{(N)}(\alpha_N) \times \left[\sum_{k=1}^{N} \left(\widetilde{u}_\xi(\alpha_k) - u_\xi(\alpha_k) \right) \right]^2 \left[\sum_{k=1}^{N} \left(\widetilde{u}_\gamma(\alpha_k) - u_\gamma(\alpha_k) \right) \right]^2 d\alpha_1 ... d\alpha_N. \tag{3.23}$$

Expanding, and appealing to isotropy and symmetry of the spherical vortex, we find

$$D_{iiii} = N \int \Psi^{(k)}(\alpha_k) \left(\widetilde{u}_i(\alpha_k) - u_i(\alpha_k) \right)^4 d\alpha_k + 3N(N-1) \frac{D_{ii}^2}{N^2}, \tag{3.24}$$

where $i = \xi$ or γ, and

$$D_{\xi\xi\gamma\gamma} = N \int \Psi^{(k)}(\alpha_k) \left(\widetilde{u}_\xi(\alpha_k) - u_\xi(\alpha_k) \right)^2 \left(\widetilde{u}_\gamma(\alpha_k) - u_\gamma(\alpha_k) \right)^2 d\alpha_k + N(N-1) \frac{D_{\xi\xi} D_{\gamma\gamma}}{N^2} + 2N(N-1) \frac{D_{\xi\gamma}^2}{N^2}. \tag{3.25}$$

Isotropy ensures $D_{\xi\gamma}$ is zero. However, it has been retained in the above equation so that equation (3.25) agrees with equation (3.24) for the lateral component $D_{\xi\xi\xi\xi}$ upon contracting the indices, ξ and γ as required. The spherical vortex model will also be used to predict the lateral component of the sixth order structure function tensor,

$$D_{\xi\xi\xi\xi\xi\xi} = N \int \Psi^{(k)}(\alpha_k) \left(\widetilde{u}_\xi(\alpha_k) - u_\xi(\alpha_k) \right)^6 d\alpha_k + 15N(N-1) \frac{D_{\xi\xi} D_{\xi\xi\xi\xi}}{N^2}. \tag{3.26}$$

Since the symmetry in the Hill's spherical vortex causes the odd order structure

functions to vanish, terms in the above expansions involving D_{ijk} and D_{ijklm} are zero.

Chapter 4 Second order statistics for the velocity and pressure field

4.1 The second order velocity structure function

The two non-zero second order structure functions $D_{\xi\xi}$ and $D_{\gamma\gamma}$ are related through equation (1.26) by the following equations obtained by expanding $(\tilde{u}_i - u_i)^2$, imposing isotropy and then averaging:

$$D_{\xi\xi}(\xi) = 2\left\langle u^2 \right\rangle [1 - f(\xi)], \tag{4.1}$$

$$D_{\gamma\gamma}(\xi) = 2\left\langle u^2 \right\rangle [1 - g(\xi)]. \tag{4.2}$$

We will calculate the two quantities independently for the spherical vortex model and use these relationships and equation (1.26) to verify our final results. We begin by decomposing the distribution function as in equation (2.4) and impose homogeneity and isotropy on $\mu(l_i)$ and $\sigma(\mathbf{x}_i)$. We find that the second order structure function is given by

$$D_{ii} = \frac{n}{4\pi} \int d\mathbf{x} \int d\Omega (\tilde{u}_i - u_i)^2, \tag{4.3}$$

where the dependence of u_i and $\tilde{u}_i$ on a single vortex characterized by the vector α_k is understood. We are momentarily disregarding the distribution in type and have introduced n as the vortex number density, N/V. The longitudinal structure function is given by the second moment of the increments Δu_ξ, defined by (4.3) for $i = \xi$, and the lateral structure function is given by the second moment of the increments Δu_γ,

defined by (4.3) for $i = \gamma$. Let $\tilde{u}_i = \tilde{c}_{ij} l^j$, where

$$\tilde{c}_{ij} = \begin{cases} \tilde{\alpha}_{ij} & \tilde{r} \geq a \\ \tilde{\beta}_{ij} & \tilde{r} \leq a \end{cases} \tag{4.4}$$

and $u_i = c_{ij} l^j$, where

$$c_{ij} = \begin{cases} \alpha_{ij} & r \geq a \\ \beta_{ij} & r \leq a. \end{cases} \tag{4.5}$$

Substituting into (4.3) we find

$$D_{ii} = \int d\mathbf{x} \int d\Omega [(\tilde{c}_{ij} - c_{ij}) l^j]^2. \tag{4.6}$$

Let A_o denote the point at position $\mathbf{x}$, and $\tilde{A}_o$ denote the point at position $\mathbf{x} + \xi$. In general two-point correlations involve moving the separation vector through all of space and allowing it to take on all orientations. Mathematically, this is equivalent to holding points, A_o and $\tilde{A}_o$, fixed, and rotating a single vortex through its Euler angles, and allowing it take on all positions in space. Upon expanding the integrand, and averaging with respect to direction, i.e., $\overline{l^i l^j} = \frac{1}{3}\delta_{ij}$, the second order structure function becomes

$$D_{ii} = \frac{n}{3} \int (c_{ij} c_i^j - 2 c_{ij} \tilde{c}_i^j + \tilde{c}_{ij} \tilde{c}_i^j) d\mathbf{x}. \tag{4.7}$$

As the vortex is moved through space, the velocity at point A_o is fixed by the tensor α_{ij} or β_{ij} depending on the distance between the vortex center and A_o. The same is true for the velocity at point $\tilde{A}_o$. Since the formal expressions for the velocity field are different depending on the vortex position, integrating over the volume requires partitioning the domain of integration into three regions when $\xi > 2a$ and four regions when $\xi < 2a$, figures (4.1) and (4.2).

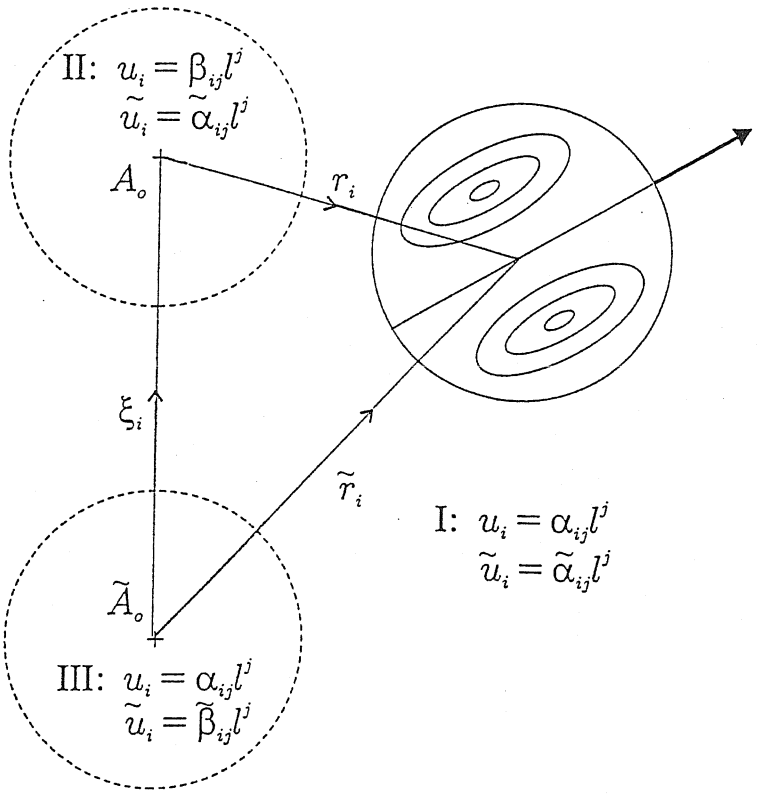

Figure 4.1: Case 1: When the vortex diameter is less than the distance between points A_o and $\tilde{A}_o$ the volume can be partitioned into three distinct regions depending on the relative position of the vortex and the two points.

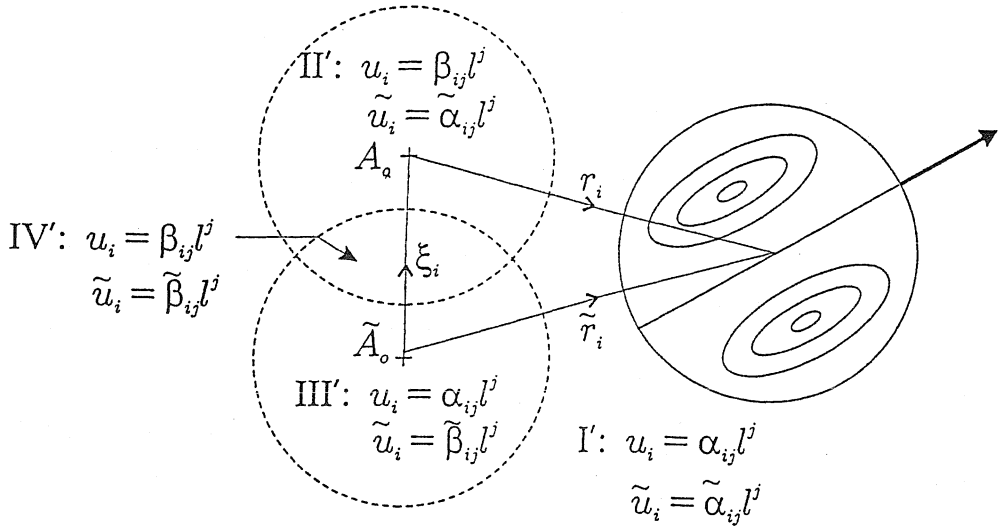

Figure 4.2: Case 2: When the vortex diameter exceeds the separation distance there is a region in which rotational flow is induced at both points A_o and $\tilde{A}_o$. In this case there are four distinct regions to be considered.

4.1.1 Case 1: $\xi \geq 2a$

When the magnitude of the separation vector exceeds the vortex diameter, there are three distinct regions. In region I, both points, A_o and $\tilde{A}_o$, are secluded from rotational flow, while in regions II and III one point is in the interior of the spherical vortex, while the other point is outside the vortex within the potential flow region. Specifically,

$$\begin{aligned} D_{ii}(\xi) &= \frac{n}{3}\left\{\int_I (\tilde{\alpha}_{ij}\tilde{\alpha}_i^j - 2\tilde{\alpha}_{ij}\alpha_i^j + \alpha_{ij}\alpha_i^j)d\mathbf{x} \right. && (4.8)\\ &+ \int_{II} (\tilde{\alpha}_{ij}\tilde{\alpha}_i^j - 2\tilde{\alpha}_{ij}\beta_i^j + \beta_{ij}\beta_i^j)d\mathbf{x} && (4.9)\\ &+ \left.\int_{III} (\tilde{\beta}_{ij}\tilde{\beta}_i^j - 2\tilde{\beta}_{ij}\alpha_i^j + \alpha_{ij}\alpha_i^j)d\mathbf{x}\right\}. && (4.10) \end{aligned}$$

Using the fact that $\alpha_{ij} = \frac{\partial \varphi_i}{\partial x_j}$, and appealing to continuity, we can rewrite our integral as

$$\begin{aligned} D_{ii}(\xi) &= \frac{n}{3}\left\{\int_I \frac{\partial}{\partial x_j}(\tilde{\alpha}_i^j\tilde{\varphi}_i - 2\tilde{\alpha}_i^j\varphi_i + \alpha_i^j\varphi_i)d\mathbf{x} \right. && (4.11)\\ &+ \int_{II}[\frac{\partial}{\partial x_j}(\tilde{\alpha}_i^j\tilde{\varphi}_i - 2\beta_i^j\tilde{\varphi}_i) + \beta_{ij}\beta_i^j]d\mathbf{x} \\ &+ \left.\int_{III}[\tilde{\beta}_i^j\tilde{\beta}_{ij} + \frac{\partial}{\partial x}(\alpha_i^j\varphi_i - 2\tilde{\beta}_i^j\varphi_i)]d\mathbf{x}.\right. \end{aligned}$$

With the aid of Green's theorem, some of the terms in the above integrals transform into surface integrals over Σ_{II}, Σ_{III} and an infinite sphere. The integral over the infinite sphere vanishes since the velocity is zero at infinity. Using the fact that $\alpha_{ij} = \beta_{ij}$ on Σ_{II} and $\tilde{\alpha}_{ij} = \tilde{\beta}_{ij}$ on Σ_{III}, we find

$$\begin{aligned} D_{ii}(\xi) &= \frac{n}{3}\left\{\int_{\Sigma_{II}} (2\tilde{\alpha}_i^j\varphi_i - \alpha_i^j\varphi_i - 2\beta_i^j\tilde{\varphi}_i)n_j d\sigma - \int_{\Sigma_{III}} \tilde{\alpha}_i^j\tilde{\varphi}_i n_j d\,\tilde{\sigma}\right. \\ &+ \left.\int_{II}\beta_{ij}\beta_i^j d\tau + \int_{III}\tilde{\beta}_{ij}\tilde{\beta}_i^j d\tau\right\}. && (4.12) \end{aligned}$$

Thus far it has been convenient to study the problem in Cartesian coordinates. In E(3) the velocity field generated by the vortex is proportional to the direction

cosines of the vortex velocity vector referred to an arbitrary set of coordinate axes. Hence, the average over orientation can be carried out independently of the average over space, and the vanishing of all odd order structure functions is a consequence of averaging over an odd number of direction cosines. In addition Cartesian coordinates facilitate the transformation of some of the volume integrals into surface integrals, a great simplification considering the domain is infinite.

At this point, however, the remaining integration is simplified by changing to toroidal coordinates $(r, \tilde{r}, \varphi)$, figure (4.3). This is a natural coordinate system for studying two-point correlation type problems. Every point, P, in space is specified by the distances, $A_oP, \tilde{A}_oP$, and the polar angle φ. Presently, the integrands are functions of r_i and $\tilde{r}_i$, and the magnitudes r and $\tilde{r}$. Simple geometry enables us to express the components r_i and $\tilde{r}_i$ in terms of $r, \tilde{r}$, and φ. Let T be the transformation that takes $(\mathbf{r},\tilde{\mathbf{r}}) \rightarrow (r,\tilde{r},\varphi)$,

$$T \equiv \begin{cases} r_1 = r\sin\alpha\cos\varphi & = f(r,\ \tilde{r})\cos\varphi \\ r_2 = r\sin\alpha\sin\varphi & = f(r,\ \tilde{r})\sin\varphi \\ r_3 = r\cos\alpha & = \frac{\tilde{r}^2-r^2-\xi^2}{2\xi} \\ \tilde{r}_1 = \tilde{r}\sin\beta\cos\varphi & = f(r,\ \tilde{r})\cos\varphi \\ \tilde{r}_2 = \tilde{r}\sin\beta\sin\varphi & = f(r,\ \tilde{r})\sin\varphi \\ \tilde{r}_3 = \tilde{r}\cos\beta & = \frac{\tilde{r}^2-r^2+\xi^2}{2\xi} \end{cases} \tag{4.13}$$

where

$$f(r,\tilde{r}) = \left(\frac{r^2+\tilde{r}^2}{2} - \frac{(\tilde{r}^2-r^2)^2}{4\xi^2} - \frac{\xi^2}{4}\right)^{\frac{1}{2}}. \tag{4.14}$$

Let $\alpha_{ij} \xrightarrow{T} \Lambda_{ij}$, $\beta_{ij} \xrightarrow{T} \Theta_{ij}$, $\varphi_{ij} \xrightarrow{T} \Phi_{ij}$, and $n_j \xrightarrow{T} \nu_j$. As detailed in appendix A, the measure of volume integration in the chosen coordinate system is given by

$$dV = \frac{r\tilde{r}dr d\tilde{r} d\phi}{\xi}. \tag{4.15}$$

Switching to toroidal coordinates facilitates the definition of the various regions of

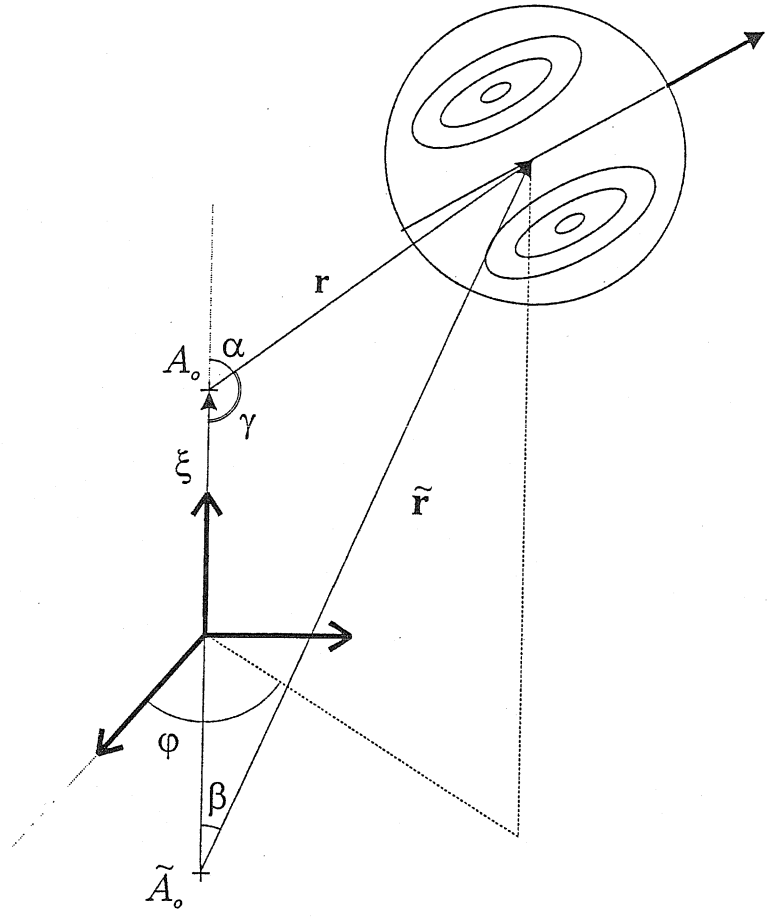

Figure 4.3: The toroidal coordinate system. Each point in space is specified by $r = \|\mathbf{r}\|$, $\tilde{r} = \|\tilde{\mathbf{r}}\|$ and the polar angle φ.

integration, figure (4.4). Surfaces, Σ_{II}, and Σ_{III} are defined by surfaces of constant r, and $\tilde{r}$ respectively. By symmetry, the two volume integrals in equation (4.12) are equivalent. Under the coordinate transformation $D_{ii}(\xi)$ becomes

$$\begin{aligned} D_{ii}(\xi) &= \frac{n}{3}\left\{\int_0^{2\pi} d\phi \int_{\xi-a}^{\xi+a} d\tilde{r}\frac{a\tilde{r}}{\xi}(2\tilde{\Lambda}_i^j\Phi_i - \Lambda_i^j\Phi_i - 2\Theta_i^j\tilde{\Phi}_i)\nu_j \right. \\ &\quad - \int_0^{2\pi} d\phi \int_{\xi-a}^{\xi+a} dr\frac{ar}{\xi}\,\tilde{\Lambda}_i^j\tilde{\Phi}_i\tilde{\nu}_j \qquad (4.16) \\ &\quad \left. + 2\int_0^{2\pi} d\phi \int_0^{a} dr \int_{\xi-a}^{\xi+a} d\tilde{r}\,\frac{r\tilde{r}}{\xi}\Theta_{ij}\Theta_i^j\right\}. \qquad (4.17) \end{aligned}$$

The coordinate system has been oriented so that $\hat{e}_3$ lies along the direction of the vector ξ ($\hat{e}_3 = \hat{e}_\xi$). Therefore, $D_{\xi\xi}$ corresponds to $i = 3$, and $D_{\gamma\gamma}$ corresponds to $i = 2$. Upon representing the integrand in toroidal coordinates, and performing the above integration, we find

$$D_{\xi\xi}(\xi) = \tfrac{4}{21}na^3\pi U^2\left(10 - 7\left(\tfrac{a}{\xi}\right)^3\right) \quad \xi \geq 2a, \qquad (4.18)$$

$$D_{\gamma\gamma}(\xi) = \tfrac{2}{21}na^3\pi U^2\left(20 + 7\left(\tfrac{a}{\xi}\right)^3\right) \quad \xi \geq 2a. \qquad (4.19)$$

The mean-square velocity is given by

$$\langle u^2\rangle = \frac{1}{2}\lim_{\xi\to\infty} D_{\xi\xi}(\xi) = \frac{1}{2}\lim_{\xi\to\infty} D_{\gamma\gamma}(\xi) = \frac{20}{21}na^3\pi U^2. \qquad (4.20)$$

4.1.2 Case 2: $\xi \leq 2a$

When the distance separating the two points is less than the vortex diameter, there is a region in space where the vortex induces rotational flow at both points. Referring

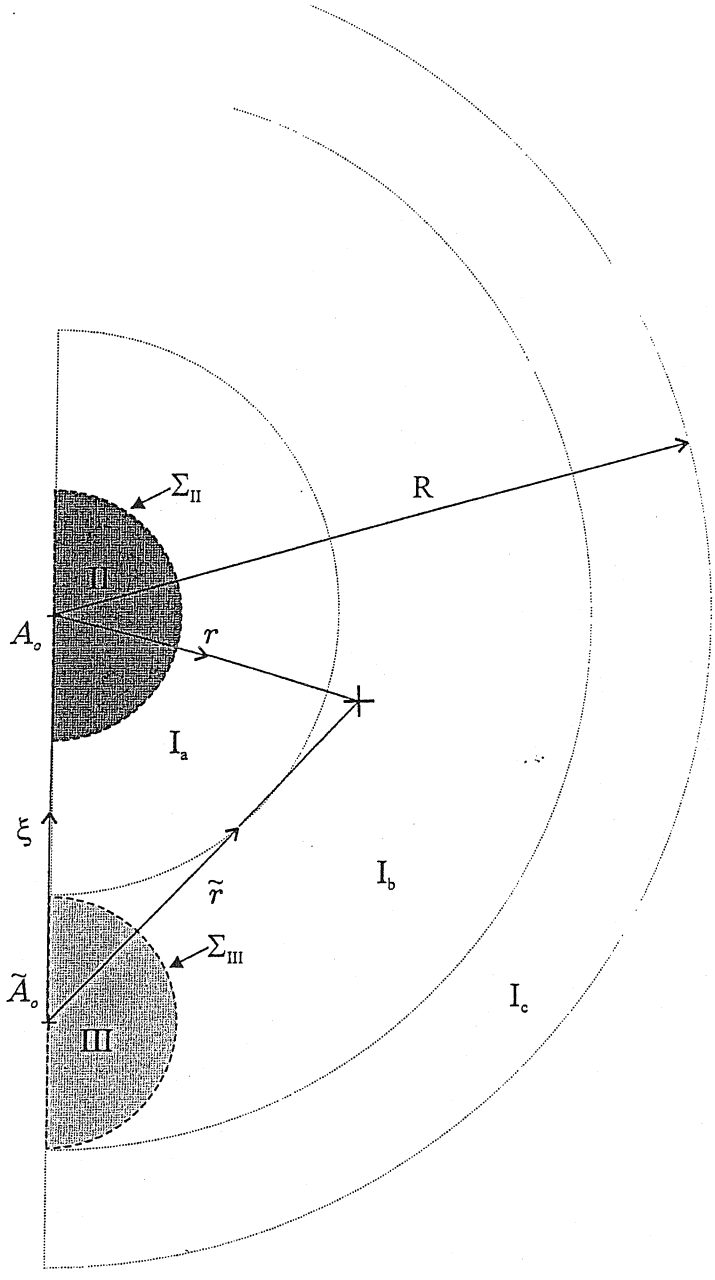

Figure 4.4: Case 1

$$\begin{aligned}\int d\mathbf{x} &= \int_{I_a} d\mathbf{x} + \int_{I_b} d\mathbf{x} + \int_{I_c} d\mathbf{x} + \int_{II} d\mathbf{x} + \int_{III} d\mathbf{x} \\ &= \int_0^{2\pi} d\varphi \left\{ \int_a^{\xi-a} dr \int_{\xi-r}^{\xi+r} d\tilde{r} \frac{r\tilde{r}}{\xi} + \int_{\xi-a}^{\xi+a} dr \int_a^{\xi+r} d\tilde{r} \frac{r\tilde{r}}{\xi} \right. \\ &\quad \left. + \int_{\xi+a}^{\infty} dr \int_{r-\xi}^{\xi+r} d\tilde{r} \frac{r\tilde{r}}{\xi} + \int_0^a dr \int_{\xi-r}^{\xi+r} d\tilde{r} \frac{r\tilde{r}}{\xi} + \int_0^a d\tilde{r} \int_{\xi-\tilde{r}}^{\xi+\tilde{r}} dr \frac{r\tilde{r}}{\xi} \right\}\end{aligned}$$

to figure (4.2),

$$\begin{aligned} D_{ii}(\xi) &= \frac{n}{3}\left\{\int_{I'}(\tilde{\alpha}_{ij}\tilde{\alpha}_i^j - 2\tilde{\alpha}_{ij}\alpha_i^j + \alpha_{ij}\alpha_i^j)d\tau \right. \\ &+ \int_{II'}(\tilde{\alpha}_{ij}\tilde{\alpha}_i^j - 2\tilde{\alpha}_{ij}\beta_i^j + \beta_{ij}\beta_i^j)d\tau \\ &+ \int_{III'}(\tilde{\beta}_{ij}\tilde{\beta}_i^j - 2\tilde{\beta}_{ij}\alpha_i^j + \alpha_{ij}\alpha_i^j)d\tau \\ &\left. + \int_{IV'}(\tilde{\beta}_{ij}\tilde{\beta}_i^j - 2\tilde{\beta}_{ij}\beta_i^j + \beta_{ij}\beta_i^j)d\tau\right\}. \end{aligned} \tag{4.21}$$

Upon introducing the potential φ_i, we can invoke Green's theorem again to simplify the above integral. Appealing to similar symmetry arguments used in case 1, we find

$$\begin{aligned} D_{ii}(\xi) &= \frac{n}{3}\left\{\int_{\Sigma_{II'}}(2\tilde{\alpha}_i^j\varphi_i - \alpha_i^j\varphi_i - 2\beta_i^j\tilde{\varphi}_i)n_j d\sigma \right. \\ &- \int_{\Sigma_{III'}}\tilde{\alpha}_i^j\tilde{\varphi}_i\tilde{n}_j d\tilde{\sigma} + 2\int_{III'}\tilde{\beta}_{ij}\tilde{\beta}_i^j d\tau \\ &+2\int_{IV'}\left(\beta_i^j\beta_{ij} - \tilde{\beta}_i^j\beta_{ij}\right)d\tau \\ &\left. + 2\int_{\Sigma_{IV'a}}\left(2\beta_i^j\tilde{\varphi}_i - \tilde{a}_i^j\tilde{\varphi}_i\right)\tilde{n}_j d\tilde{\sigma}\right\}. \end{aligned} \tag{4.22}$$

Under the transformation T, and referring to figure (4.5),

$$\begin{aligned} D_{ii}(\xi) &= \frac{n}{3}\left\{\int_0^{2\pi}d\varphi\int_a^{\xi+a}d\tilde{r}\frac{a\tilde{r}}{\xi}(2\tilde{\Lambda}_i^j\Phi_i - \Lambda\Phi_i - 2\Theta_i^j\tilde{\Phi}_i)\nu_j \right. \\ &- \int_0^{2\pi}d\varphi\int_a^{\xi+a}d\ r\frac{ar}{\xi}\tilde{\Lambda}_i^j\tilde{\Phi}_i\tilde{\nu}_j + 2\int_0^{2\pi}d\phi\int_a^{\xi+a}dr\int_{\xi-r}^{a}d\tilde{r}\frac{r\tilde{r}}{\xi}\tilde{\Theta}_i^j\tilde{\Theta}_{ij} \\ &+2\int_0^{2\pi}d\varphi\int_{\xi-a}^{a}dr\int_{\xi-r}^{a}d\tilde{r}\frac{r\tilde{r}}{\xi}\left(\Theta_i^j\Theta_{ij} - \tilde{\Theta}_i^j\Theta_{ij}\right) \\ &\left. + 2\int_0^{2\pi}d\varphi\int_{\xi-a}^{a}dr\frac{ar}{\xi}\left(2\Theta_i^j\tilde{\Phi}_i - \tilde{\Lambda}_i^j\tilde{\Phi}_i\right)\tilde{\nu}_j\right\}. \end{aligned} \tag{4.23}$$

Setting $i = 3$, and carrying out the above integration,

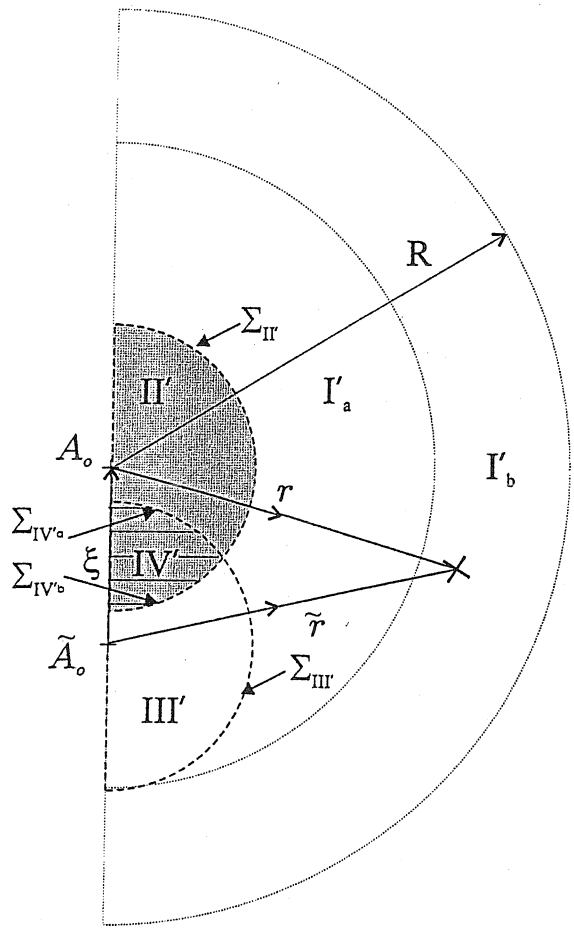

Figure 4.5: Case 2

$$\begin{aligned}\int d\mathbf{x} &= \int_{I'_a} d\mathbf{x} + \int_{I'_b} d\mathbf{x} + + \int_{II'} d\mathbf{x} + \int_{III'} d\mathbf{x} + \int_{IV'} d\mathbf{x} \\ &= \int_0^{2\pi} d\varphi \left\{ \int_a^{\xi+a} dr \int_a^{\xi+r} d\tilde{r} \frac{r\tilde{r}}{\xi} + \int_{\xi+a}^{\infty} dr \int_{r-\xi}^{\xi+r} d\tilde{r} \frac{r\tilde{r}}{\xi} + \int_a^{\xi+a} d\tilde{r} \int_{\xi-\tilde{r}}^{a} dr \frac{r\tilde{r}}{\xi} \right. \\ &\quad \left. + \int_a^{\xi+a} dr \int_{\xi-r}^{a} d\tilde{r} \frac{r\tilde{r}}{\xi} + \int_{\xi-a}^{a} dr \int_{\xi-r}^{a} d\tilde{r} \frac{r\tilde{r}}{\xi} \right\}\end{aligned}$$

$$D_{\xi\xi}(\xi) = \; na^3\pi U^2\left[2\left(\tfrac{\xi}{a}\right)^2 - \tfrac{25}{24}\left(\tfrac{\xi}{a}\right)^3 + \tfrac{5}{64}\left(\tfrac{\xi}{a}\right)^5 - \tfrac{3}{896}\left(\tfrac{\xi}{a}\right)^7\right] \quad (\xi \le 2a)\,. \tag{4.24}$$

For the lateral function, $i = 2$,

$$D_{\gamma\gamma}(\xi) = \; na^3\pi U^2\left[\tfrac{21504}{5376}\left(\tfrac{\xi}{a}\right)^2 - \tfrac{14000}{5376}\left(\tfrac{\xi}{a}\right)^3 + \tfrac{1470}{5376}\left(\tfrac{\xi}{a}\right)^5 - \tfrac{81}{5376}\left(\tfrac{\xi}{a}\right)^7\right] \quad (\xi \le 2a)\,. \tag{4.25}$$

Under the assumption of local isotropy, the second order structure function is related to the longitudinal and transverse velocity correlation coefficients, $f(\xi)$ and $g(\xi)$ by equations (4.1) and (4.2). Solving for $f(\xi)$ and $g(\xi)$, we obtain results consistent with Synge and Lin,

$$f(\xi) = \begin{cases} \tfrac{7}{10}\left(\tfrac{a}{\xi}\right)^3 & (\xi \ge 2a) \\ 1 - \tfrac{21}{20}\left(\tfrac{\xi}{a}\right)^2 + \tfrac{35}{64}\left(\tfrac{\xi}{a}\right)^3 - \tfrac{21}{512}\left(\tfrac{\xi}{a}\right)^5 + \tfrac{9}{5120}\left(\tfrac{\xi}{a}\right)^7 & (\xi \le 2a)\,, \end{cases} \tag{4.26}$$

$$g(\xi) = \begin{cases} -\tfrac{7}{20}\left(\tfrac{a}{\xi}\right)^3 & (\xi \ge 2a) \\ 1 - \tfrac{21}{10}\left(\tfrac{\xi}{a}\right)^2 + \tfrac{175}{128}\left(\tfrac{\xi}{a}\right)^3 - \tfrac{147}{1024}\left(\tfrac{\xi}{a}\right)^5 + \tfrac{81}{10240}\left(\tfrac{\xi}{a}\right)^7 & (\xi \le 2a)\,. \end{cases} \tag{4.27}$$

It should be noted that the results of Synge and Lin contain a slight error in their expression for $g(\xi)$. Their coefficient of $\left(\frac{\xi}{a}\right)^5$ is off by a factor of 2. Knowledge of $f(\xi)$ enables us to compute the Taylor microscale, λ, and the macro length scale, L in terms of the vortex size a,

$$\lambda = \left[-\left(\frac{d^2 f}{d\xi^2}\right)_{\xi=0}\right]^{-\frac{1}{2}} = \sqrt{\frac{10}{21}}a, \tag{4.28}$$

$$L = \int_0^\infty f(\xi)\, d\xi = \frac{35}{32}a. \tag{4.29}$$

Synge and Lin used the statistical model outlined here to compute the second order

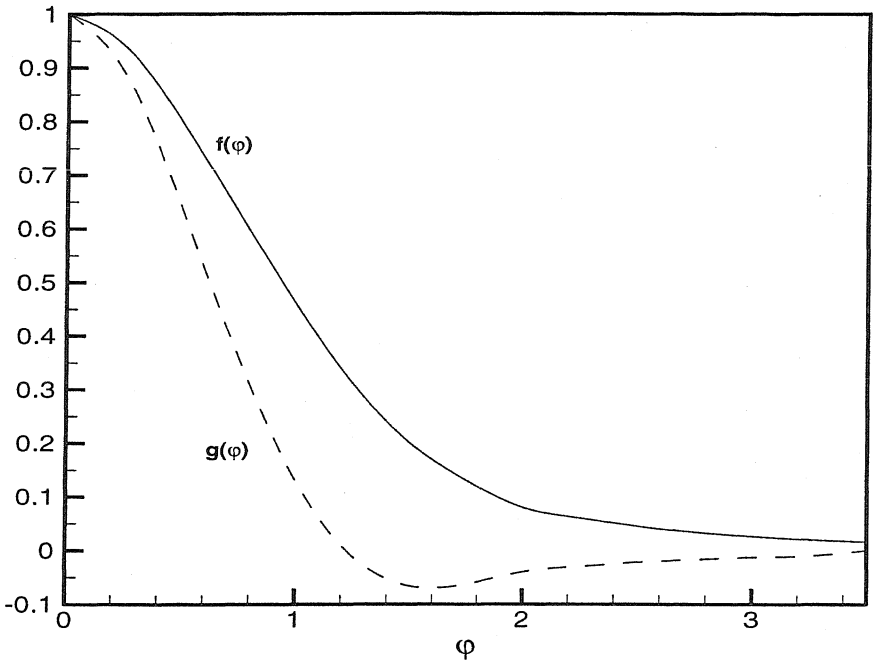

Figure 4.6: Second order longitudinal and lateral correlation functions due to a single vortex type, $\varphi = \xi/a$.

velocity correlation and the turbulent length scales λ and L. They found the shape of the correlation functions to be consistent with experiment. We depart from the statistical model of Synge and Lin and introduce an average over vortex type which is physically motivated by the fractal structure of the energy cascade.

4.2 Average over vortex type

Thus far we have considered a state of homogeneous, isotropic turbulence generated by a field of Hill's vortices of the same type. Turbulent flows, however, interact nonlinearly across a wide range of scales. Since it is likely that the statistics of a turbulent flow are highly influenced by this multitude of length scales, we proceed with an average over vortex type.

We begin by assuming vortex speed remains constant across the observations but that a continuous distribution exists for vortex size. We assume the vortex radii form a set of independent random variables and that the average vortex size at a given point in space is the cumulative effect of all neighboring vortices. Rough use of the Central Limit Theorem would yield an asymptotically normal probability distribution. However, a more physically viable consideration of the vortex type density function would include some type of interdependence between the random variables, a_i, in an attempt to characterize the fractal nature of turbulent flow patterns.

In 1941, Kolmogorov was able to show that a process consisting of a sequence of discrete particle fragmentations yields an asymptotically normal distribution for the logarithm of the particle size. Obukhov and Kolmogorov [12] later used particle fragmentation as a model for eddy breakdown to develop the log-normal hypothesis for the energy dissipation rate, ε (**x**,t). This was eventually formalized by Yaglom [55] in a model for self-similar eddy breakdown. More recently, Bernal [14] investigated the statistics of large scale vortex structure in turbulent mixing layers and deduced that the distribution of vortex circulation is also log-normal. The self similar manner in which scales increase in the turbulent mixing layer can be naively modeled by an inverse fragmentation process. Large scale vortices increase their scale only in

response to discrete amalgamation events. In the mixing layer, the leading approximation for the vortex circulation is proportional to the vortex wavelength, hence, the distributions of vortex scale and circulation are intimately connected. In contrast to the mixing layer, the spherical vortex model is based on an ensemble of independent, i.e., non-interacting vortex spheres. Amalgamation mechanisms are assumed to be extreme, statistically insignificant events. It is reasonable to assume fluctuations in vortex size in such a field are responses to energy dissipation. Hence, appealing to the Yaglom model for self-similar eddy breakdown, we are returned to the natural assumption of a log-normal distribution function for the random variables a_i,

$$\zeta\left(\frac{a}{a_o},\sigma\right) = \begin{cases} \frac{(2\pi)^{-1/2}}{\sigma(a/a_o)} \exp\left[-\frac{1}{2}\left(\frac{\log\left(\frac{a}{a_o}\right)}{\sigma}\right)^2\right] & (a>0) \\ 0 & (a\leq 0)\,. \end{cases} \tag{4.30}$$

The distribution function is expressed in non-dimensional form for convenience. The variance of the distribution, σ, is a dimensionless parameter introduced into the model and a_o is a length scale defined formally by the mean of $\log a$. It should be kept in mind that the assumption of log-normality for ε (**x**,t), and consequently a_i, has significant implications. It models a uni-directional energy transfer for developed turbulence, and in the case of the mixing layer, successive scale amplification. Transfer of energy from small to large scales, and tearing and amalgamation mechanisms, are required to be statistically negligible.

Upon averaging over vortex position and vortex orientation, the second order structure function has the form

$$D_{ii}\left(\frac{\xi}{a}, na^3, U^2\right) = D_{ii,<}\ H\left(2-\frac{\xi}{a}\right) + D_{ii,>}\ H\left(\frac{\xi}{a}-2\right). \tag{4.31}$$

H denotes the usual heaviside function. $D_{ii,<}$ and $D_{ii,>}$ correspond to the second order structure functions for case 2 and case 1 respectively. Recasting D_{ii} in a more

suitable form prior to averaging, we find

$$D_{ii}\left(\frac{\xi}{a_o},\frac{a}{a_o},na_o^3,U^2\right)=\hat{D}_{ii,<}\ H\left(\frac{a}{a_o}-\frac{\xi}{2a_o}\right)+\hat{D}_{ii,>}\ H\left(\frac{\xi}{2a_o}-\frac{a}{a_o}\right). \tag{4.32}$$

Specifically, for the longitudinal and lateral function, we have

$$\begin{aligned}\hat{D}_{\xi\xi,<} &= \pi U^2 na_o^3\left[2\left(\frac{\xi}{a_o}\right)^2\left(\frac{a}{a_o}\right)-\frac{25}{24}\left(\frac{\xi}{a_o}\right)^3+\frac{5}{64}\left(\frac{\xi}{a_o}\right)^5\left(\frac{a_o}{a}\right)^2\right. \qquad (4.33)\\ &\quad \left.-\frac{3}{896}\left(\frac{\xi}{a_o}\right)^7\left(\frac{a_o}{a}\right)^4\right],\\ \hat{D}_{\xi\xi,>} &= \pi U^2 na_o^3\frac{4}{21}\left[10\left(\frac{a}{a_o}\right)^3-7\left(\frac{a_o}{\xi}\right)^3\left(\frac{a}{a_o}\right)^6\right], \qquad (4.34)\end{aligned}$$

and

$$\begin{aligned}\hat{D}_{\gamma\gamma,<} &= \pi U^2 na_o^3\left[4\left(\frac{\xi}{a_o}\right)^2\left(\frac{a}{a_o}\right)-\frac{125}{48}\left(\frac{\xi}{a_o}\right)^3+\frac{35}{128}\left(\frac{\xi}{a_o}\right)^5\left(\frac{a_o}{a}\right)^2\right. \qquad (4.35)\\ &\quad \left.-\frac{27}{1792}\left(\frac{\xi}{a_o}\right)^7\left(\frac{a_o}{a}\right)^4\right],\\ \hat{D}_{\gamma\gamma,>} &= \pi U^2 na_o^3\frac{40}{21}\left[\left(\frac{a}{a_o}\right)^3+\frac{2}{3}\left(\frac{a_o}{\xi}\right)^3\left(\frac{a}{a_o}\right)^6\right]. \qquad (4.36)\end{aligned}$$

The average over vortex size is therefore given by

$$\begin{aligned}\overline{D_{ii}}^a\left(\frac{\xi}{a_o},na_o^3,U^2,\sigma\right) &= \int_0^\infty \zeta\left(\frac{a}{a_o},\sigma\right)\left[\hat{D}_{ii,<}\ H\left(\frac{a}{a_o}-\frac{\xi}{2a_o}\right)\right. \qquad (4.37)\\ &\quad \left.+\hat{D}_{ii,>}\ H\left(\frac{\xi}{2a_o}-\frac{a}{a_o}\right)\right] d\left(\frac{a}{a_o}\right). \qquad (4.38)\end{aligned}$$

Evaluation of the above integral is carried out numerically owing to the complexity of the kernel, $\zeta\left(\frac{a}{a_o},\sigma\right)$. When $\overline{D_{ii}}^a$ is non-dimensionalized by the mean-square velocity, the parameters na_o^3 and U^2 cancel, leaving the variance as the only remaining parameter. As previously stated the value of σ is fixed by comparing the theoretical results to experiment. Data for $D_{\xi\xi}$, $D_{\xi\xi\xi\xi}$, and $D_{\xi\xi\xi\xi\xi\xi}$ versus ξ/λ, where λ is the measured Taylor microscale, is borrowed from the low temperature helium gas

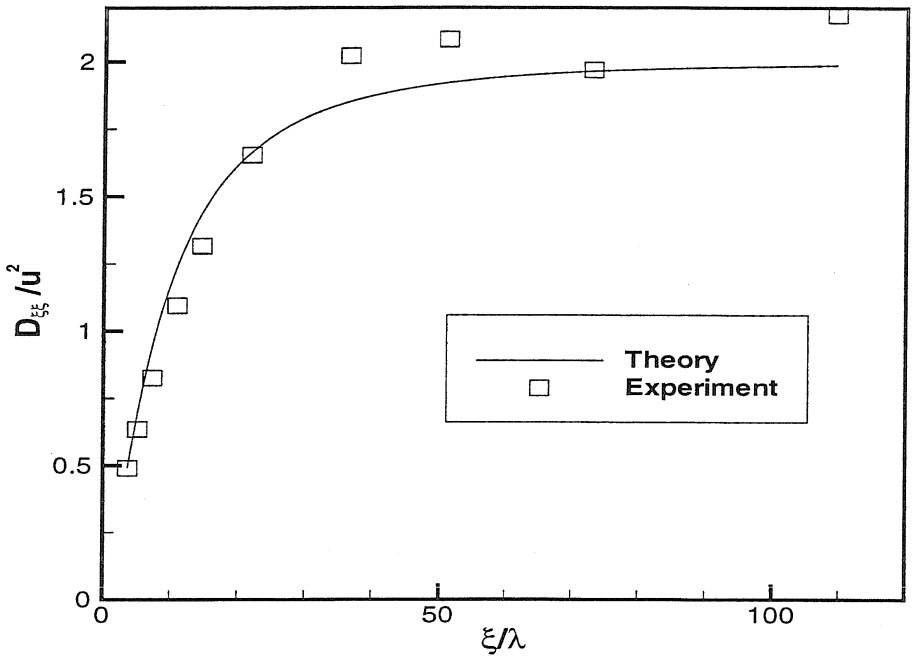

Figure 4.7: Normalized second order longitudinal velocity structure function for the spherical vortex model plotted against the normalized separation. Comparison is being made against the low temperature helium gas experiments of Tabeling et al. [1].

experiments of Tabeling, et al. [1]. To compare the spherical vortex model with experiment, the type averaged Taylor microscale must first be computed so that the ratio of λ/a_o can be obtained and used to rescale the theoretical predictions which are given as functions of ξ/a_o. Upon fixing σ, and averaging over vortex size, we obtain the Taylor micro-scale and the integral length scale in terms of a_o. A satisfactory fit between theory and data for $D_{\xi\xi}$ occurs when $\sigma = 0.85$. The type averaged Taylor and integral scales become

$$\overline{\lambda}^a = \sqrt{\frac{10}{21}} a_o \int_0^\infty \zeta\left(\frac{a}{a_o}, 0.85\right)\left(\frac{a}{a_o}\right) d\left(\frac{a}{a_o}\right) \simeq 0.99 a_o, \tag{4.39}$$

$$\overline{L}^a = \frac{35}{64} a_o \int_0^\infty \zeta\left(\frac{a}{a_o}, 0.85\right)\left(\frac{a}{a_o}\right) d\left(\frac{a}{a_o}\right) \simeq 1.57 a_o. \tag{4.40}$$

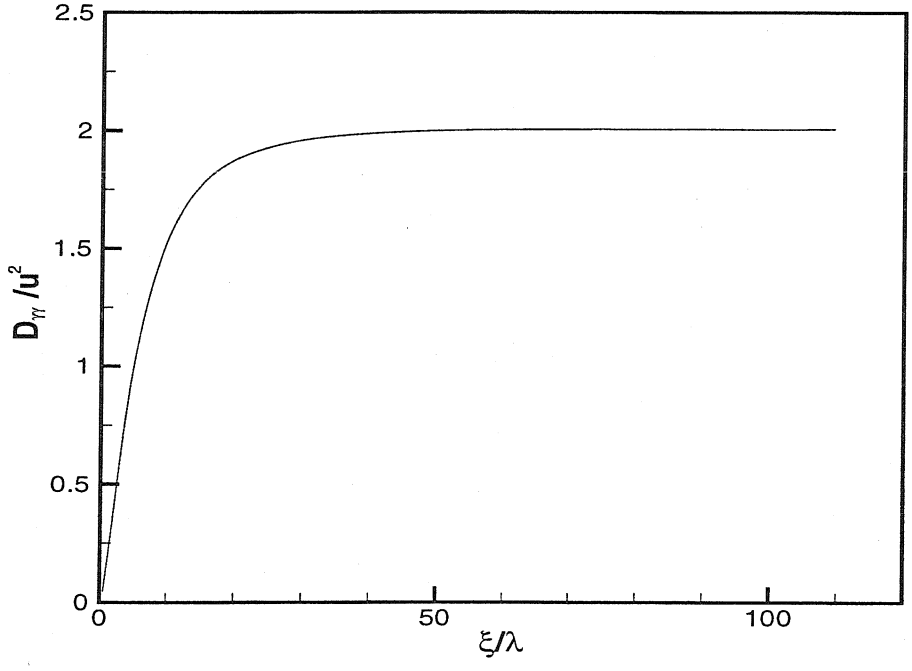

Figure 4.8: Normalized second order transverse velocity structure function for the spherical vortex model plotted against the normalized separation.

We non-dimensionalize the p^{th} order structure function by the mean square velocity (4.20). Averaging over vortex size,

$$\overline{u^2}^a = \frac{20}{21}\pi U^2 n a_o^3 \int_0^\infty \zeta\left(\frac{a}{a_o}, 0.85\right)\left(\frac{a}{a_o}\right)^3 d\left(\frac{a}{a_o}\right) \simeq 24.6 n a_o^3 \pi U^2. \tag{4.41}$$

Hence, the non-dimensional form for the structure function of arbitrary order is given by

$$\frac{\overline{\underbrace{D_{ij\ldots s}}}^a}{\langle u^2\rangle^{\frac{p}{2}}} = C\left(n a_o^3\right)^{1-\frac{p}{2}} fn\left(\frac{\xi}{a_o}\right). \tag{4.42}$$

The remaining parameter, na_o^3, is fixed by fitting results for the fourth-order structure function with experimental data. The sixth-order results are entirely parameter free.

4.3 Dissipation properties

We are interested in a range of scales in which a balance between energy injected to the large scales and viscous dissipation by the small scales has been achieved. The spherical vortex is an exact solution to the Navier-Stokes equation for zero viscosity, so we expect less reliable predictions near the Kolmogorov scale. Although the model is an inviscid one, we can compute an instantaneous energy dissipation at the exact moment viscosity is turned on for the assumed field. The rate of removal of energy is given by

$$\epsilon = 2\nu \int_0^\infty \kappa^2 E(\kappa)\, d\kappa. \tag{4.43}$$

The relation between the dissipation and the Taylor microscale is given by equation (1.33). Substituting the Taylor scale for the spherical vortex model (4.39), the type

averaged energy dissipation is

$$\bar{\epsilon}^a = 89\nu\pi U^2 n a_o. \tag{4.44}$$

The Kolmogorov length scale follows from the energy dissipation,

$$\eta = \left(\frac{\nu^3}{\epsilon}\right)^{\frac{1}{4}} = \nu^{\frac{1}{2}} \left(89\pi U^2 n a_o\right)^{-\frac{1}{4}}. \tag{4.45}$$

4.4 Pressure correlation

Equation (2.42) provides a mathematical model for the explicit calculation of the ensemble average based on the pressure field for Hill's spherical vortex. The pressure correlation depends on the mean pressure as well as the two point correlation due to the presence of a single vortex. We will only consider the behavior of the fluctuating component, $P(\xi) = \frac{N}{\rho^2}\langle p_m \tilde{p}_m \rangle$, which is consistent with the data acquired from simulation and experiment. We will, however, compute the mean pressure for completeness. Because the formal expressions for the pressure field vary depending on radial distance from the vortex center, the domain of spatial integration must be partitioned into two regions to determine the mean pressure, equation (2.43). We introduce R_1 defined by $|r| < a$ and R_2 defined by $|r| \geq a$. Temporarily disregarding the distribution in vortex size,

$$\langle P \rangle = N \langle p_m \rangle = \frac{n}{4\pi} \left\{ \int d\Omega \int_{R_1} d\mathbf{x}\; p_l + \int d\Omega \int_{R2} d\mathbf{x}\; p_g \right\}, \tag{4.46}$$

where p_l refers to the pressure within the sphere, equation (3.12), while p_g refers to the pressure in the potential region, equation (3.13). For incompressible flow we are free to add any constant pressure to the field; therefore, the value of Π in (3.12) and (3.13) is entirely arbitrary. For simplicity, we choose Π so that the pressure is zero at

infinity, i.e.,

$$\Pi = \rho\mathcal{V} - \frac{29}{32}\rho U^2. \tag{4.47}$$

For $u = r^2 - \frac{1}{2}a^2$, $v = -4\left(\frac{a}{r}\right)^3 - \left(\frac{a}{r}\right)^6$, and $w = \frac{3}{r^2}\left[4\left(\frac{a}{r}\right)^3 - \left(\frac{a}{r}\right)^6\right]$,

$$p_l = \frac{9\rho U^2}{8a^4}\left[\frac{-29a^4}{36} + u^2 + 2\left(r_i l^i\right)^2\left(a^2 - u\right)\right], \tag{4.48}$$

$$p_g = \frac{\rho U^2}{8}\left[v + w\left(r_i l^i\right)^2\right]. \tag{4.49}$$

The evaluation of equation (4.46) can be carried out efficiently in spherical polar coordinates. Let S be the transformation that takes $(r_1, r_2, r_3) \rightarrow (r, \theta, \phi)$, and let the direction cosines l^i be functions of the spherical polar coordinates α and β, respectively,

$$S \equiv \begin{cases} r_1 = r\sin\theta\cos\phi \\ r_2 = r\sin\theta\sin\phi \\ r_3 = r\cos\theta \end{cases} \tag{4.50}$$

and

$$l^i \equiv \begin{cases} l^1 = \sin\alpha\cos\beta \\ l^2 = \sin\alpha\sin\beta \\ l^3 = \cos\alpha. \end{cases} \tag{4.51}$$

Let $p_l \xrightarrow{S} \hat{p}_l$, and $p_g \xrightarrow{S} \hat{p}_g$. Explicitly, the mean pressure is given by

$$\langle P\rangle = \frac{n}{4\pi}\left\{\int_0^a dr\ r^2 \int_0^{2\pi} d\phi \int_0^{\pi} d\theta\ \sin\theta \int_0^{2\pi} d\alpha \int_0^{\pi} d\beta\ \sin\beta\ \hat{p}_l \right. \tag{4.52}$$

$$\left. + \int_a^{\infty} dr\ r^2 \int_0^{2\pi} d\phi \int_0^{\pi} d\theta\ \sin\theta \int_0^{2\pi} d\alpha \int_0^{\pi} d\beta\ \sin\beta\ \hat{p}_g \right\}. \tag{4.53}$$

The above integral is straightforward and yields the mean pressure

$$\langle P \rangle = \frac{-20na^3\pi\rho U^2}{21}. \tag{4.54}$$

This is an expected result, as the mean pressure and the mean-square velocity (4.20) are related through Bernoulli's equation. A similar calculation yields the mean-square pressure,

$$P(0) = \frac{1}{\rho^2}\langle p^2 \rangle = \frac{157na^3\pi U^4}{231}. \tag{4.55}$$

To compute the two point pressure correlation due to the presence of a single vortex of size a, we appeal to the same method used to compute the velocity field statistics. Unlike $\mathbf{u}$, the pressure field is not proportional to the direction cosines of the vortex advancement vector. Therefore, the average over orientation cannot be carried out prior to decomposing the domain of spatial integration. We must again distinguish between two cases in the evaluation of $\langle p_m \tilde{p_m} \rangle$ depending on the separation between the two observed points. Representing the average over orientation by $\overline{()}^{\Omega}$, and referring to figures (4.1) and (4.2), we have

$$\langle p_m \tilde{p_m} \rangle = \frac{1}{4\pi V}\left\{ \int_I \overline{p_g \tilde{p_g}}^{\Omega} d\tau + 2\int_{II} \overline{p_l \tilde{p_g}}^{\Omega} d\tau \right\} \qquad \xi \geq 2a, \tag{4.56}$$

$$\begin{aligned} \langle p_m \tilde{p_m} \rangle \;=\; & \frac{1}{4\pi V}\left\{ \int_{I'} \overline{p_g \tilde{p_g}}^{\Omega} d\tau + 2\int_{II'} \overline{p_l \tilde{p_g}}^{\Omega} d\tau \qquad \xi \leq 2a. \right. \\ & \left. + \int_{IV'} \overline{p_l \tilde{p_l}}^{\Omega} d\tau \right\} \end{aligned} \tag{4.57}$$

4.4.1 Case 1: $\xi > 2a$

When the vortex diameter is less than the separation ξ, the spatial domain must be decomposed into three regions. Symmetry allows us to restrict our attention to regions I and II. The exact limits of integration are given in figure (4.4). Let $p_l \xrightarrow{T} \mathcal{P}_l$ and $p_g \xrightarrow{T} \mathcal{P}_g$ where T is the transformation into toroidal coordinates.

Under the transformation the covariance of the fluctuating pressure is given by

$$\begin{aligned}\langle p_m \tilde{p_m} \rangle &= \frac{1}{4\pi V}\left\{2\int_0^{2\pi} d\varphi \int_0^{a} dr \int_{\xi-r}^{\xi+r} d\,\tilde{r}\frac{r\tilde{r}}{\xi}\int_0^{2\pi} d\beta \int_0^{\pi} d\alpha \sin\alpha \mathcal{P}_l \bar{\mathcal{P}}_g \right. \\ &+ \int_0^{2\pi} d\varphi \int_a^{\xi-a} dr \int_{\xi-r}^{\xi+r} d\,\tilde{r}\frac{r\tilde{r}}{\xi}\int_0^{2\pi} d\beta \int_0^{\pi} d\alpha \sin\alpha \mathcal{P}_g \bar{\mathcal{P}}_g \\ &+ \int_0^{2\pi} d\varphi \int_{\xi-a}^{\xi+a} dr \int_{a}^{\xi+r} d\,\tilde{r}\frac{r\tilde{r}}{\xi}\int_0^{2\pi} d\beta \int_0^{\pi} d\alpha \sin\alpha \mathcal{P}_g \bar{\mathcal{P}}_g \\ &+ \left.\int_0^{2\pi} d\varphi \int_{\xi+a}^{\infty} dr \int_{r-\xi}^{\xi+r} d\,\tilde{r}\frac{r\tilde{r}}{\xi}\int_0^{2\pi} d\beta \int_0^{\pi} d\alpha \sin\alpha \mathcal{P}_g \bar{\mathcal{P}}_g \right\}. \end{aligned} \tag{4.58}$$

Upon integrating, we multiply by N, the number of vortices present, and simultaneously pass to the limits $N \to \infty$ and $V \to \infty$. Non-dimensionalizing by the mean square pressure, we obtain the fluctuating component of the pressure covariance,

$$\begin{aligned}\frac{N\langle p_m \tilde{p_m}\rangle_>}{\rho^2 P(0)} &= \frac{K_o}{\varphi^8(\varphi+1)^6(\varphi-1)^8}\sum_{i=0}^{15} C_i \varphi^i \\ &+ \frac{L_o}{\varphi^9}\left(D_1 + D_2\varphi^8 + D_3\varphi^{10}\right)\log\left(\frac{\varphi-1}{\varphi+1}\right), \\ &= g_>(\varphi). \end{aligned} \tag{4.59}$$

We have introduced φ as the ratio of separation to vortex size, ξ/a. The subscript $>$ denotes the case for $\xi \geq 2a$. The coefficients K_o, L_o, D_j $(j = 1, 2, 3)$, and C_i $(i = 0, 1, ...15)$ are provided in table (4.1). As required, in the limit of infinite separation, the covariance goes to zero,

$$\lim_{\varphi\to\infty} \frac{N\langle p_m \tilde{p_m}\rangle_>}{\rho^2 P(0)} = 0. \tag{4.60}$$

4.4.2 Case 2: $\xi \leq 2a$

When the vortex diameter exceeds the distance between the two observed points, there is a region in the domain in which both points are simultaneously included in

Case 1: $\xi \geq 2a$		Case 2: $\xi \leq 2a$	
K_o	$\frac{-77}{25120}$	K'_o	$\frac{3}{803840}$
C_0	2205	C'_0	905520
C_1	11025	C'_1	452760
C_2	20580	C'_2	-150920
C_3	14700	C'_3	75460
C_4	-3969	C'_4	-45276
C_5	-13965	C'_5	30184
C_6	-10416	C'_6	-21560
C_7	-5040	C'_7	16170
C_8	-2887	C'_8	199930
C_9	-2051	C'_9	250288
C_{10}	-810	C'_{10}	-432432
C_{11}	1030	C'_{11}	-375760
C_{12}	2603	C'_{12}	350768
C_{13}	2655	C'_{13}	33528
C_{14}	1350	C'_{14}	-101640
C_{15}	270	C'_{15}	11055
L_0	$\frac{693}{10048}$	C'_{16}	11055
D_1	49	C'_{17}	-924
D_2	-3	C'_{18}	-924
D_3	-6	C'_{19}	36
		C'_{20}	36
		L'_0	$\frac{693}{10048}$
		D'_1	49
		D'_2	-3
		D'_3	-6

Table 4.1: Coefficients for equations (4.59) and (4.62) for the type averaged pressure covariance for the Hill's spherical vortex model.

a region of rotational flow. Referring to figure (4.5),

$$\begin{aligned}\langle p_m \tilde{p_m} \rangle &= \frac{1}{4\pi V}\left\{2\int_0^{2\pi} d\varphi \int_a^{\xi+a} dr \int_{\xi-r}^{a} d\,\tilde{r}\frac{r\tilde{r}}{\xi}\int_0^{2\pi} d\beta \int_0^{\pi} d\alpha \sin\alpha \mathcal{P}_g\,\tilde{\mathcal{P}}_l\right. \\ &+ \int_0^{2\pi} d\varphi \int_{\xi-a}^{a} dr \int_{\xi-r}^{a} d\,\tilde{r}\frac{r\tilde{r}}{\xi}\int_0^{2\pi} d\beta \int_0^{\pi} d\alpha \sin\alpha \mathcal{P}_l\,\tilde{\mathcal{P}}_l \\ &+ \int_0^{2\pi} d\varphi \int_a^{\xi+a} dr \int_a^{\xi+r} d\,\tilde{r}\frac{r\tilde{r}}{\xi}\int_0^{2\pi} d\beta \int_0^{\pi} d\alpha \sin\alpha \mathcal{P}_g\,\tilde{\mathcal{P}}_g \\ &+ \left.\int_0^{2\pi} d\varphi \int_{\xi+a}^{\infty} dr \int_{r-\xi}^{\xi+r} d\,\tilde{r}\frac{r\tilde{r}}{\xi}\int_0^{2\pi} d\beta \int_0^{\pi} d\alpha \sin\alpha \mathcal{P}_g\,\tilde{\mathcal{P}}_g\right\}.\end{aligned} \tag{4.61}$$

Performing the integration and non-dimensionalizing by the mean square pressure, we obtain the following result for the fluctuating component of the pressure covariance,

$$\begin{aligned}\frac{N\langle p_m \tilde{p_m}\rangle_<}{\rho^2 P(0)} &= \frac{K_o'}{\varphi^8(\varphi+1)}\sum_{i=0}^{20} C_i'\varphi^i \\ &+ \frac{L_o'}{\varphi^9}\left(D_1' + D_2'\varphi^8 + D_3'\varphi^{10}\right)\log\left(\frac{1}{\varphi+1}\right), \\ &= g_<(\varphi).\end{aligned} \tag{4.62}$$

The subscript $<$ denotes the case for $\xi \leq 2a$. The coefficients K_o', L_o', D_j' $(j = 1, 2, 3)$, and C_i' $(i = 0, 2, ...20)$ are provided in table (4.1). As required, as the separation tends to zero, the normalized covariance tends to 1,

$$\lim_{\varphi\to 0}\frac{N\langle p_m \tilde{p_m}\rangle_<}{\rho^2 P(0)} = 1. \tag{4.63}$$

Note that while the normalized covariance has the appropriate limiting behavior, it becomes highly oscillatory for $0 < \varphi \leq .03$. Introducing the heaviside function H,

$$\frac{P(\varphi)}{P(0)} = g_<\ H(2-\varphi) + g_>\ H(\varphi-2). \tag{4.64}$$

Results for the fluctuating component of the pressure covariance owing to the presence of a single sized vortex distribution are provided in figure (4.9). Comparison

is being made between the theoretical prediction and direct numerical simulation at four separate Reynolds numbers. The spherical vortex model is essentially an infinite Reynolds number prediction. The numerical data is taken from DNS predictions [2] of the pressure spectrum defined as

$$\Pi(\mathbf{k}) = \frac{1}{8\pi^3} \int\int\int P(\xi)\, e^{-i\mathbf{k}\cdot\xi} d\xi. \tag{4.65}$$

The inverse Fourier transform of the pressure spectrum yields the pressure correlation. For isotropic turbulence, the spectrum is independent of the angle components of $\mathbf{k}$. Changing the inverse transform to spherical polar coordinates in k-space and carrying out the angle integration, we find

$$P(\xi) = \int_0^\infty E_p(k) \frac{\sin(k\xi)}{k\xi} d\mathrm{k}, \tag{4.66}$$

where the shell summed spectral function, $E_p(k)$, for isotropic turbulence has the simple form,

$$E_p(k) = 4\pi k^2 \Pi(k). \tag{4.67}$$

Knowledge of $E_p(k)$ enables us to compute the pressure correlation. Dimensional arguments suggest $E_p(k)$ behaves according to the well-known $k^{-\frac{7}{3}}$ law,

$$E_p(k) = \overline{\varepsilon}^{\frac{4}{3}} k^{-\frac{7}{3}} g(k\eta). \tag{4.68}$$

Substituting this into equation (4.66), and making the change of variables, $K = k\eta$, $\Psi = \frac{\xi}{\lambda}$, and $L = \frac{\lambda}{\eta}$, we find

$$P(\Psi) = \overline{\varepsilon}\nu \int_0^\infty K^{-\frac{7}{3}} g(K) \frac{\sin(K\Psi L)}{K\Psi L} dK. \tag{4.69}$$

The numerical data used for comparison provides values of $g(K)$ and L for a range of K for various values of the Taylor Reynolds number. In all cases, $g(K)$ decays

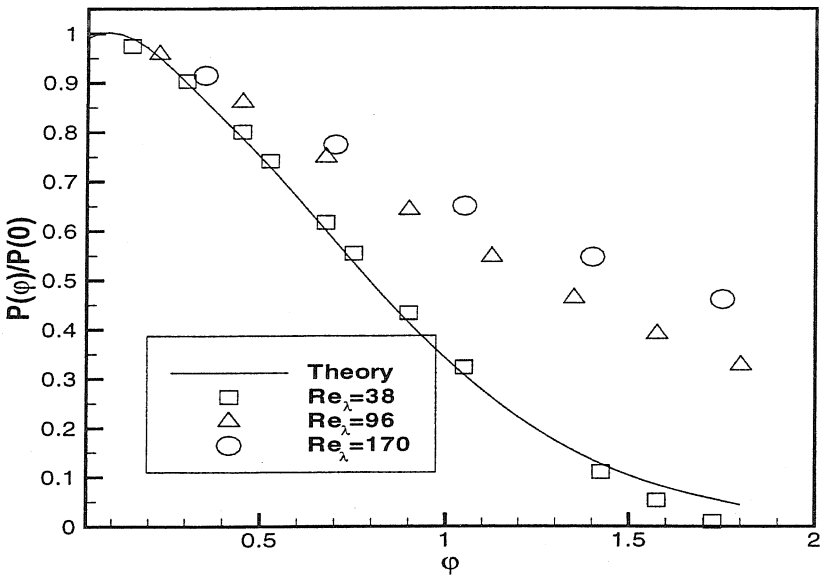

Figure 4.9: Two point pressure correlation for the Hill's spherical vortex based on a disribution of single sized vortices. Comparison is being made with DNS data taken from [2].

sufficiently rapidly so that the infinite integration is reasonably approximated by a numerical integration over the range of K provided. Straight-forward quadrature yields results provided in figure (4.9).

4.4.3 Joint-normal hypothesis for the velocity field

Before we proceed with averaging the pressure covariance over vortex size, we consider the joint-Gaussian hypothesis used by Heisenberg [47], Obukhov [53] and Batchelor [44]. We can appeal to the HSV turbulence model to test the supposition that departures from normality increase in response to decreasing ξ by comparing $P_{JNH}(\xi)$, equation (2.23), which depends on the scalar function $f(\xi)$, to $P(\xi)$, derived independently from an appropriate average of the pressure field associated with the spherical vortex. For isotropic turbulence assuming the joint-probability distribution of $\mathbf{u}$ and $\tilde{\mathbf{u}}$ is normal, the pressure covariance is given by (2.23) which is an integral relation involving the derivative of the scalar function f. For the spherical vortex model, the

scalar function $f\left(\frac{\xi}{a}\right)$ is different for $\xi \leq 2a$ and $\xi \geq 2a$. For $\varphi = \xi/a$,

$$f'(\varphi) = \left(-\frac{21}{10}\varphi + \frac{105}{64}\varphi^2 - \frac{105}{512}\varphi^4 + \frac{63}{5120}\varphi^6\right) H(2-\varphi) + \left(-\frac{21}{10}\varphi^{-4}\right) H(\varphi - 2). \tag{4.70}$$

Substituting this decomposition into (2.23), we find that the pressure correlation for the HSV turbulence model under the joint-Gaussian supposition is given by

$$P(\varphi)_{\varphi\leq 2} = 2u^4 \int_{\varphi}^{2} \left(y - \frac{\varphi^2}{y}\right)\left(-\frac{21}{10}y + \frac{105}{64}y^2 - \frac{105}{512}y^4 + \frac{63}{5120}y^6\right)^2 dy + \int_{2}^{\infty} \left(y - \frac{\varphi^2}{y}\right)\left(-\frac{21}{10}y^{-4}\right)^2 dy, \tag{4.71}$$

$$= \frac{21u^4}{52428800}\{2170880 - 3875840\varphi^2 + 5505024\varphi^4 - 4587520\varphi^5 + 1120000\varphi^6 + 245760\varphi^7 - 140000\varphi^8 - 8192\varphi^9 + 10290\varphi^{10} - 420\varphi^{12} + 9\varphi^{14}\}, \tag{4.72}$$

$$P(\varphi)_{\varphi\geq 2} = 2u^4 \int_{\varphi}^{\infty} \left(y - \frac{\varphi^2}{y}\right)\left(-\frac{21}{10}y^{-4}\right)^2 dy, \tag{4.73}$$

$$= \frac{147}{400}\varphi^{-6}. \tag{4.74}$$

As required, $P(\varphi)_{\varphi\leq 2}$ and $P(\varphi)_{\varphi\geq 2}$ join smoothly at $\varphi = 2$. The mean-square pressure fluctuation is given by (4.71) with $\varphi = 0$,

$$P(0) = 2u^4 \int_{0}^{2} y\left(-\frac{21}{10}y + \frac{105}{64}y^2 - \frac{105}{512}y^4 + \frac{63}{5120}y^6\right)^2 dy + \int_{2}^{\infty} y\left(-\frac{21}{10}y^{-4}\right)^2 dy, \tag{4.75}$$

$$= \frac{1113}{1280}u^4. \tag{4.76}$$

In figure (4.10), we see that the joint-normal hypothesis appears to be a good assumption for the spherical vortex model. One might conjecture that the highly symmetrical spherical vortex coupled with assumptions regarding statistical independence, homogeneity, and isotropy generate a model for a joint-Gaussian velocity field. Departures

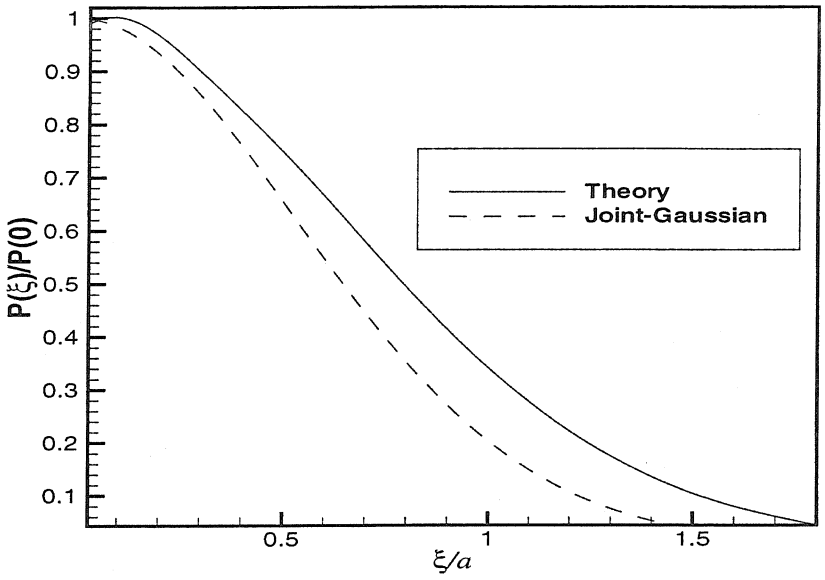

Figure 4.10: Pressure correlation based on the joint-normal hypothesis for the velocity field.

from normality, measured partly by the skewness, vanish as appropriate to a Gaussian distribution.

4.4.4 Average of the pressure field over vortex size

To complete our treatment of the pressure field statistics, we allow the vortex size to vary continuously across the observations. The variance of the log-normal distribution has already been fixed by the velocity statistics. The type averaged mean-square pressure is given by

$$\overline{P(0)}^{a} = \frac{157 n a_o^3 \pi U^4}{231} \int_0^\infty \zeta\left(\frac{a}{a_o}, \sigma = .85\right) \left(\frac{a}{a_o}\right)^3 d\left(\frac{a}{a_o}\right), \tag{4.77}$$

$$\simeq 17.55\, n a_o^3 \pi U^4. \tag{4.78}$$

From (4.55) and (4.64) the fluctuating two point pressure correlation has the form

$$P(\varphi) = \frac{157 n a_o^3 \pi U^4}{231} \left\{ g_<(\varphi) \;\; H(2-\varphi) + g_>(\varphi) \;\; H(\varphi - 2) \right\}. \tag{4.79}$$

To simplify the average over vortex size, we make the substitutions, $\varphi = \psi\mathcal{L}/u$, $\mathcal{L} = \overline{\lambda}^a/a_o$, and $u = a/a_o$. The variable ψ becomes the normalized separation parameter, and u is the variable over which the integration over size is performed. $\mathcal{L}$ is fixed by averaging the Taylor scale over size (4.39). Equation (4.79) becomes

$$\begin{aligned} P(\psi,\mathcal{L},u) &= \frac{157na_o^3\pi U^4}{231}\left\{\hat{g}_<(\psi,\mathcal{L},u)\ H\left(u-\frac{\psi\mathcal{L}}{2}\right)\right. \\ &\left. +\hat{g}_>(\psi,\mathcal{L},u)\ H\left(\frac{\psi\mathcal{L}}{2}-u\right)\right\}. \end{aligned} \tag{4.80}$$

The type averaged pressure correlation is therefore given by $\int_0^\infty P(\psi,\mathcal{L},u)\,du$,

$$\begin{aligned} \overline{P(\psi)}^a &= \frac{157na_o^3\pi U^4}{231}\left\{\int_{\frac{\psi\mathcal{L}}{2}}^\infty \hat{g}_<(\psi,\mathcal{L},u)\,du\right. \\ &\left. +\int_0^{\frac{\psi\mathcal{L}}{2}} \hat{g}_>(\psi,\mathcal{L},u)\,du\right\}. \end{aligned} \tag{4.81}$$

The normalized results of (4.81) are given in figure (4.11). We see that averaging over vortex size moves the asymptotic zero separation value for the covariance from approximately 1.8 to 20.0. This is consistent with the second order velocity structure function results—the asymptotic value of 2.0 was achieved near $\xi/\lambda \simeq 20.0$. Unfortunately, this result is not in agreement with the DNS data for box turbulence at a Taylor Reynolds number of 170. Larger deviations exist for the lower Reynolds number simulations. There are several possible explanations for this discrepancy. The pressure covariance is derived from the pressure field of the spherical vortex assuming the N vortices make additive contributions to the pressure field. While this ansatz is reasonable for the velocity field, it may not be valid for the pressure field. Given a particular velocity field, the pressure is fixed by the Navier-Stokes equation, in particular the nonlinear term $(\mathbf{U}\cdot\nabla)\,\mathbf{U}$. Substituting an *additive velocity field*, $U_j = \sum_{i=1}^N (u_j)_i$ into (1.6) does not produce a similar *additive pressure field*, $P = \sum_{i=1}^N p_i$, due to the nonlinearities which dominate turbulent flows. Hence, the validity of the model equation (2.42) is unresolved. Alternatively, the disagreement may result from an insufficient Reynolds number for the simulated flow. The stochastic model is essen-

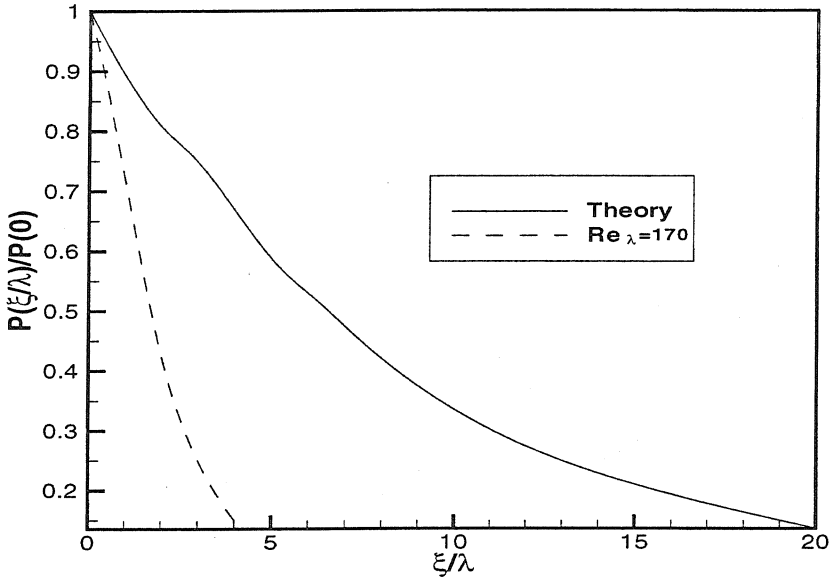

Figure 4.11: The type averaged prediction for the normalized two point pressure correlation as a function of the normalized separation compared with DNS data [2].

tially an infinite Reynolds number model with the full range of eddy scales described by the log-normal distribution. It is possible that $Re_\lambda = 170$ is not large enough to capture the dynamic significance of the range of scales present in the vortex model. It should be kept in mind that the Taylor Reynolds number of the experimental data taken from Tabeling et al. [1] is 507.

Chapter 5 Fourth order velocity structure function and the second order pressure structure function

The second order velocity structure function has clear significance as it relates directly to the spectrum tensor $\Phi_{ij}(k)$ which forms the foundation of most theories regarding the decay of energy containing eddies. However, there are other statistical quantities, in particular higher order incremental velocity product mean values which are physically meaningful and arise in practical theories for turbulence.

The next higher order quantity is the third order velocity structure function which, when normalized by the second order structure function, measures the skewness factor, S, of the probability distribution of Δu_ξ. In a symmetric distribution, every odd order moment about the mean is equal to zero. Any such moment which is not zero may thus be considered as a measure of the asymmetry or *skewness* of the distribution. S is the simplest of these measures and is defined explicitly by

$$S = \frac{\left\langle (\tilde{u}_\xi - u_\xi)^3 \right\rangle}{\left\langle (\tilde{u}_\xi - u_\xi)^2 \right\rangle^{\frac{3}{2}}}. \tag{5.1}$$

The third order structure function plays an important role in the statistical theory of turbulence and is known generally to be non-zero by the Kármán-Howarth equation (1.32). The skewness factor as a function of separation is sensitive to varying Reynolds number. However, the trend from maximum at zero separation to zero at large separation is consistent across a full range of Reynolds numbers. Measurements of S have been available since R. W. Stewart first published skewness data in 1951 [52]. Non-zero values for the skewness reflect the generally accepted theory that the two-point joint probability distribution of the velocity field is non-Gaussian. As already mentioned all odd order moments for the spherical vortex model vanish due to its high

degree of symmetry. While the model does not violate the Kármán-Howarth equation (1.32). it does suggest the existence of an inherent problem and should be addressed in future continuations of the work. Suggestions for ways of breaking the symmetry will be provided in the concluding remarks. The fourth moment of the incremental velocity difference defines the flatness factor, or kurtosis, when non-dimensionalized by second order structure function,

$$F = \frac{\left\langle (\tilde{u}_\xi - u_\xi)^4 \right\rangle}{\left\langle (\tilde{u}_\xi - u_\xi)^2 \right\rangle^2}. \tag{5.2}$$

Probability densities must always vanish as $x \to \pm\infty$, so higher moments such as the fourth order structure function provide information regarding unlikely large values of Δu_ξ. For this reason the higher order structure functions give us insight into extreme events in the turbulent velocity field.

5.1 Calculation of D_{ijkl} and the flatness factor

The fourth order velocity structure function tensor for isotropic turbulence is defined by (2.13). In our preferred coordinate system, the fourth order tensor D_{ijkl} is fully defined by the three independent functions $D_{\xi\xi\xi\xi}$, $D_{\gamma\gamma\gamma\gamma}$, and $D_{\xi\xi\gamma\gamma}$. Respectively these are the longitudinal, transverse and mixed structure functions defined by (3.24) and (3.25). Imposing isotropy and homogeneity on $\mu(l_i)$ and $\sigma(\mathrm{x}_i)$ and introducing results for $D_{\xi\xi}$ and $D_{\gamma\gamma}$, these equations become

$$D_{iiii} = \frac{n}{4\pi} \int d\mathbf{x} \int d\Omega \left(\tilde{u}_i - u_i\right)^4 + 3D_{ii}^2, \tag{5.3}$$

where $i = \xi$ or γ, and

$$D_{\xi\xi\gamma\gamma} = \frac{n}{4\pi} \int d\mathbf{x} \int d\Omega \left(\tilde{u}_\xi - u_\xi\right)^2 \left(\tilde{u}_\gamma - u_\gamma\right)^2 + D_{\xi\xi} D_{\gamma\gamma}. \tag{5.4}$$

We begin with D_{iiii} and let $\tilde{u}_i = \tilde{c}_{ij} l^j$ and $u_i = c_{ij} l^j$ where $\tilde{c}_{ij}$ and c_{ij} are defined

by (4.4) and (4.5) respectively. Substituting, we find

$$D_{iiii} = \frac{n}{4\pi} \int d\mathbf{x} \int d\Omega \left[\left(\tilde{c}_{i1} - c_{i1} \right) l^1 + \left(\tilde{c}_{i2} - c_{i2} \right) l^2 + \left(\tilde{c}_{i3} - c_{i3} \right) l^3 \right]^4 + 3D_{ii}^2. \quad (5.5)$$

Expanding and using (3.20) to average over orientation,

$$\begin{aligned} D_{iiii} &= \frac{n}{5} \int d\mathbf{x} \left[\left(\tilde{c}_{i1} - c_{i1} \right)^4 + \left(\tilde{c}_{i2} - c_{i2} \right)^4 + \left(\tilde{c}_{i3} - c_{i3} \right)^4 \right. \\ &\quad + 2 \left(\tilde{c}_{i1} - c_{i1} \right)^2 \left(\tilde{c}_{i2} - c_{i2} \right)^2 + 2 \left(\tilde{c}_{i2} - c_{i2} \right)^2 \left(\tilde{c}_{i3} - c_{i3} \right)^2 \\ &\quad \left. + 2 \left(\tilde{c}_{i1} - c_{i1} \right)^2 \left(\tilde{c}_{i3} - c_{i3} \right)^2 \right] + 3D_{ii}^2. \end{aligned} \quad (5.6)$$

We next partition the domain of spatial integration as in figures (4.1) and (4.2) and substitute the rotational and irrotational tensors for $\tilde{c}_{ij}$ and c_{ij} appropriately. Symmetry arguments allow us to restrict our attention to regions I and II when the magnitude of the separation vector exceeds the vortex diameter and to regions I', II', and IV' when the separation distance is less than the vortex diameter. Let

$$\begin{aligned} fn\left(\tilde{c}_{ij}, c_{ij} \right) &= \left(\tilde{c}_{i1} - c_{i1} \right)^4 + \left(\tilde{c}_{i2} - c_{i2} \right)^4 + \left(\tilde{c}_{i3} - c_{i3} \right)^4 \\ &\quad + 2 \left(\tilde{c}_{i1} - c_{i1} \right)^2 \left(\tilde{c}_{i2} - c_{i2} \right)^2 + 2 \left(\tilde{c}_{i2} - c_{i2} \right)^2 \left(\tilde{c}_{i3} - c_{i3} \right)^2 \\ &\quad + 2 \left(\tilde{c}_{i1} - c_{i1} \right)^2 \left(\tilde{c}_{i3} - c_{i3} \right)^2 . \end{aligned} \quad (5.7)$$

$D_{iiii,>}$ and $D_{iiii,<}$ are then given by

$$D_{iiii,>} = 3D_{ii,>}^2 + \frac{n}{5} \left\{ \int_I d\mathbf{x} \;\; fn\left(\tilde{\alpha}_{ij}, \alpha_{ij} \right) + 2 \int_{II} d\mathbf{x} \;\; fn\left(\tilde{\alpha}_{ij}, \beta_{ij} \right) \right\}, \quad (5.8)$$

and

$$\begin{aligned} D_{iiii,<} &= 3D_{ii,<}^2 + \frac{n}{5} \left\{ \int_{I'} d\mathbf{x} \;\; fn\left(\tilde{\alpha}_{ij}, \alpha_{ij} \right) + 2 \int_{II'} d\mathbf{x} \;\; fn\left(\tilde{\alpha}_{ij}, \beta_{ij} \right) \right. \\ &\quad \left. + \int_{IV'} d\mathbf{x} \;\; fn\left(\tilde{\beta}_{ij}, \beta_{ij} \right) \right\}. \end{aligned} \quad (5.9)$$

Under the transformation to the toroidal coordinate system, where $\alpha_{ij} \xrightarrow{T} \Lambda_{ij}$, and

$\beta_{ij} \xrightarrow{T} \Theta_{ij}$, (5.8) and (5.9) become

$$\begin{aligned} D_{iiii,>} &= 3D_{ii,>}^2 + \frac{n}{5}\left\{2\int_0^{2\pi} d\varphi \int_0^a dr \int_{\xi-r}^{\xi+r} d\tilde{r}\ \frac{r\tilde{r}}{\xi}\ fn\left(\tilde{\Lambda}_{ij}, \Theta_{ij}\right)\right. \\ &+ \int_0^{2\pi} d\varphi \int_a^{\xi-a} dr \int_{\xi-r}^{\xi+r} d\tilde{r}\ \frac{r\tilde{r}}{\xi}\ fn\left(\tilde{\Lambda}_{ij}, \Lambda_{ij}\right) \\ &+ \int_0^{2\pi} d\varphi \int_{\xi-a}^{\xi+a} dr \int_a^{\xi+r} d\tilde{r}\ \frac{r\tilde{r}}{\xi}\ fn\left(\tilde{\Lambda}_{ij}, \Lambda_{ij}\right) \\ &+ \left.\int_0^{2\pi} d\varphi \int_{\xi+a}^{\infty} dr \int_{r-\xi}^{\xi+r} d\tilde{r}\ \frac{r\tilde{r}}{\xi}\ fn\left(\tilde{\Lambda}_{ij}, \Lambda_{ij}\right)\right\}, \end{aligned} \tag{5.10}$$

and

$$\begin{aligned} D_{iiii,<} &= 3D_{ii,<}^2 + \frac{n}{5}\left\{2\int_0^{2\pi} d\varphi \int_a^{\xi+a} dr \int_{\xi-r}^{a} d\tilde{r}\ \frac{r\tilde{r}}{\xi}\ fn\left(\tilde{\Theta}_{ij}, \Lambda_{ij}\right)\right. \\ &+ \int_0^{2\pi} d\varphi \int_{\xi-a}^{a} dr \int_{\xi-r}^{a} d\tilde{r}\ \frac{r\tilde{r}}{\xi}\ fn\left(\tilde{\Theta}_{ij}, \Theta_{ij}\right) \\ &+ \int_0^{2\pi} d\varphi \int_a^{\xi+a} dr \int_a^{\xi+r} d\tilde{r}\ \frac{r\tilde{r}}{\xi}\ fn\left(\tilde{\Lambda}_{ij}, \Lambda_{ij}\right) \\ &+ \left.\int_0^{2\pi} d\varphi \int_{\xi+a}^{\infty} dr \int_{r-\xi}^{\xi+r} d\tilde{r}\ \frac{r\tilde{r}}{\xi}\ fn\left(\tilde{\Lambda}_{ij}, \Lambda_{ij}\right)\right\}. \end{aligned} \tag{5.11}$$

The mixed fourth order velocity structure function for the proposed turbulence model is the result of substituting the longitudinal and transverse components of the velocity field induced by Hill's vortex into (3.25). Partitioning the domain of spatial integration so that the appropriate tensor representation can be substituted for the velocities u_i and $\tilde{u}_i$ and changing to toroidal coordinates, we find that the two cases, $D_{\xi\xi\gamma\gamma,>}$ and $D_{\xi\xi\gamma\gamma,<}$, are given by

$$\begin{aligned} D_{\xi\xi\gamma\gamma,>} &= D_{\xi\xi,>}D_{\gamma\gamma,>} + \frac{n}{5}\left\{2\int_0^{2\pi} d\varphi \int_0^a dr \int_{\xi-r}^{\xi+r} d\tilde{r}\ \frac{r\tilde{r}}{\xi}\ gn\left(\tilde{\Lambda}_{ij}, \Theta_{ij}\right)\right. \\ &+ \int_0^{2\pi} d\varphi \int_a^{\xi-a} dr \int_{\xi-r}^{\xi+r} d\tilde{r}\ \frac{r\tilde{r}}{\xi}\ gn\left(\tilde{\Lambda}_{ij}, \Lambda_{ij}\right) \\ &+ \int_0^{2\pi} d\varphi \int_{\xi-a}^{\xi+a} dr \int_a^{\xi+r} d\tilde{r}\ \frac{r\tilde{r}}{\xi}\ gn\left(\tilde{\Lambda}_{ij}, \Lambda_{ij}\right) \\ &+ \left.\int_0^{2\pi} d\varphi \int_{\xi+a}^{\infty} dr \int_{r-\xi}^{\xi+r} d\tilde{r}\ \frac{r\tilde{r}}{\xi}\ gn\left(\tilde{\Lambda}_{ij}, \Lambda_{ij}\right)\right\}, \end{aligned} \tag{5.12}$$

and

$$
\begin{aligned}
D_{\xi\xi\gamma\gamma,<} &= D_{\xi\xi,<}D_{\gamma\gamma,<} + \frac{n}{5}\left\{2\int_0^{2\pi} d\varphi \int_a^{\xi+a} dr \int_{\xi-r}^{a} d\tilde{r}\ \frac{r\tilde{r}}{\xi}\ gn\left(\tilde{\Theta}_{ij}, \Lambda_{ij}\right)\right. \\
&+ \int_0^{2\pi} d\varphi \int_{\xi-a}^{a} dr \int_{\xi-r}^{a} d\tilde{r}\ \frac{r\tilde{r}}{\xi}\ gn\left(\tilde{\Theta}_{ij}, \Theta_{ij}\right) \qquad (5.13) \\
&+ \int_0^{2\pi} d\varphi \int_a^{\xi+a} dr \int_a^{\xi+r} d\tilde{r}\ \frac{r\tilde{r}}{\xi}\ gn\left(\tilde{\Lambda}_{ij}, \Lambda_{ij}\right) \\
&\left.+ \int_0^{2\pi} d\varphi \int_{\xi+a}^{\infty} dr \int_{r-\xi}^{\xi+r} d\tilde{r}\ \frac{r\tilde{r}}{\xi}\ gn\left(\tilde{\Lambda}_{ij}, \Lambda_{ij}\right)\right\},
\end{aligned}
$$

where $gn\left(\tilde{c}_{ij} - c_{ij}\right)$ is given by

$$
\begin{aligned}
gn\left(\tilde{c}_{ij}, c_{ij}\right) &= \left(\tilde{c}_{31} - c_{31}\right)^2\left(\tilde{c}_{21} - c_{21}\right)^2 \qquad (5.14) \\
&+ \left(\tilde{c}_{32} - c_{32}\right)^2\left(\tilde{c}_{22} - c_{22}\right)^2 + \left(\tilde{c}_{33} - c_{33}\right)^2\left(\tilde{c}_{23} - c_{23}\right)^2 \\
&+ \frac{1}{3}\left[\left(\tilde{c}_{32} - c_{32}\right)^2\left(\tilde{c}_{21} - c_{21}\right)^2 + \left(\tilde{c}_{33} - c_{33}\right)^2\left(\tilde{c}_{21} - c_{21}\right)^2\right. \\
&+ \left(\tilde{c}_{31} - c_{31}\right)^2\left(\tilde{c}_{22} - c_{22}\right)^2 + \left(\tilde{c}_{33} - c_{33}\right)^2\left(\tilde{c}_{22} - c_{22}\right)^2 \\
&\left.+ \left(\tilde{c}_{31} - c_{31}\right)^2\left(\tilde{c}_{23} - c_{23}\right)^2 + \left(\tilde{c}_{32} - c_{32}\right)^2\left(\tilde{c}_{23} - c_{23}\right)^2\right] \\
&+ \frac{4}{3}\left[\left(\tilde{c}_{31} - c_{31}\right)\left(\tilde{c}_{32} - c_{32}\right)\left(\tilde{c}_{21} - c_{21}\right)\left(\tilde{c}_{22} - c_{22}\right)\right. \\
&+ \left(\tilde{c}_{31} - c_{31}\right)\left(\tilde{c}_{33} - c_{33}\right)\left(\tilde{c}_{21} - c_{21}\right)\left(\tilde{c}_{23} - c_{23}\right) \\
&\left.+ \left(\tilde{c}_{32} - c_{32}\right)\left(\tilde{c}_{33} - c_{33}\right)\left(\tilde{c}_{22} - c_{22}\right)\left(\tilde{c}_{23} - c_{23}\right)\right].
\end{aligned}
$$

Analytical evaluation of (5.10), (5.11), (5.12), and (5.13) can be carried out efficiently with the aid of symbolic manipulation programs such as *Mathematica.* The integrands involve terms like $r^{\alpha}\tilde{r}^{\beta}\tau\left(\varphi\right)$ where $\tau\left(\varphi\right)$ is a trigonometric function. The large number of such terms involved and the complicated limits of integration render the problem intractable without the aid of such technical computing software. Furthermore, it is necessary to break the evaluation of (5.10), (5.11), (5.12), and (5.13) into several pieces so as not to exceed the memory capacity of the computer. Upon evaluating both cases $D_{iiii,>}$ and $D_{iiii,<}$ separately for $i = \xi = 3$ and $i = \gamma = 2$ and evaluating both cases for the mixed structure function, we obtain preliminary results for the fourth order longitudinal, lateral and mixed structure functions due

to the presence of a single vortex type. The exact expressions are too lengthy and complicated for publication.

To average the fourth order statistics over vortex size, we introduce the heaviside function H and make the substitutions $\varphi = \psi\mathcal{L}/u$, $\mathcal{L} = \overline{\lambda}^a/a_o$, and $u = a/a_o$. The type averaged integrals for $D_{\xi\xi\xi\xi}$, $D_{\gamma\gamma\gamma\gamma}$, and $D_{\xi\xi\gamma\gamma}$ are given as follows:

$$\begin{aligned}\overline{D_{\xi\xi\xi\xi}}^a(\psi, na_o^3) &= na_o^3\pi U^4 \int_0^\infty \zeta(u, \sigma = .85)\left[\hat{D}_{\xi\xi\xi\xi,>}\ H\left(u - \frac{\varphi}{2}\right)\right. \\ &\quad \left. + \hat{D}_{\xi\xi\xi\xi,>}\ H\left(\frac{\varphi}{2} - u\right)\right] du \\ &\quad + 3\left\{\int_0^\infty \zeta(u, \sigma = .85)\left[\hat{D}_{\xi\xi,<}\ H\left(u - \frac{\varphi}{2}\right)\right.\right. \\ &\quad \left.\left. + \hat{D}_{\xi\xi,>}\ H\left(\frac{\varphi}{2} - u\right)\right] du\right\}^2, \end{aligned} \tag{5.15}$$

$$\begin{aligned}\overline{D_{\gamma\gamma\gamma\gamma}}^a(\psi) &= na_o^3\pi U^4 \int_0^\infty \zeta(u, \sigma = .85)\left[\hat{D}_{\gamma\gamma\gamma\gamma,<}\ H\left(u - \frac{\varphi}{2}\right)\right. \\ &\quad \left. + \hat{D}_{\gamma\gamma\gamma\gamma,>}\ H\left(\frac{\varphi}{2} - u\right)\right] du \\ &\quad + 3\left\{\int_0^\infty \zeta(u, \sigma = .85)\left[\hat{D}_{\gamma\gamma,<}\ H\left(u - \frac{\varphi}{2}\right)\right.\right. \\ &\quad \left.\left. + \hat{D}_{\gamma\gamma,>}\ H\left(\frac{\varphi}{2} - u\right)\right] du\right\}^2, \end{aligned} \tag{5.16}$$

$$\begin{aligned}\overline{D_{\xi\xi\gamma\gamma}}^a(\psi) &= na_o^3\pi U^4 \int_0^\infty \zeta(u, \sigma = .85)\left[\hat{D}_{\xi\xi\gamma\gamma,<}\ H\left(u - \frac{\varphi}{2}\right)\right. \\ &\quad \left. + \hat{D}_{\xi\xi\gamma\gamma,>}\ H\left(\frac{\varphi}{2} - u\right)\right] du \\ &\quad + \left\{\int_0^\infty \zeta(u, \sigma = .85)\left[\hat{D}_{\xi\xi,<}\ H\left(u - \frac{\varphi}{2}\right)\right.\right. \\ &\quad \left.\left. + \hat{D}_{\xi\xi,>}\ H\left(\frac{\varphi}{2} - u\right)\right] du\right\}\left\{\int_0^\infty \zeta(u, \sigma = .85)\left[\hat{D}_{\gamma\gamma,<}\ H\left(u - \frac{\varphi}{2}\right)\right.\right. \\ &\quad \left.\left. + \hat{D}_{\gamma\gamma,>}\ H\left(\frac{\varphi}{2} - u\right)\right] du\right\}, \end{aligned} \tag{5.17}$$

where $\hat{D}_{\xi\xi\xi\xi}$, $\hat{D}_{\gamma\gamma\gamma\gamma}$, and $\hat{D}_{\xi\xi\gamma\gamma}$ are the longitudinal, lateral and mixed structure functions respectively with the quantity $na_o^3\pi U^4$ factored out. We note the explicit functional dependence of $\overline{D_{\xi\xi\xi\xi}}^a$ on na_o^3 while $\overline{D_{\gamma\gamma\gamma\gamma}}^a$ and $\overline{D_{\xi\xi\gamma\gamma}}^a$ are parameter free.

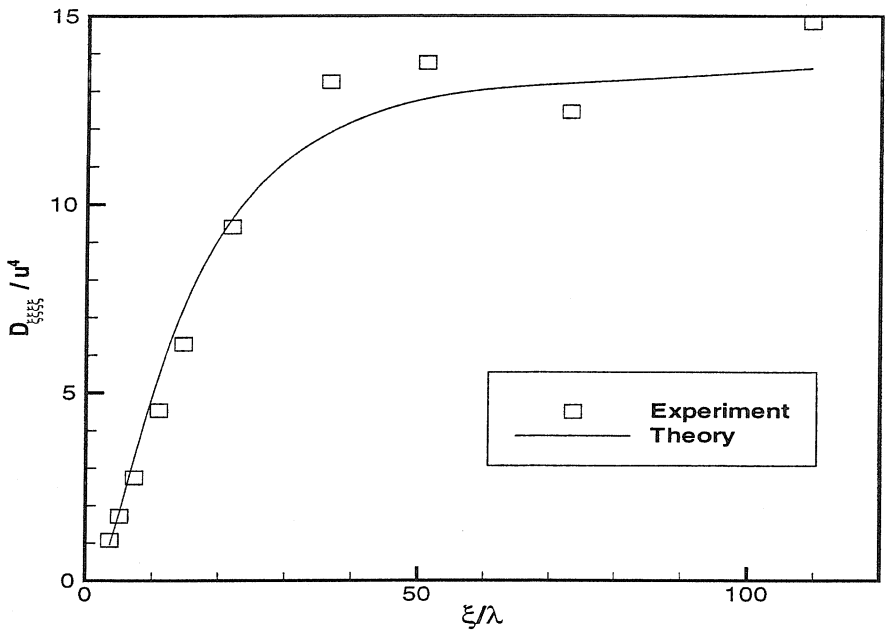

Figure 5.1: Fourth order normalized longitudinal velocity structure function for HSV model plotted against normalized separation and compared with experiment [1].

Upon non-dimensionalizing by the root-mean-square velocity raised to the order of the statistic, the n^{th} order structure function contains the quantity $(na_o^3)^{1-n/2}$. This term conveniently vanishes for $n = 2$, allowing us to tune the variance σ in the size distribution so that respectable agreement with experimental data can be achieved. Satisfactory results were obtained for $\sigma = 0.85$. We choose to fix the remaining parameter na_o^3 by fitting the fourth order longitudinal prediction to experimental data [1]. A satisfactory fit between the statistical model and experiment occurs when $na_o^3 = 0.02$. Quadrature results for (5.15), (5.16) and (5.17) are provided in figures (5.1), (5.2) and (5.3). It should be emphasized that the lateral and mixed results are pure predictions.

Figure (5.4) shows the functional dependence of the flatness factor on separation for the HSV model. If the joint-probability distribution of $\tilde{u}_i$ and u_i were normal, the flatness factor of Δu_ξ given by (5.1) would be 3.0. We see that the model predicts an asymptotic value near 3.45 for large separation. At small separation the flatness factor departs significantly from this.

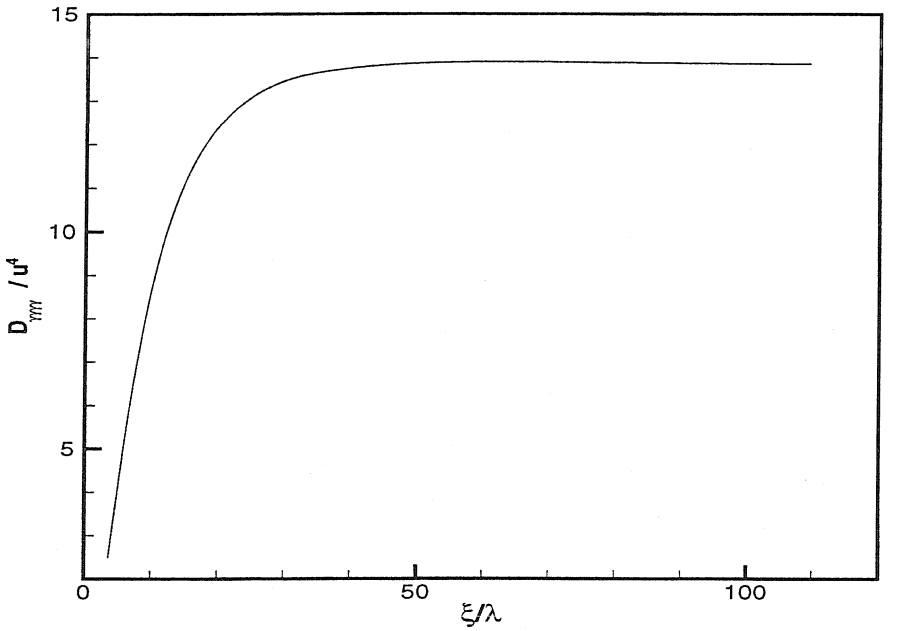

Figure 5.2: Fourth order normalized transverse velocity structure function for HSV model plotted against normalized separation.

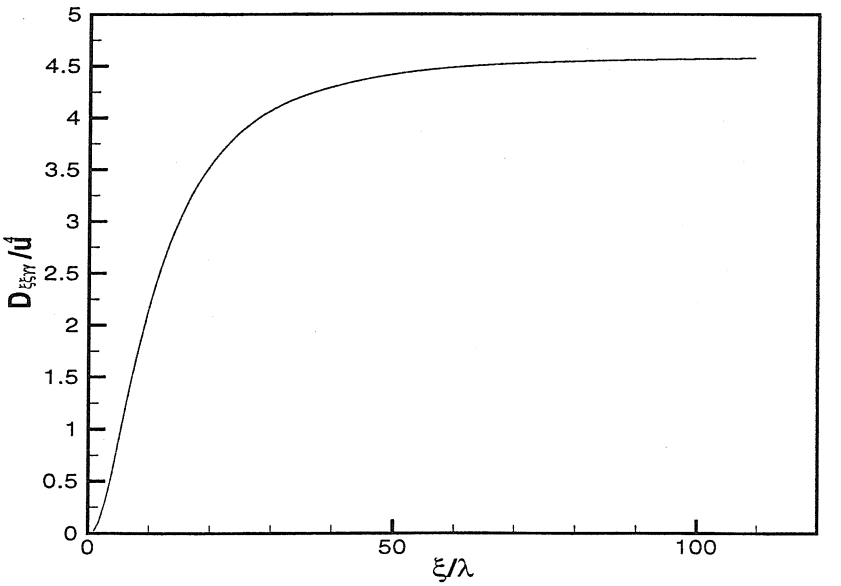

Figure 5.3: Fourth order mixed structure function for HSV model plotted against the normalized separation.

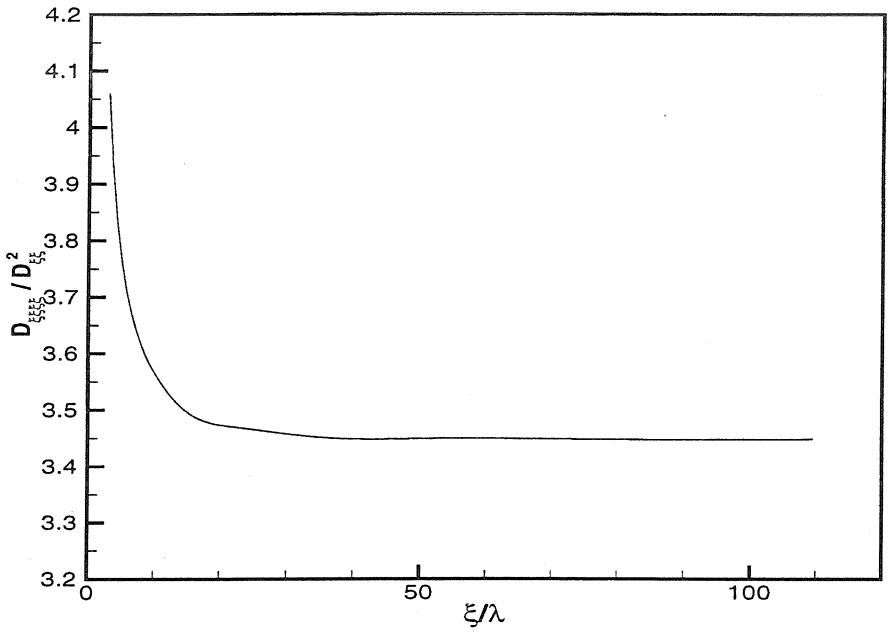

Figure 5.4: Flatness factor for HSV model.

5.2 Scaling of the longitudinal and transverse structure functions

The relative scaling of the transverse structure functions to their longitudinal counterparts has received considerable attention by experimentalists and DNS experts [56, 57, 58, 59]. Some of the measurements suggest that the scaling exponents of the two functions are equal to within experimental error [57], while other measurements suggest that the scaling exponent of the transverse structure function is measurably smaller than the longitudinal exponent for orders greater than 2 [58, 59]. Recently, the transverse structure functions, orders 2-6, were obtained for DNS simulations of high Reynolds number atmospheric flows [56]. They concluded that the scaling exponents of the longitudinal and transverse functions are indeed different. We can use the results of the spherical vortex model to test their conclusions since both functions have been computed for orders 2 and 4. We begin by considering the ratio of the

longitudinal to the lateral velocity structure function of order n,

$$R_n = \frac{\langle |\Delta u_\xi|^n \rangle}{\langle |\Delta u_\gamma|^n \rangle}. \tag{5.18}$$

If the structure functions demonstrate power law (inertial range) behavior, the index R_n provides the difference between the longitudinal and lateral scaling exponents. By isotropy, the ratio R_2 should have zero slope over the inertial range. This arises by assuming $f(\xi) \sim \xi^\alpha$ and $g(\xi) \sim \xi^\beta$ and imposing the isotropic relation $g = f + \frac{1}{2}\xi f'$,

$$\begin{aligned} g &= f + \frac{1}{2}\xi f' \Rightarrow \xi^\beta = \xi^\alpha + \frac{\alpha}{2}\xi^\alpha \\ \Rightarrow \quad \beta &= \alpha. \end{aligned} \tag{5.19}$$

Using the results for $D_{\xi\xi}(\xi/\lambda)$, $D_{\gamma\gamma}(\xi/\lambda)$, $D_{\xi\xi\xi\xi}(\xi/\lambda)$, and $D_{\gamma\gamma\gamma\gamma}(\xi/\lambda)$, the ratios R_2 and R_4 are plotted in figures (5.5), (5.6), (5.7) and (5.8). The results are consistent with the findings of [56]. By fitting a power law to their measurements for R_2 and a least squares fit to their measurements for R_4, they concluded that R_2 has an index around 0.02, while R_4 demonstrates larger departures with an index around 0.07. The spherical vortex model confirms this result with scaling indices of 0.04 and 0.09 for R_2 and R_4 respectively. This has great implications to small scale phenomenologists and might even challenge the existence of strict scaling rules altogether.

5.3 The pressure structure function for isotropic turbulence

Equation (2.37) provides an exact relationship between the pressure structure function and the three independent fourth order velocity structure functions, $D_{\xi\xi\xi\xi} = \langle \Delta u_\xi^4 \rangle$, $D_{\gamma\gamma\gamma\gamma} = \langle \Delta u_\gamma^4 \rangle$ and $D_{\xi\xi\gamma\gamma} = \langle \Delta u_\xi^2 \Delta u_\gamma^2 \rangle$. Following the approach of [60], we recast (2.37) into a form in which the relative contributions of the longitudinal, transverse and mixed structure functions to the pressure structure function can be examined

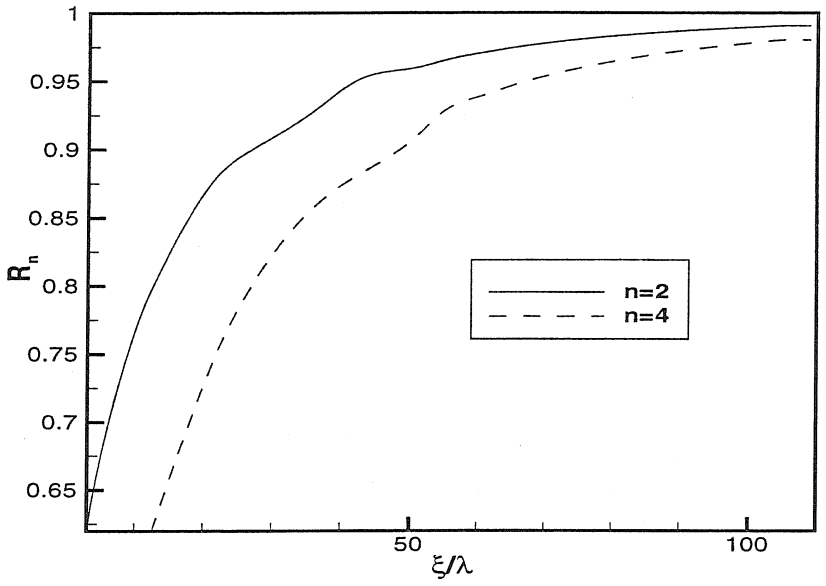

Figure 5.5: Ratio of the longitudinal structure function to the lateral structure function for orders 2 and 4.

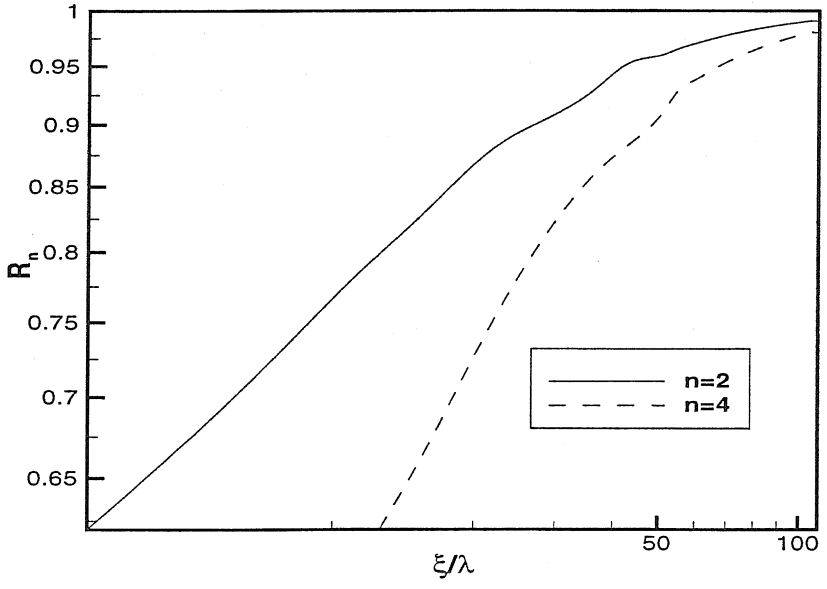

Figure 5.6: Ratio of the longitudinal structure function to the lateral structure function for orders 2 and 4. The log scale suggests power law behavior in two different regions.

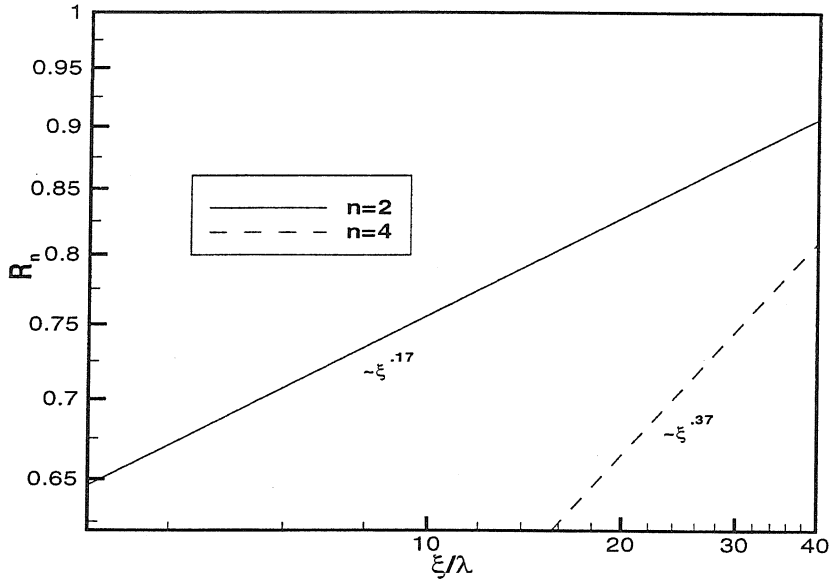

Figure 5.7: Ratio of the longitudinal structure function to the lateral structure function for orders 2 and 4 for small separation.

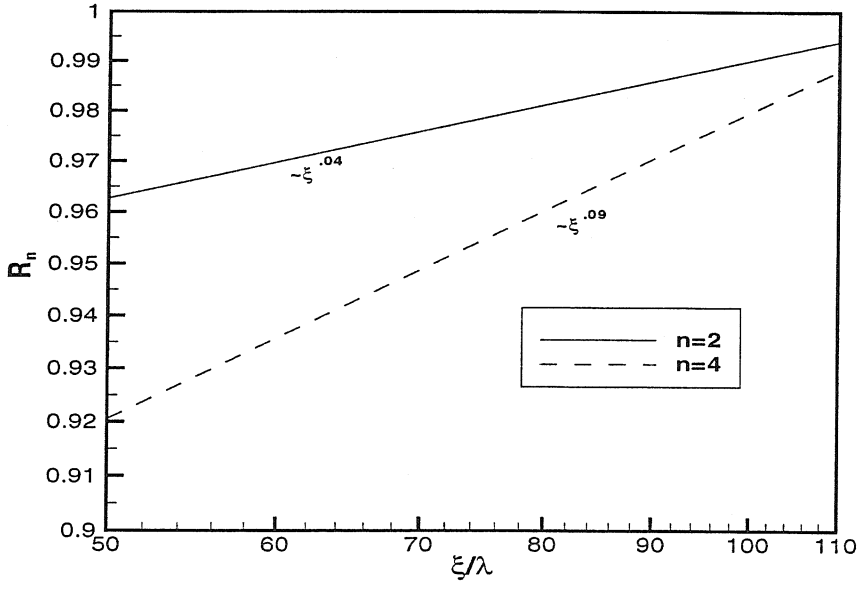

Figure 5.8: Ratio of the longitudinal structure function to the lateral structure function for orders 2 and 4 for large separation.

separately. If we let $D_p\left[\Delta u_\xi^4\right]$, $D_p\left[\Delta u_\gamma^4\right]$, and $D_p\left[\Delta u_\xi^2 \Delta u_\gamma^2\right]$ denote their individual respective contributions, we find

$$D_p(\xi) = D_p\left[\Delta u_\xi^4\right] + D_p\left[\Delta u_\gamma^4\right] - D_p\left[\Delta u_\xi^2 \Delta u_\gamma^2\right]. \tag{5.20}$$

Introducing the integral operator $I_{\geq}$ which determines the effect of scales larger than ξ on $D_p(\xi)$ and $I_{\leq}$, its small scale counterpart, yields

$$I_{\geq} A(\xi) = \frac{4}{3}\xi^2 \int_\xi^\infty y^{-3} A(y)\, dy, \tag{5.21}$$

$$I_{\leq} A(\xi) = \frac{4}{3}\int_0^\xi y^{-1} A(y)\, dy. \tag{5.22}$$

Comparison with equation (2.37) yields the explicit form of (5.20),

$$\begin{aligned} D_p(\xi) &= \left[I_{\geq} - 1/3\right]\left\langle \Delta u_\xi^4 \right\rangle + \left[I_{\leq} + I_{\geq}\right]\left\langle \Delta u_\gamma^4 \right\rangle \\ &\quad - \left[3I_{\leq} + 6I_{\geq}\right]\left\langle \Delta u_\xi^2 \Delta u_\gamma^2 \right\rangle. \end{aligned} \tag{5.23}$$

Using the results for the fourth order velocity structure functions, the right-hand side of (5.23) is integrated numerically. The results are plotted in figures (5.9) and (5.10).

Through DNS simulations, Nelkin and Chen [60] found that the cancellation between $D_p\left[\Delta u_\xi^4\right] + D_p\left[\Delta u_\gamma^4\right]$ and $D_p\left[\Delta u_\xi^2 \Delta u_\gamma^2\right]$ is almost complete. This suggests that the second order pressure structure function is highly sensitive to scaling deviations among the three independent fourth order quantities. They concluded that the large degree of cancellation generates a scaling exponent for $D_p(\xi)$ which is significantly smaller than the scaling exponents for the fourth order quantities. Figures (5.11) and (5.12) confirm the results of Nelkin and Chen. The contributions from both $D_p\left[\Delta u_\xi^4\right] + D_p\left[\Delta u_\gamma^4\right]$ and $D_p\left[\Delta u_\xi^2 \Delta u_\gamma^2\right]$ for the spherical vortex model have been computed separately and are plotted over a range of ξ/λ. Unfortunately, the origin of the strong cancellation is not well understood. However, it is the bias of [60] that this result elucidates a fundamental property of the statistical pressure field for isotropic

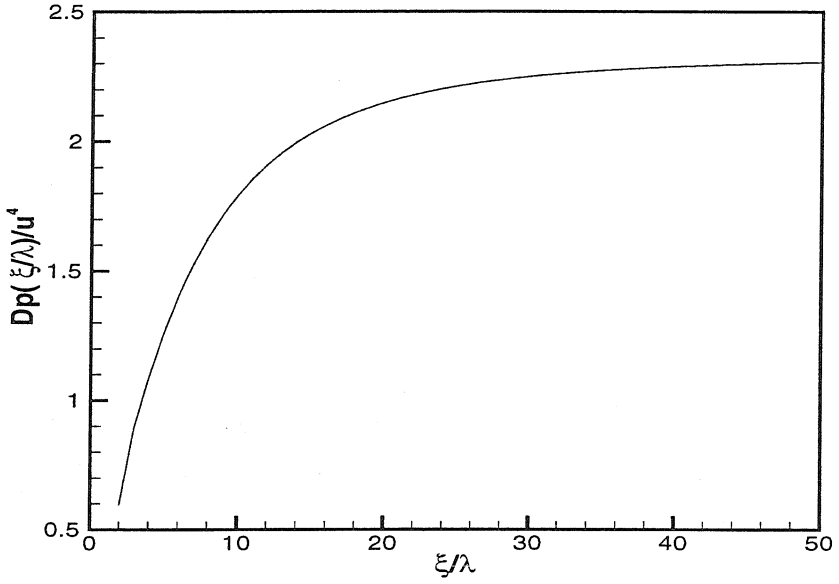

Figure 5.9: The pressure structure function based on the fourth order velocity statistics of the HSV model, equation (2.37).

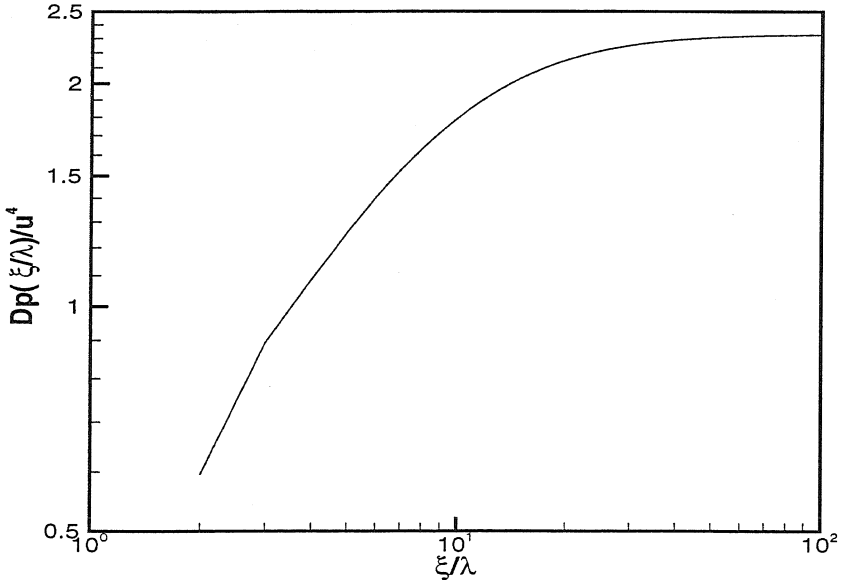

Figure 5.10: Log-log plot of the pressure structure function derived from (2.37).

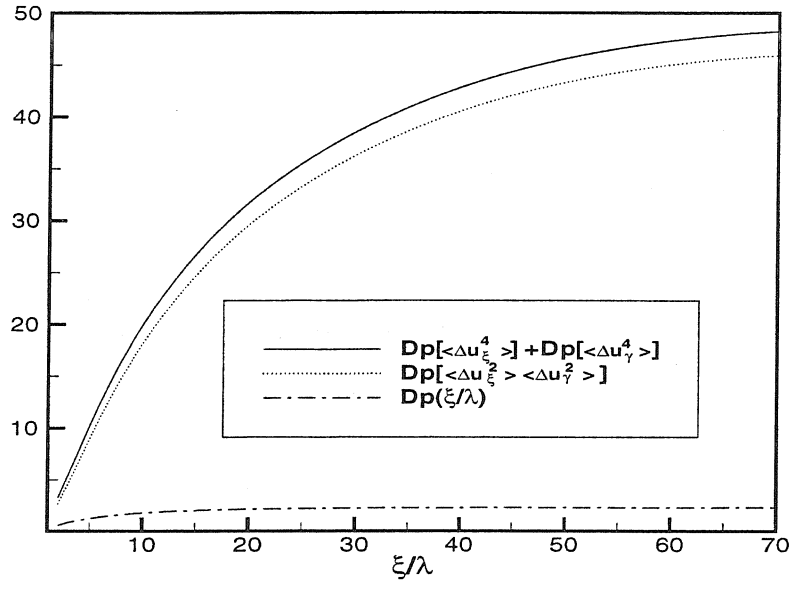

Figure 5.11: The cancellation between the positive contribution to $D_p(\xi)$ from the longitudinal and transverse fourth order structure functions and the negative contribution from the mixed structure function is almost complete. The residual between the two curves, $D_p\left[\Delta u_\xi^4\right] + D_p\left[\Delta u_\gamma^4\right]$ and $D_p\left[\Delta u_\xi^2 \Delta u_\gamma^2\right]$, gives D_p.

turbulence.

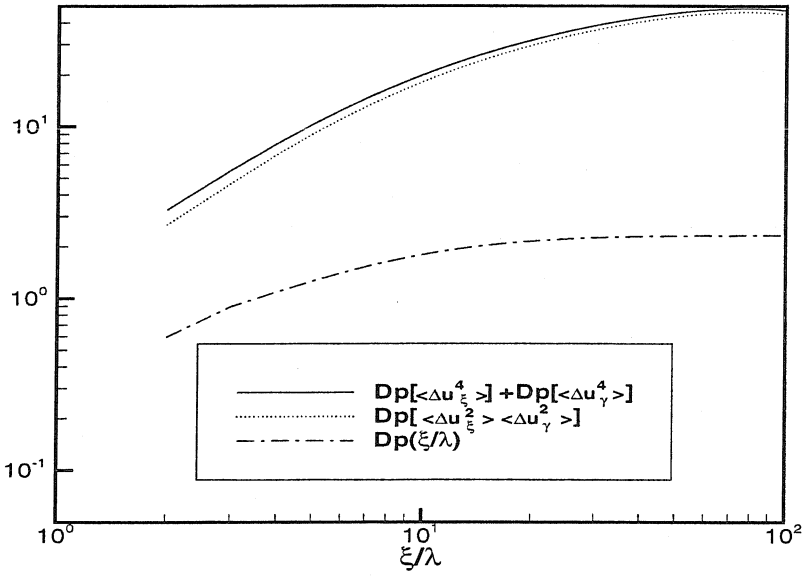

Figure 5.12: Log-log plot of $D_p\left[\Delta u_\xi^4\right]+D_p\left[\Delta u_\gamma^4\right]$ and $D_p\left[\Delta u_\xi^2 \Delta u_\gamma^2\right]$ and their residual D_p.

Chapter 6 Sixth order longitudinal velocity structure function

We are now equipped with a parameter free statistical model for homogeneous isotropic turbulence and are interested in making a prediction for the sixth order longitudinal velocity structure function, $D_{\xi\xi\xi\xi\xi\xi}$. For N statistically independent vortices, this particular moment is defined by (3.26). Imposing isotropy and homogeneity in the usual way, we find

$$D_{\xi\xi\xi\xi\xi\xi} = \frac{n}{4\pi}\int d\mathbf{x}\int d\Omega\,(\tilde{u}_i - u_i)^6 + 15D_{\xi\xi}D_{\xi\xi\xi\xi}. \tag{6.1}$$

Expanding and averaging over orientation, we obtain the volume integral for $D_{\xi\xi\xi\xi\xi\xi}$,

$$\begin{aligned} D_{\xi\xi\xi\xi\xi\xi} = \frac{n}{7}\int d\mathbf{x}\,\big[&(\tilde{c}_{31}-c_{31})^6 + (\tilde{c}_{32}-c_{32})^6 + (\tilde{c}_{33}-c_{33})^6 \\ &+3\,(\tilde{c}_{31}-c_{31})^4(\tilde{c}_{32}-c_{32})^2 + 3\,(\tilde{c}_{32}-c_{32})^4(\tilde{c}_{33}-c_{33})^2 \\ &+3\,(\tilde{c}_{31}-c_{31})^4(\tilde{c}_{33}-c_{33})^2 + 3\,(\tilde{c}_{31}-c_{31})^2(\tilde{c}_{32}-c_{32})^4 \\ &+3\,(\tilde{c}_{32}-c_{32})^2(\tilde{c}_{33}-c_{33})^4 + 3\,(\tilde{c}_{31}-c_{31})^2(\tilde{c}_{33}-c_{33})^4 \\ &+6\,(\tilde{c}_{31}-c_{31})^2(\tilde{c}_{32}-c_{32})^2(\tilde{c}_{33}-c_{33})^2\big] + 15D_{\xi\xi}D_{\xi\xi\xi\xi}. \end{aligned} \tag{6.2}$$

For notational simplicity, we introduce the function $hn\,(\tilde{c}_{ij}, c_{ij})$,

$$\begin{aligned} hn\,(\tilde{c}_{ij}, c_{ij}) = &(\tilde{c}_{31}-c_{31})^6 + (\tilde{c}_{32}-c_{32})^6 + (\tilde{c}_{33}-c_{33})^6 \\ &+3\,(\tilde{c}_{31}-c_{31})^4(\tilde{c}_{32}-c_{32})^2 + 3\,(\tilde{c}_{32}-c_{32})^4(\tilde{c}_{33}-c_{33})^2 \\ &+3\,(\tilde{c}_{31}-c_{31})^4(\tilde{c}_{33}-c_{33})^2 + 3\,(\tilde{c}_{31}-c_{31})^2(\tilde{c}_{32}-c_{32})^4 \\ &+3\,(\tilde{c}_{32}-c_{32})^2(\tilde{c}_{33}-c_{33})^4 + 3\,(\tilde{c}_{31}-c_{31})^2(\tilde{c}_{33}-c_{33})^4 \\ &+6\,(\tilde{c}_{31}-c_{31})^2(\tilde{c}_{32}-c_{32})^2(\tilde{c}_{33}-c_{33})^2. \end{aligned} \tag{6.3}$$

We next refer to figures (4.1) and (4.2) and substitute the appropriate rotational and irrotational tensors for $\tilde{c}_{ij}$ and c_{ij}. Appealing to symmetry we find that for case 1,

$$\begin{aligned} D_{\xi\xi\xi\xi\xi\xi\xi,>} &= \frac{n}{7}\left\{\int_I d\mathbf{x}\ \ hn\left(\tilde{\alpha}_{ij},\alpha_{ij}\right)+2\int_{II} d\mathbf{x}\ \ hn\left(\tilde{\alpha}_{ij},\beta_{ij}\right)\right\} \\ &\quad +15D_{\xi\xi,>}D_{\xi\xi\xi\xi,>}, \end{aligned} \tag{6.4}$$

and for case 2,

$$\begin{aligned} D_{\xi\xi\xi\xi\xi\xi\xi,<} &= \frac{n}{7}\left\{\int_{I'} d\mathbf{x}\ \ hn\left(\tilde{\alpha}_{ij},\alpha_{ij}\right)+2\int_{II'} d\mathbf{x}\ \ hn\left(\tilde{\alpha}_{ij},\beta_{ij}\right)\right. \\ &\quad \left.+\int_{IV'} d\mathbf{x}\ \ hn\left(\tilde{\beta}_{ij},\beta_{ij}\right)\right\}+15D_{\xi\xi,<}D_{\xi\xi\xi\xi,<}. \end{aligned} \tag{6.5}$$

Equations (6.4) and (6.5) are solved in the usual way by transforming to toroidal coordinates and defining the regions of integration following figures (4.4) and (4.5). Using *Mathematica* to assist in the calculus, we obtain preliminary results. The final type averaged result is given by

$$\begin{aligned} \overline{D_{\xi\xi\xi\xi\xi\xi\xi}}^{a}(\psi) &= na_o^3\pi U^6\int_0^\infty \zeta\left(u,\sigma=.85\right)\left[\hat{D}_{\xi\xi\xi\xi\xi\xi\xi,>}\ \ H\left(u-\frac{\varphi}{2}\right)\right. \\ &\quad \left.+\hat{D}_{\xi\xi\xi\xi\xi\xi\xi,>}\ \ H\left(\frac{\varphi}{2}-u\right)\right]du \\ &\quad +15\left\{\int_0^\infty \zeta\left(u,\sigma=.85\right)\left[\hat{D}_{\xi\xi,<}\ \ H\left(u-\frac{\varphi}{2}\right)\right.\right. \\ &\quad \left.+\hat{D}_{\xi\xi,>}\ \ H\left(\frac{\varphi}{2}-u\right)\right]du\times \\ &\quad \int_0^\infty \zeta\left(u,\sigma=.85\right)\left[\hat{D}_{\xi\xi\xi\xi,<}\ \ H\left(u-\frac{\varphi}{2}\right)\right. \\ &\quad \left.\left.+\hat{D}_{\xi\xi\xi\xi,>}\ \ H\left(\frac{\varphi}{2}-u\right)\right]du\right\}. \end{aligned} \tag{6.6}$$

Quadrature results for (6.6) are given in figure (6.1). These results are extremely powerful because the prediction is parameter free. We see that Hill's spherical vortex coupled with details on the probability distribution of $(\tilde{u}_i-u_i)$ produce a turbulence model consistent with experimental velocity structure function data orders 2, 4, and 6.

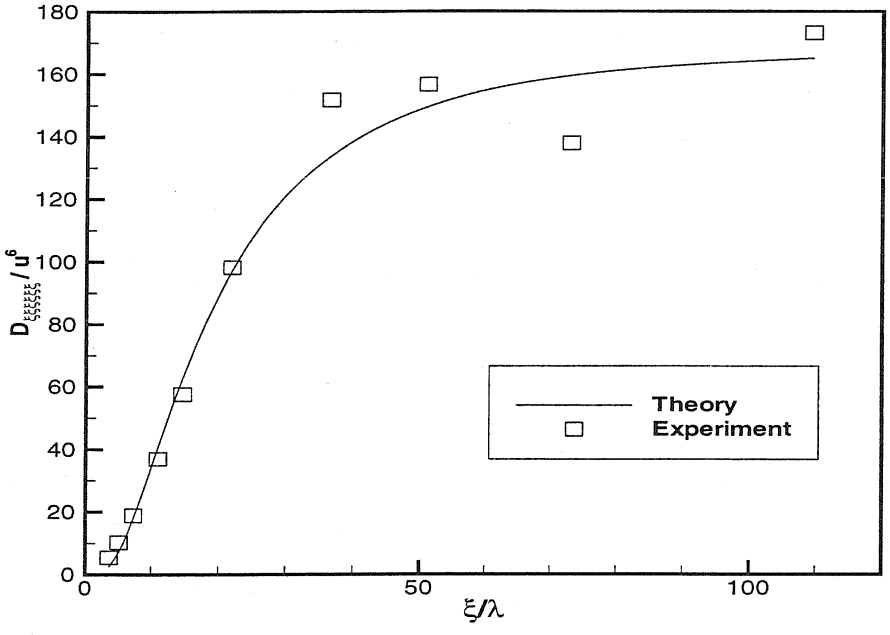

Figure 6.1: Sixth order longitudinal velocity structure function based on Hill's spherical vortex compared with experimental data [1].

Chapter 7 Concluding remarks

In the pioneering work of Synge and Lin, theoretical second order velocity correlation curves were obtained which demonstrated fair agreement with experiment. We have modified their original work with a physically motivated vortex size distribution and have extended the statistical analysis beyond the second order velocity correlation functions. We derived a mathematical model for computing the ensemble average and obtained complete velocity structure function information for orders two and four and the lateral component of the sixth order tensor. In addition to analyzing the relative scaling of longitudinal and lateral results, we investigated the second order pressure statistics.

The spherical vortex model seems to predict theoretical results consistent with experimental observation which indicates its general correctness for homogeneous isotropic turbulence. In fact, it appears that no other physical model has been as robust in capturing the statistical properties measured in the lab or via numerical simulation. In summary the model was developed around the longitudinal second and fourth order velocity structure functions. The two parameters introduced by the model were fixed at the junctures of both calculations so that results for these particular statistics would be in fair agreement with empirical data for high Reynolds number isotropic flows. The second order lateral structure function was derived independently of $\langle \Delta u_\xi^2 \rangle$ as verification of the longitudinal results. The model was then used to predict the higher order velocity statistics, $\langle \Delta u_\gamma^4 \rangle$, $\langle \Delta u_\gamma^2 \Delta u_\xi^2 \rangle$, and $\langle \Delta u_\xi^6 \rangle$. While we are presently lacking both experimental and numerical data for the lateral and mixed fourth order structure functions, we found striking agreement between experiment and the sixth order longitudinal prediction. This is probably the result of greatest merit for the model.

In addition to the velocity statistics, the second order pressure structure function was investigated. The model equation which used the pressure field of the spherical

vortex did not generate a shape for $D_p(\xi)$ consistent with simulation. Several explanations for this were presented including the unresolved question as to whether a pressure field based on the sum of the induced pressures of N non-interacting vortices has any physical or mathematical validity as a consequence of the Navier-Stokes equation. One might further conjecture that the pressure statistics are largely determined by the small scale dynamics which conflicts with the vortex size distribution which biases the statistics towards contributions from the large scales. It was found, however, that prior to averaging over vortex size, the theoretical pressure correlation was in good agreement with low Reynolds number turbulent flows and, additionally, modeled the behavior of $P(\xi)$ owing to the joint-Gaussian assumption. Motivated by the success of the shape of $\langle \Delta u_\xi^4 \rangle$, we computed $D_p(\xi)$ from an isotropic relation which depends on the three independent fourth order velocity structure functions. During this calculation we found that the pressure structure function is the result of large positive and large negative contributions which suggests that the pressure structure function is sensitive to minor scaling idiosyncracies among the three fourth order velocity statistics. The relative scaling of the transverse structure functions to the longitudinal structure functions was considered for the spherical vortex model. The theoretical prediction that the two functions scale differently, at least for orders two and four, was shown to be consistent with simulation.

While the model appears robust in its predictive capability, it is not without inconsistencies and unsatisfactory points. Foremost, the high degree of symmetry causes all odd-order structure functions to vanish which is contrary to theory, experiment and simulation. One suggestion for breaking the symmetry is to add helicity to the flow [61]. While this would probably be a more physically viable model, the analytical tractability would be quickly lost. Furthermore, the spherical vortex is not a perfect model for a turbulent eddy. The velocity field is continuous across the vortex surface, but there is a discontinuity in the tangential rate of shear. In a viscous fluid this discontinuity would become dynamically significant and would quickly alter the motion. A model better suited to understand the general decay of turbulence would not contain such a defect and would include some type of viscous dissipation mechanism.

One such approach would be to seek a viscous perturbation of Hill's spherical vortex by introducing a small amount of viscosity on the vortex surface.

Appendix A The toroidal coordinate system

To evaluate the integration over space, we introduce a coordinate transformation $T : (\mathbf{r}, \tilde{\mathbf{r}}) \rightarrow (r, \tilde{r}, \varphi)$ where $\|\mathbf{r}\| = r$ and $\|\tilde{\mathbf{r}}\| = \tilde{r}$.

In figure (4.3) the vortex has its center at the point $A(\mathbf{x})$ and the two points where turbulent fluctuations are being observed have positions $A_o(\mathbf{x}_o)$ and $\tilde{A}_o(\tilde{\mathbf{x}}_o)$. We begin by positioning a Cartesian system at the midpoint of the separation vector ξ with the $\hat{e}_3$ axis aligned with ξ. The vortex position is thus given by

$$\begin{aligned} \mathbf{x} &= \left(r_1, r_2, r\cos\alpha + \frac{\xi}{2}\right), \\ &= \left(\tilde{r}_1, \tilde{r}_2, \tilde{r}\cos\beta - \frac{\xi}{2}\right). \end{aligned} \tag{A.1}$$

Referring to figure (4.3), we see that the Cartesian coordinates (r_1, r_2, r_3) and $(\tilde{r}_1, \tilde{r}_2, \tilde{r}_3)$ are given by

$$\begin{aligned} r_1 &= r\sin\alpha\cos\varphi, \\ r_2 &= r\sin\alpha\sin\varphi, \\ r_3 &= r\cos\alpha, \\ \tilde{r}_1 &= \tilde{r}\sin\beta\cos\varphi, \\ \tilde{r}_2 &= \tilde{r}\sin\beta\sin\varphi, \\ \tilde{r}_3 &= \tilde{r}\cos\beta. \end{aligned} \tag{A.2}$$

By the law of cosines,

$$\begin{aligned} r^2 &= \tilde{r}^2 + \xi^2 - 2\tilde{r}\xi\cos\beta, \\ \tilde{r}^2 &= r^2 + \xi^2 - 2r\xi\cos\gamma, \end{aligned} \tag{A.3}$$

so that

$$\begin{aligned} \cos\gamma &= \frac{r^2 - \tilde{r}^2 + \xi^2}{2r\xi}, \\ \cos\beta &= \frac{\tilde{r}^2 - r^2 + \xi^2}{2\tilde{r}\xi}. \end{aligned} \tag{A.4}$$

The cosine of the angle γ is equal to $\cos(\pi - \alpha) = -\cos\alpha$. Therefore, by equation $(A.4)$,

$$\cos\alpha = \frac{\tilde{r}^2 - r^2 - \xi^2}{2r\xi}. \tag{A.5}$$

By $(A.1)$ and $(A.5)$,

$$r\sin\alpha = \tilde{r}\sin\beta, \tag{A.6}$$

and

$$\xi = \tilde{r}\cos\beta - r\cos\alpha. \tag{A.7}$$

Squaring $(A.7)$ we find

$$\xi^2 = \tilde{r}^2\left(1 - \sin^2\beta\right) + r^2\left(1 - \sin^2\alpha\right) - 2r\tilde{r}\cos\beta\cos\alpha. \tag{A.8}$$

We next substitute equations $(A.4)$ and $(A.5)$ for $\cos\beta$ and $\cos\alpha$ and use $(A.6)$ to substitute $\frac{\tilde{r}}{r}\sin\beta$ for $\sin\alpha$. This enables us to solve for $\sin\beta$ and thence for $\sin\alpha$:

$$\sin\beta = \left[\frac{1}{2} + \frac{1}{2}\left(\frac{r}{\tilde{r}}\right)^2 - \frac{1}{4}\left(\frac{\tilde{r}^2 - r^2}{\tilde{r}\xi}\right)^2 - \frac{1}{4}\left(\frac{\xi}{\tilde{r}}\right)^2\right]^{1/2}, \tag{A.9}$$

$$\sin\alpha = \left[\frac{1}{2} + \frac{1}{2}\left(\frac{\tilde{r}}{r}\right)^2 - \frac{1}{4}\left(\frac{\tilde{r}^2 - r^2}{r\xi}\right)^2 - \frac{1}{4}\left(\frac{\xi}{r}\right)^2\right]^{1/2}. \tag{A.10}$$

Using the fact that $r\sin\alpha = \tilde{r}\sin\beta$, we introduce the function $f(r, \tilde{r})$ and define the

coordinate transformation as follows. Let $T : (\mathbf{r}, \tilde{\mathbf{r}}) \rightarrow (r, \tilde{r}, \varphi)$ such that

$$T \equiv \begin{cases} r_1 &= r\sin\alpha\cos\varphi &= f\,(r,\ \tilde{r})\cos\varphi \\ r_2 &= r\sin\alpha\sin\varphi &= f\,(r,\ \tilde{r})\sin\varphi \\ r_3 &= r\cos\alpha &= \frac{\tilde{r}^2-r^2-\xi^2}{2\xi} \\ \tilde{r}_1 &= \tilde{r}\sin\beta\cos\varphi &= f\,(r,\ \tilde{r})\cos\varphi \\ \tilde{r}_2 &= \tilde{r}\sin\beta\sin\varphi &= f\,(r,\ \tilde{r})\sin\varphi \\ \tilde{r}_3 &= \tilde{r}\cos\beta &= \frac{\tilde{r}^2-r^2+\xi^2}{2\xi} \end{cases} \tag{A.11}$$

where

$$f(r,\tilde{r}) = \left(\frac{r^2+\tilde{r}^2}{2} - \frac{(\tilde{r}^2-r^2)^2}{4\xi^2} - \frac{\xi^2}{4}\right)^{\frac{1}{2}}. \tag{A.12}$$

We now have r_i and $\tilde{r}_i$ expressed in terms of the bipolar components $(r, \tilde{r}, \varphi)$. It remains to establish the measure of integration dV. In a Cartesian system (x, y, z) a differential volume element is given by the exterior product of dx, dy, and dz,

$$dV = dx \wedge dy \wedge dz = dxdydz. \tag{A.13}$$

Referring to figure (4.3), let $\rho = (x, y, z)$, where

$$\begin{aligned} x &= r\sin\alpha\cos\varphi = f(r,\tilde{r})\cos\varphi, \\ y &= r\sin\alpha\sin\varphi = f(r,\tilde{r})\sin\varphi, \\ z &= r\cos\alpha = \frac{\tilde{r}^2-r^2}{2\xi}. \end{aligned} \tag{A.14}$$

The differentials dx, dy, dz are therefore

$$\begin{aligned} dx &= \cos\varphi df - f(r,\tilde{r})\sin\varphi d\varphi, \\ dy &= \sin\varphi df + f(r,\tilde{r})\cos\varphi d\varphi, \\ dz &= \frac{1}{\xi}\left(\tilde{r}d\tilde{r} - rdr\right), \end{aligned} \tag{A.15}$$

where df is given by

$$df = \frac{1}{2f}\left[\left(1+\frac{\tilde{r}^2-r^2}{\xi^2}\right)rdr+\left(1-\frac{\tilde{r}^2-r^2}{\xi^2}\right)\tilde{r}d\tilde{r}\right]. \tag{A.16}$$

We now form the exterior product $dx \wedge dy \wedge dz$,

$$\begin{aligned} dV &= (\cos\varphi df - f\sin\varphi d\varphi)\wedge(\sin\varphi df+\cos\varphi d\varphi)\wedge\frac{1}{\xi}(\tilde{r}d\tilde{r}-rdr), \\ &= \frac{1}{\xi}\left(f\cos^2\varphi df d\varphi + f\sin^2\varphi df d\varphi\right)\wedge(\tilde{r}d\tilde{r}-rdr), \\ &= \frac{1}{\xi}f df d\varphi\,(\tilde{r}d\tilde{r}-rdr), \\ &= \frac{r\tilde{r}}{\xi}dr d\tilde{r} d\varphi. \end{aligned} \tag{A.17}$$

Bibliography

[1] P. Tabeling, G. Zocchi, F. Belin, J. Maurer, and H. Willaime. Probability density functions, skewness and flatness in large reynolds number turbulence. *Phys. Rev. E*, 1995.

[2] D. I. Pullin. Pressure spectra for vortex models of homogeneous turbulence. *Phys. Fluids*, 7:849–56, 1995.

[3] M. Lesieur. *Turbulence in Fluids.* Martinus Nijhoff Publishers, 1987.

[4] B. E. Launder and D. B. Spalding. *Mathematical Models of Turbulence.* Academic Press, 1972.

[5] M. Farge, N. Kevlahan, V. Perrier, and E. Goirand. Wavelets in turbulence. *Proc. IEEE*, 84(4):639–669, Apr 1996.

[6] V. Yakhot and S. A. Orszag. Renormalization group analysis of turbulence. *J. Sc. Comp.*, 1(1):3–51, 1986.

[7] G. I. Taylor. Statistical theory of turbulence. parts 1-4. *Proc. Roy. Soc. A*, 151:421, 1935.

[8] A. N. Kolmogorov. The local structure of turbulence in incompressible viscous fluid for very large reynolds numbers. *C. R. Acad. Sc. USSR*, 30:301–305, 1941.

[9] A. N. Kolmogorov. On degeneration of isotropic turbulence in an incompressible viscous liquid. *C. R. Acad. Sc. USSR*, 31:538, 1941.

[10] A. N. Kolmogorov. Dissipation of energy in locally isotropic turbulence. *C. R. Acad. Sc. USSR*, 32:16, 1941.

[11] A. M. Obukhov. On the distribution of energy in the spectrum of turbulent flow. *C. R. Acad. Sci. URSS*, 32:19, 1941.

[12] A. N. Kolmogorov. A refinement of previous hypotheses concerning the local structure of turbulence in a viscous incompressible fluid at high reynolds number. *J. Fluid Mech.*, 12:82–85, 1962.

[13] G. Brown and A. Roshko. On density effects and large structure in turbulent mixing layers. *J. Fluid Mech.*, 64:775–816, 1974.

[14] L. P. Bernal. The statistics of the organized vortical structure in turbulent mixing layers. *Phys. Fluids*, 31(9):2533–2543, 1988.

[15] M. Lesieur and O. Metias. New trends in large eddy simulation. *Annu. Rev. Fluid Mech.*, 28:45–82, 1996.

[16] H. M. Blackburn, N. N. Mansour, and B. J. Cantwell. Topology of fine-scale motions in turbulent channel flow. *J. Fluid Mech.*, 310:269–292, 1996.

[17] W. T. Ashurst, A. R. Kerstein, R. M. Kerr, and C. H. Gibson. Alignment of vorticity and scalar gradient with strain rate in simulated navier-stokes turbulence. *Phys. Fluids*, 30(8):2343–2353, 1987.

[18] A. Vincent and M. Meneguzzi. The spatial and statistical properties of homogeneous turbulence. *J. Fluid Mech.*, 225:1–20, 1991.

[19] A. Vincent and M. Meneguzzi. The dynamics of vorticity tubes in homogeneous turbulence. *J. Fluid Mech.*, 258:245–254, 1994.

[20] J. L. Synge and C. C. Lin. On a statistical model of isotropic turbulence. *Trans. Roy. Soc. Can.*, 37:45, 1943.

[21] A. A. Townsend. On the fine scale structure of turbulence. *Proc. Roy. Soc. London Ser. A*, 208:534, 1951.

[22] S. Corrsin. Turbulent dissipation fluctuations. *Phys. Fluids*, 5:1301, 1962.

[23] A. A. Tennekes. Simple model for the small-scale structure of turbulence. *Phys. Fluids*, 11:669, 1968.

[24] P. G. Saffman. Lectures on homogeneous turbulence. In N. J. Zabusky, editor, *Topics in Nonlinear Physics*. Springer-Verlag, 1968.

[25] T. S. Lundgren. Strained spiral vortex model for turbulent fine structure. *Phys. Fluids*, 25:2193, 1982.

[26] J. M. Burgers. A mathematical model illustrating the theory of turbulence. *Adv. Appl. Mech.*, 1:171–199, 1948.

[27] D. I. Pullin and P. G. Saffman. Vortex dynamics in turbulence. *Annu. Rev. Fluid Mech.*, 30:31–51, 1998.

[28] P. G. Saffman and D. I. Pullin. Calculation of velocity structure functions for vortex models of isotropic turbulence. *Phys. Fluids*, 8:3072–84, 1996.

[29] T. S. Lundgren. A small-scale turbulence model. *Phys. Fluids A*, 5(6):1472–1483, 1983.

[30] D. Segel. The higher moments in the lundgren model conform with kolmogorov scaling. *Phys. Fluids*, 7(12):3072–77, Dec 1995.

[31] D. I. Pullin and P. G. Saffman. On the lundgren-townsend model of turbulent fine scales. *Phys. Fluids A*, 5:126–45, 1993.

[32] D. I. Pullin, J. D. Buntine, and P. G. Saffman. On the spectrum of a stretched spiral vortex. *Phys. Fluids*, 6(9):3010–3027, Sep 1994.

[33] T. S. Lundgren. The concentration spectrum of the product of a fast biomolecular reaction. *Chem. Eng. Sci.*, 40:1641–52, 1985.

[34] A. Roshko. *J. Fluid Mech.*, 10:345, 1961.

[35] Y. Couder, S. Douady, and O. Cadot. Vorticity filaments. In Tabeling and Cardoso, editors, *Turbulence: A Tentative Dictionary*. Plenum, 1994.

[36] J. C. McWilliams. The emergence of isolated coherent vortices in turbulent flow. In G. Holloway and B. J. West, editors, *AIP Conference Proceedings*, volume 106, pages 205–221. LaJolla Institute, 1984.

[37] L. E. Reichl. *A Modern Course in Statistical Physics.* Edward Arnold, London, 1980.

[38] L. D. Landau and E. M. Lifshitz. *Fluid Mechanics*, volume 6 of *Course of Theoretical Physics.* Pergamon Press, 1959.

[39] O. Reynolds. On the dynamical theory of incompressible viscous fluids and the determination of the criterion. *Phil. Trans. Roy. Soc. London*, 186:123–164, 1894.

[40] H. P. Robertson. The invariant theory of isotropic turbulence. *Proc. Camb. Phil. Soc.*, 36:209, 1940.

[41] G. K. Batchelor. *The Theory of Homogeneous Turbulence.* Cambridge University Press, 1953.

[42] A. S. Monin and A. M. Yaglom. *Statistical Fluid Mechanics: Mechanics of Turbulence.* MIT Press, 1975.

[43] F. Anselmet, Y. Gagne, E. J. Hopfinger, and R. A. Antonia. High-order velocity structure function in turbulent shear flows. *J. Fluid Mech.*, 140:63–89, 1984.

[44] G. K. Batchelor. Pressure fluctuations in isotropic turbulence. *Proc. Camb. Phil. Soc.*, 47:359–374, 1951.

[45] A. M. Obukhov. Pressure pulsation in a turbulent flow. *Dokl. Akad. Nauk. SSSR*, 66:17–20, 1949.

[46] A. M. Yaglom. On the field of accelerations in turbulent flow. *Dokl. Akad. Nauk. SSSR*, 67:795–798, 1949.

[47] W. Heisenberg. Zur statistichen theorie der turbulenz. *Z. Physik*, 124:628–657, 1948.

[48] A. M. Obukhov and A. M. Yaglom. The microstructure of turbulent flow. *Prikl. Mat. Mekh.*, 15:3–26, 1951.

[49] R. J. Hill. Relationships between several fourth-order velocity statistics and the pressure structure function for isotropic, incompressible turbulence. Technical report, NOAA Tech. Rep. ERL 449-ETL 65, 1993. Order no. PB94-187309. Available from the author or the National Technical Information Service, 5285 Port Royal Rd, Springfield, VA 22161, USA.

[50] R. J. Hill and J. M. Wilczak. Pressure structure functions and spectra for locally isotropic turbulence. *J. Fluid Mech.*, 296:247–269, 1995.

[51] M. Millionshtchikov. On the theory of homogeneous isotropic turbulence. *C. R. Acad. Sci. URSS*, 32:615, 1941.

[52] R. W. Stewart. Triple velocity correlations in isotropic turbulence. *Proc. Camb. Phil. Soc.*, 47:146, 1951.

[53] A. M. Obukhov. Pressure pulsation in a turbulent flow. *Dokl. Akad. Nauk. SSSR*, 66:17–20, 1949.

[54] M. J. M. Hill. On a spherical vortex. *Phil. Trans. Roy. Soc. London*, 185:213–245, 1894.

[55] A. M. Yaglom. Lagrangian turbulence characteristics in a diabatic atmospheric surface layer and in convective jets. *Izvestiya AN SSSR, Ser. fiz. atmos. i okeana*, 1(2):157–166, 1965.

[56] B. Dhruva, Y. Tsuji, and K. Sreenivasan. Transverse structure functions in high reynolds-number turbulence. *Phys. Rev. E*, 56(5):56–58, 1997.

[57] A. Noullez, G. Wallace, W. Lempert, R. Miles, and U. Frisch. Transverse velocity increments in turbulent flow using the relief technique. *J. Fluid Mech.*, 339:287, 1997.

[58] O. N. Boratov and R. B. Pelz. Structures and structure functions in the inertial range of turbulence. *Phys. Fluids*, 9:1400, 1997.

[59] S. Chen, K. Sreenivasan, M. Nelkin, and N. Cao. Refined similarity hypothesis for transverse structure functions in fluid turbulence. *Phys. Rev. Let.*, 79:2253, 1997.

[60] M. Nelkin and S. Chen. The scaling of pressure in isotropic turbulence. *Phys. Fluids*, 10(9):2119–2121, 1998.

[61] P. G. Saffman. *Vortex Dynamics.* Cambridge University Press, 1992.